

Multiband Diagnostics of Unidentified 1FGL Sources with Suzaku and Swift X-ray Observations

Y. Takeuchi¹, J. Kataoka¹, K. Maeda¹, Y. Takahashi¹, T. Nakamori², M. Tahara¹

uto_of_take@suou.waseda.jp

ABSTRACT

We have analyzed all the archival X-ray data of 134 unidentified (unID) gamma-ray sources listed in the first *Fermi/LAT* (1FGL) catalog and subsequently followed up by *Swift/XRT*. We constructed the spectral energy distributions (SEDs) from radio to gamma-rays for each X-ray source detected, and tried to pick up unique objects that display anomalous spectral signatures. In these analysis, we target all the 1FGL unID sources, using updated data from the second *Fermi/LAT* (2FGL) catalog on their LAT position and spectra. We found several potentially interesting objects, particularly three sources, 1FGL J0022.2-1850, 1FGL J0038.0+1236 and 1FGL J0157.0-5259, which were then more deeply observed with *Suzaku* as a part of an AO7 program in 2012. We successfully detected an X-ray counterpart for each source whose X-ray spectra were well fitted by a single power-law function. The positional coincidence with a bright radio counterpart (currently identified as AGN) in the 2FGL error circles suggests these are definitely the X-ray emission from the same AGN, but their SEDs show a wide variety of behavior. In particular, the SED of 1FGL J0038.0+1236 is difficult to be explained by conventional emission models of blazars. The source 1FGL J0022.2-1850 may be in a transition state between a low-frequency peaked BL Lac and a high-frequency peaked BL Lac object, and 1FGL J0157.0-5259 could be a rare kind of extreme blazar. We discuss the possible nature of these three sources observed with *Suzaku*, together with the X-ray identification results and SEDs of all 134 sources observed with *Swift/XRT*.

Subject headings: galaxies:active - gamma rays:general - radiation mechanism:general - X-rays:general

¹Research Institute for Science and Engineering, Waseda University, 3-4-1 Okubo, Shinjuku, Tokyo, 169-8555, Japan.

²Department of Physics, Faculty of Science, Yamagata University, 990-8560

1. Introduction

Since the successful launch of the *Fermi* Gamma-ray Space Telescope in 2008 June, we now have a new opportunity to study gamma-ray emission from different types of high energy sources with much improved sensitivity and localization capabilities than with the EGRET instrument onboard the *Compton Gamma-Ray Observatory* (CGRO). With the field of view covering 20% of the sky at every moment (five times larger than EGRET), and its improved sensitivity (by more than an order of magnitude with respect to EGRET), the Large Area Telescope (LAT; Atwood et al. 2009) aboard *Fermi* surveys the entire sky each day down to photon flux levels of $F_{>100\text{MeV}} \simeq \text{few} \times 10^{-7} \text{ph cm}^{-2} \text{s}^{-1}$. The number of detected gamma-ray sources has increased, with the 2nd *Fermi*-LAT Catalog (2FGL; Nolan et al. 2012) containing 1873 gamma-ray sources in the 100 MeV to 100 GeV range, while 271 objects were previously listed in the 3rd EGRET Catalog (3EG; Hartman et al. 1999). More than 1,000 gamma-ray sources included in the 2FGL are proposed to be associated with active galactic nuclei (AGNs) and 87 sources with pulsars (PSRs; Abdo et al. 2010a), including 21 millisecond pulsars (MSPs). Other associations included supernova remnants (SNRs; Abdo et al. 2010d), low-mass/high-mass X-ray binaries (Abdo et al. 2009), pulsar wind nebulae (Abdo et al. 2010e), normal and starburst galaxies (Abdo et al. 2010c), and the giant lobes of a radio galaxy (Abdo et al. 2010f).

However, no obvious counterparts at longer wavelength have been found for as much as 31% of the 2FGL *Fermi*-LAT objects so that several hundreds of GeV sources currently remain unassociated with any known astrophysical systems. In other words the nature of unassociated gamma-ray sources are still one of the major puzzles, and the mystery has never been solved yet. Fortunately, an improved localization capabilities of the *Fermi*-LAT (typical 95% confidence radii $r_{95} \sim 0^\circ.1 - 0^\circ.2$, and even $0^\circ.005 - 0^\circ.01$ for the brightest sources; (Nolan et al. 2012)), when compared to that of EGRET (typical $r_{95} \sim 0^\circ.4 - 0^\circ.7$), enables more effective follow-up studies at radio, optical, and X-ray frequencies, which can help to unravel the nature of the unID gamma-ray emitters. Indeed for example, a lot of *Fermi* sources were identified using WISE IR data (D’Abrusco et al. 2013; Massaro et al. 2013).

In this context, we started a new project to investigate the nature of unID *Fermi*-LAT objects through X-ray follow-up observations with the XIS sensor onboard the *Suzaku* X-ray satellite (see section 2). For example, the results of the first-year campaign conducted in *Suzaku* AO-4 (2009) were presented in (Maeda et al. 2011). In this campaign, the X-ray counterpart for one of the brightest unassociated *Fermi*-LAT objects, 1FGL J1231.1-1410 (also detected by EGRET as 3EG J1234-1318 and EGR J1231-1412), was discovered for the first time. The X-ray spectrum was well fitted by a blackbody with an additional power-law component, supporting the recent identification of this source with a MSP. In the second-year campaign (AO-5), another seven unID *Fermi*-LAT sources were subsequently observed with *Suzaku* (Takahashi et al. 2012). In particular,

this paper presented a convenient method to classify the objects into “AGN-like” and “PSR-like” by comparing their multiwavelength properties with those of known AGNs and pulsars. In the third-year (AO-6), 1FGL J2339.7-0531 (Yatsu et al. 2013 in prep; also Romani & Shaw 2011) and 1FGL J1311.7-3429 (Romani 2012; Kataoka et al. 2012) were intensively monitored with a total exposure time of 200 ksec. Both sources are now suggested to be “black widow” MSP systems and newly categorized as “radio-quiet” MSPs. As these projects show, the X-ray follow-up observations especially using *Suzaku* provided various fruitful results to clarify the nature of unassociated gamma-ray sources, and was able to find a new type of gamma-ray emitter.

To complete a series of X-ray follow-up programs described above, we further carried out the analysis of all the archival X-ray data of 134 unID gamma-ray sources in the 1FGL catalog of point sources (1FGL; Abdo et al. 2010b) with *Swift*/XRT. Note that, all these 134 sources have been detected in the 2FGL catalog, hence the updated data on their LAT position and spectra were available from the 2nd *Fermi*/LAT catalog so are used throughout this work. This allowed us to construct the SEDs (SEDs) of each objects from radio to gamma-rays (see Section 2 and appendix) for the first time. Note that we target all the 1FGL unID sources that satisfy our selections (see Section 2), using updated/improved information from the 2FGL catalog on their LAT positions and spectra in this paper. Moreover, three sources that displayed potentially interesting SEDs, 1FGL J0022.2-1850 (or 2FGL J0022.2-1853), 1FGL J0038.0+1236 (or 2FGL J0037.8+1238) and 1FGL J0157.0-5259 (or 2FGL J0157.2-5259), were deeply observed with *Suzaku* as a part of AO7 campaign in 2012. In the 2FGL catalog, both 1FGL J0022.2-1850 and 1FGL J0157.0-5259 are categorized as active galaxies of uncertain type (agu), while 1FGL J0038.0+1236 was classified as a BL Lac type of blazar (bzb) based on the positional coincidences to sources observed at another wavelength. But as we see below, the unique SEDs of these three objects are not well understood as conventional blazars. In Section 2 we first describe the analysis of the 134 1FGL unID sources with *Swift*. Subsequently in Section 3, deep *Suzaku* follow-up observations of the selected three sources, 1FGL J0022.2-1850, 1FGL J0038.0+1236 and 1FGL J0157.0-5259 are shown. The results of the analysis are given in Section 4. The discussion and summary are presented in Section 5 and 6, respectively.

2. *Swift* analysis of 134 1FGL unID sources

2.1. Observation and Data Reduction

Swift (Geherels et al. 2004) is a gamma-ray observatory launched on 2004 November 20. The primary goal of this mission is to explore and follow-up the gamma-ray burst, but high mobility and sensitivity to localize sources especially using the XRT (Burrows et al. 2005) and UVOT (Roming

et al. 2005), makes it also viable to follow-up unID gamma-ray objects discovered by *Fermi*-LAT . In fact, *Swift* follow-up observations helped study many unID *Fermi*-LAT sources (Cognard et al. 2011; Keith et al. 2011; Ransom et al. 2011; Theureau et al. 2011; Cheung et al. 2012; Kong et al. 2012). Here we tried to perform a systematic and uniform analysis of unID gamma-ray sources observed thus far with *Swift* using the archival data. The selection criteria is given as follows; (1) categorized as unID sources in 1FGL catalog, (2) localized at high Galactic latitude $|b| > 10^\circ$, (3) observational data are in public at the time of October 2011, (4) the positional center of *Swift* field-of-view is within 12 arcmin from the 1FGL sources. Among 630 unID sources listed in the 1FGL catalog, this selection yields 134 sources which we analyzed here. In the reduction and the analysis of the *Swift*/XRT and UVOT data, HEADAS software version 6.11 and the most recent calibration databases (CALDB) as of 2011 October 20 were used. We did not use BAT data because most sources are not bright enough to be detected within short exposure of typically 10 ksec or less. In the XRT analysis, we only use the PC mode data, while only image data taken from photometry observation is used in the UVOT analysis.

2.2. XRT Analysis

Two types of XRT archival data can be obtained from the *Swift* Data Center, Level 1 and 2. Level 2 cleaned data have gone through the standard pipeline process; however, we calibrated the Level 1 data ourselves in a way recommended by *Swift* team¹. Particularly, we selected the good time interval (GTI) from the Level 1 data using `xrtpipeline`. In this process, we only changed the default `xrtpipeline` selection in the temperature of CCDs from " ≤ -47 " to " ≤ -50 ", where the former is the default value. In the XRT image analysis, we tried to detect the X-ray counterparts of 1FGL unID sources, and localize each source. First, we extracted X-ray images in the energy range of 0.3–10 keV using `xselect`. Next by using `ximage`, we searched for “possible” X-ray sources which were $> 3\sigma$ confidence level in photon statistics against background. The position of these sources are determined with a typical accuracy of $\sim 5''$ using `xrtcentroid`. The results of X-ray source detection is listed in Table 6 (see, appendix). In the appendix, we also show the XRT images corresponding to each of the 134 1FGL unID gamma-ray sources indicating also the 2FGL error ellipses (Figure 11). In these images, bright radio sources and X-ray sources listed in The ROSAT All-Sky Survey Bright Source Catalogue (1RXS; Voges et al. 1999) corresponding to the XRT sources are also plotted as magenta crosses. Finally, if the X-ray sources were detected were within the 2FGL 95% position error ellipse, we performed X-ray spectral analysis for those sources. We note that very bright X-ray sources with more than 0.6 c/s should cause se-

¹The SWIFT XRT Data Reduction Guide:http://heasarc.nasa.gov/docs/swift/analysis/xrt_swguide_v1.2.pdf

rious pile-up effects in the XRT CCD, however, there were no such bright sources in our analyzed sample.

In the XRT spectral analysis, PHA files were extracted from event files with `xselect` and exposure maps were made using `xrtexpomap`. We made auxiliary response files (ARFs) using `xrtmkarf`, while we used the current redistribution matrix files (RMFs) in CALDB. We extracted photons from circles with 30 arcsec radii around the source positions as the source regions, and we set the concentric rings centered at the source positions with radius 30-180 arcsec as the background regions. In the case when some background sources appear in the field, or overall regions cannot be fitted in the CCD, we simply remove the region surrounding these background sources, or the region outside the CCD chip. If there is no source detected above 3σ inside the 2FGL error ellipse, we derived the upper limit assuming the 2FGL error ellipses as the source region of corresponding X-ray flux. The results of spectral analysis are included in the SEDs given in the appendix. We note that X-ray spectral data were binned at two different ways according to the source brightness; (a) binned with `grppha` so that at least 20 photons are included in each bin, (b) divide X-ray spectral data (0.5-10.0 keV) logarithmically into 5 bin. When the source have more than 40 counts, we used (a), but otherwise we used (b).

2.3. UVOT Analysis

We performed the analysis of UVOT data only when the X-ray counterpart of 1FGL source was found in the *Swift*/XRT field of view. *Swift*/UVOT archival data has six types of filters (*v*, *b*, *u*, *uvw1*, *uvw2* and *uvm2*), with each filter providing different wavelength data. When each filter included more than one observation, the images and exposure maps were summed using `uvotimsum`. Using `uvotdetect`, we detected the sources which have high signal-to-noise ratio ($> 3\sigma$). We set the circles around those sources with radius 5 arcsec as the sources regions if any source was found in the 90% error ellipse of the *Swift*/XRT source. Then, circles with radius 30" as the background regions were taken from the area where no sources are found. Finally, we obtained the magnitude of each filter using `uvotsource`. The correction of Galactic extinction were performed following the way described in Cardelli et al. (1998).

2.4. Multiwavelength Analysis

To construct SEDs of each 1FGL sources, we used not only the *Swift*/XRT and *Swift*/UVOT flux data analyzed in this paper, but gamma-ray fluxes listed in the 2FGL catalog, and radio fluxes mostly from the NED database and W3Browse based on a variety of catalogs. We searched for

radio counterparts associated with the XRT or UVOT objects which were mentioned above in the HEASARC/Master Radio Catalog ², (includes the NRAO VLA Sky Survey (NVSS; Condon et al. 1998, 1.4 GHz), the FIRST Survey Catalog of 1.4-GHz Radio Sources (FIRST; White et al. 1997, 1.4 GHz), Sydney University Molonglo Sky Survey Source Catalog (SUMSS; Mauch et al. 2003, 843 MHz), VLA Low-Frequency Sky Survey Discrete Source Catalog (VLSS; Cohen et al. 2007, 74 MHz), the Westerbork in the Southern Hemisphere Survey (WISH; De Breuck et al. 2002), Australia Telescope 20-GHz Survey Catalog (AT20G; Murphy et al. 2010), the Green Bank 6-cm Catalog of Radio Sources (GB6; Gregory et al. 1996), and Parkes-MIT-NRAO Southern, Tropical, Equatorial and Zenith Survey (PMN; Wright et al. 1994)) and those radio fluxes are added in the SEDs. Note that if no corresponding radio sources were found in the 2FGL 95% error ellipses, we obtained the upper limit from the most bright radio source in the error ellipse. Likewise, if no source was found in the error ellipse but some sources were found outside of the region, we used the sensitivity limits of those sources as an upper limit. Finally resultant SEDs and flux values of each wavelength are given in the appendix (Figure 12, Table 5 and 6).

3. *Suzaku* analysis of three 1FGL unID sources

3.1. Observation and Data Reduction

We observed three *Fermi*-LAT objects that exhibited potentially interesting or anomalous SEDs (which is difficult to be explained by standard emission models of blazars, i.e., SSC or external Compton models as explained in Fossati et al. (1997)) with the *Suzaku* X-ray astronomy satellite (Mitsuba et al. 2007). These were denoted in the 1FGL catalog as 1FGL J0022.2-1850, 1FGL J0038.0+1236, and 1FGL J0157.0-5259, and in the 2FGL catalog as 2FGL J0022.2-1853, 2FGL J0037.8+1238, and 2FGL J0157.2-5259, respectively. The *Suzaku* observation logs are summarized in Table 1. The observations were performed with XIS which consists of four CCD cameras each placed in the focal plane of the X-ray Telescope (XRT; Serlemitsos et al. 2007), and with the Hard X-ray Detector (HXD) which consists of Si PIN photo-diodes (HXD-PIN) and GSO scintillation counters (HXD-GSO) (HXD; Kokubun et al. 2007; Takahashi et al. 2007).

One of the XIS sensors (XIS 1) has a back-illuminated (BI) CCD, while the other three (XISs 0, 2, and 3) utilize front-illuminated (FI) CCDs. However, because of an anomaly in 2006 November, the operation of XIS2 was terminated. Hence, here we use only the three remaining CCDs. The XIS was operated in the normal full-frame clocking mode with the 3×3 or 5×5 editing mode. We analyzed the screened XIS data, reduced using the *Suzaku* software version 1.2. The screening

²<http://heasarc.nasa.gov/W3Browse/all/radio.html>

was based on the following criteria: (1) only ASCA-grade 0, 2, 3, 4, 6 events were accumulated, while hot and flickering pixels were removed from the XIS image using the `sisclean` script (Day et al. 1998), (2) the time interval after the passage of South Atlantic Anomaly was greater than 60 s, (3) the object was at least 5° and 20° above the rim of the Earth (ELV) during night and day, respectively. In addition, we also selected the data with a cutoff rigidity (COR) larger than 6 GV. In the reduction and the analysis of the *Suzaku* XIS data, HEADAS software version 6.12 and a calibration databases (CALDB) released on 2009 September 25 were used. The XIS cleaned event data-set was obtained in the combined 3×3 and 5×5 edit modes using `xselect`.

The HXD data were also processed in a standard way as follows. First, we obtained the appropriate version 2.0 “tuned” non-X-ray background file (NXB) for this observation. Because the HXD background file has a time variation, we made a new GTI file to match the Good Time Interval (GTI) between observation data and NXB data using `mgtime`. Next, using this new GTI file, We generated time-averaged HXD spectra with `xselect`. These were then dead time corrected using `hxddtcor` script. Epoch appropriate response files for XIS-nominal pointing were downloaded from the *Suzaku* CALDB website. The contribution from the Cosmic X-ray Background (CXB) was simulated following a recipe provided by the HXD team ³.

3.2. Image Analysis

We extracted the XIS images within the photon energy range of $0.4 - 10$ keV from only the two FI CCDs (XIS 0, XIS 3). In the image analysis, we excluded calibration sources at the corner of the CCD chips. The images of the NXB were obtained from the night Earth data using `xisnxbgen` (Tawa et al. 2008). Since the exposure times for the original data were different from that of NXB, we calculated the appropriate exposure-corrected original and NXB maps using `xisexpmapgen` (Ishisaki et al. 2007). The corrected NXB images were next subtracted from the corrected original images. In addition, we simulated flat sky images using `xissim` (Ishisaki et al. 2007), and applied a vignetting correction. All the images obtained with XIS0 and XIS3 were combined and re-binned by a factor of 4 (CCD pixel size $24 \mu\text{m} \times 24 \mu\text{m}$, so that 1024×1024 pixels cover an $18' \times 18'$ region on the sky; Koyama et al. 2007). Throughout these processes, we performed vignetting correction for all the images. Finally, the images were smoothed with a Gaussian function with $\sigma = 0.24'$. Note that the apparent features at the edge of these exposure corrected images are undoubtedly spurious due to low exposure in those regions.

³See http://heasarc.gsfc.nasa.gov/docs/suzaku/analysis/pin_cxb.html

3.3. Spectral Analysis

In the spectral analysis of XIS, we analyzed the three target sources as point sources, based on the result of our image analysis (See Section 5). Source regions for spectral analysis indicated by inner green circles were selected around each detected X-ray sources within the error ellipse of a gamma-ray emitters. The corresponding background regions were indicated by outer green ellipse after the removal of source regions. Moreover, if the X-ray sources other than target source was found, we excluded the region around those sources from the region for spectral analysis. We extracted the spectra from each source regions with `xselect` for each CCD (XIS 0, XIS 1, XIS 3). Next, we made redistribution matrix files (RMFs) and auxiliary response files (ARFs) using `xisrmfgen` and `xissimarfgen` (Ishisaki et al. 2007), respectively. In addition, we used the new contamination files `ae_xi0_contami_20120711.fits`, `ae_xi1_contami_20120711.fits` and `ae_xi3_contami_20120711.fits`⁴, because response function of XIS0 is imperfect for recent observations. Using these RMFs and ARFs, the corrected spectrum about energy response and the effective area of XIS were obtained. Finally, Spectral analysis and model fitting were performed with `xspec` version 12.7.0. In the spectral analysis of HXD, We also subtracted the NXB and CXB to obtain the HXD-PIN spectrum, then we performed model fitting together with XIS spectrum.

4. Results of *Suzaku* observations

We show in this section the results of X-ray image and spectral analysis for each object observed with *Suzaku*. Since we didn't detect any time-variability for each source in *Suzaku* exposures, the results of timing analysis are not shown in this paper. We detected successfully significant signals from the X-ray counterpart of 1FGL J0157.0-5259 with HXD/PIN, but below the sensitivity limit of the HXD/GSO, while other two sources were too faint to be detected either with HXD/PIN or GSO. Therefore, as for HXD analysis about 1FGL J0157.0-5259 in this paper, we only use the data from HXD/PIN.

4.1. 1FGL J0022.2-1850

In our *Suzaku* observations, we detected one X-ray point source (RA, DEC)=(5°.540, -18°.894) within the updated 2FGL error ellipse corresponding to 1FGL J0022.2-1850. Figure 1 shows the

⁴See : http://byakko.scphys.kyoto-u.ac.jp:31415/xis/XIS_Suzaku/2012_MeetRep/20120711_wada_CALDB/

corresponding X-ray image of 1FGL J0022.2-1850, as described in Section 4.1. The radio source NVSS J003750+123818 appears to be the counterpart of 1FGL J0022.2-1850, as indicated by the magenta cross at the center of this X-ray source (See section 5). Moreover, one unknown point source is detected within the background region for spectral analysis (because the central source is very bright, it is difficult to see this source in Fig 1).

In Figure 4, the X-ray spectrum of the *Suzaku* source, which we argue is the most likely counterpart of 1FGL J0022.2-1850, is shown. The XIS spectra is given for the energy range 0.6 – 7.5 keV. In the spectral analysis, the target X-ray source is so bright that we selected a source region assuming radii $3'$ (a typical half-power diameter of the XRT is $2'$: (Serlemitsos et al. 2007)). Meanwhile, we excluded one contaminating field X-ray point source detected by *Suzaku*, assuming the source region radii $2'$ from the source and background regions for spectral analysis described in Section 4.2. The spectrum is well fitted by a single power-law continuum with a photon index, $\Gamma = 2.43 \pm 0.03$, moderated by the Galactic absorption only. The Galactic hydrogen column density was fixed as $N_{\text{H}} = 2.02 \times 10^{20} \text{ cm}^{-2}$ (Dickey & Lockman 1990). The value of $\chi^2/\text{d.o.f} = 46.81/46$ indicated that this is a satisfactory model for 1FGL J0022.2-1850. The details of the fitting results are summarized in Table 2.

4.2. 1FGL J0038.0+1236

One X-ray point source (RA, DEC)=($9^{\circ}.472$, $12^{\circ}.639$) was found with *Suzaku* within the improved 2FGL error ellipse corresponding to 1FGL J0038.0+1236. The corresponding X-ray image made through the way described in Section 4.1 is shown in Figure 2. Moreover, one unknown point source is detected within the background region for spectral analysis. The radio source, NVSS J00209-185332 (shown by magenta cross; see section 6), is coincident with the X-ray position and we propose this to be the most likely counterpart of 1FGL J0038.0+1236.

Figure 2 shows the X-ray spectrum of the point source detected by *Suzaku* near the center of the 2FGL error ellipse of 1FGL J0038.0+1236 (0.6 – 7.5 keV). The source region was selected with radii $3'$, because the target source is too bright not to cover entire region of the emission from target source with radii $2'$. When we selected the background region, the region from X-ray contaminant source was excluded with radii $2'$ in order to not subtract too much as background. The spectrum could be well fitted by a single power-law continuum with $\Gamma = 2.76 \pm 0.17$, moderated by the Galactic absorption only. The Galactic hydrogen column density was fixed as $N_{\text{H}} = 5.38 \times 10^{20} \text{ cm}^{-2}$ (Dickey & Lockman 1990). The value of $\chi^2/\text{d.o.f} = 85.54/70$ indicates that this is a satisfactory model for 1FGL J0038.0+1236. The details of the fitting results are summarized in Table 3.

4.3. 1FGL J0157.0-5259

We succeeded in detecting a bright X-ray point source with *Suzaku* within the 2FGL error ellipse corresponding to 1FGL J0157.0-5259. Figure 3 shows the corresponding X-ray image (see Section 4.1). The X-ray source is located at (RA, DEC)=(29°.253, -53°.035), as shown in Figure 3. The position of the radio source, SUMSS J015657-530157, is shown by a magenta cross (see section 5). In this observation, we did not find any other contamination source like in the above two observations.

The X-ray spectrum (XIS + HXD) of the *Suzaku* source, which we propose to be the most likely counterpart of 1FGL J0157.0-5259, is shown in Figure 6 within the energy range 0.6 – 40.0 keV (XIS 0.4–10.0 keV, HXD 15.0–40.0 keV). In this spectral analysis, we set the extraction region to be a radius of 4' to encircle this bright source. On the other hand, we set the background region with the more larger radius, and the location of the center of background region displaced from the center of target source not to be over the region covering by CCD. The spectrum could be well fitted by a single power-law continuum with $\Gamma = 1.85 \pm 0.01$, moderated by the Galactic absorption only. The Galactic hydrogen column density was fixed as $N_{\text{H}} = 2.70 \times 10^{20} \text{ cm}^{-2}$ (Dickey & Lockman 1990). The value of $\chi^2/\text{d.o.f} = 3184.74/2757$ indicates that this is a satisfactory model for 1FGL J0157.0-5259. The details of the fitting results are summarized in Table 4.

5. Discussion

In the uniform analysis of archival *Swift* data, we found several objects which seemed to display anomalous SEDs that are not typical of AGNs or PSRs. Then we performed *Suzaku* X-ray follow-up observations of three such sources to more accurately determine the SEDs of each object (Figures 7, 8, and 9). Different fluxes between *Swift*/XRT and *Suzaku* /XIS seen in these SEDs indicate that these objects should have temporal variability that was not seen within the individual shorter *Suzaku* exposures. Moreover, thanks to the good sensitivity and long exposure of the *Suzaku* data, we have additional hints to reveal the nature of each source as discussed below.

An X-ray source found within the updated 2FGL error ellipse of 1FGL J0022.2-1850 is positionally consistent with the radio source NVSS J00209-185332 found in the NVSS catalog (Condon et al. 1998) (See Table 2). Moreover, infrared counterpart source WISE J002209.25-185334.7 located at (RA, DEC)=(5°.5385563, -18°.8929772) was found in the Wide Field Infrared Survey Explorer (WISE) All-Sky Release (Wright et al. 2010). The SED of 1FGL J0022.2-1850/WISE J002209.25-185334.7/NVSS J00209-185332, including our *Suzaku*/XIS data and derived XRT and UVOT fluxes from *Swift*, are shown in Figure 7. From the relatively high radio flux and flat X-ray spectrum obtained with *Swift*/XRT, this object is likely to be a low-frequency peaked BL Lac (LBL).

However, during our *Suzaku* observation, the X-ray spectrum was observed to be substantially steeper, more typical of a high-frequency peaked BL Lac (HBL). Moreover, the flat GeV gamma-ray spectrum is typical of HBLs like Mrk 421 and Mrk 501, rather than a LBL. Considering the Cherenkov Telescope Array (CTA) which is an initiative to build a next generation observatory for very-high energy gamma-rays will have an improved sensitivity by an order of magnitude with respect to current instruments ($\sim 10^{-14}$ erg/cm²/s above a few TeV), the upward shape of the *Fermi*-LAT spectrum suggests the source could be detected also in TeV energy in the near future.

In the case of 1FGL J0038.0+1236, the location of a X-ray counterpart discovered in our *Suzaku* observations is consistent with NVSS J003750+123818 described in Table 2, and each optical counterpart SDSS J003750.88+123819.9 (classified as GALAXY) located at (RA, DEC)=(9°.462, 12°.638875) and infrared counterpart WISE J003750.87+123819.9 located at (RA, DEC)=(9°.4619958, 12°.6388878), were also found in the Sloan Digital Sky Survey (SDSS) catalog (Ahn et al. 2012) and WISE catalog respectively. The constructed radio to X-ray SED together with the *Swift* XRT/UVOT and the LAT spectrum is shown in Figure 8. Since the X-ray spectrum appears very steep, this source seems to be associated with a HBL, while the steep gamma-ray spectrum observed with *Fermi*-LAT favors a FSRQ origin of this source. While optical and ultraviolet fluxes are extremely bright, this could be due to a contribution of soft photons from the host galaxy as seen in some blazar spectra (see e.g., the SED of Mrk 501; Kataoka et al. (1999)). These results show that this source is difficult to be explained by conventional leptonic models of blazars (i.e., SSC or external Compton models).

In the case of 1FGL J0157.0-5259, our *Suzaku*/XIS observations revealed the presence of a quite bright X-ray counterpart in the LAT error circle, and since the hard X-ray fluxes of this source are very high, we could also obtain data from *Suzaku*/HXD. At the position of this *Suzaku* X-ray source, the radio counterpart SUMSS J015657-530157 was found in the SUMSS catalog (Mauch et al. 2003)(Table 2). The broad-band SED of 1FGL J0157.0-5259/SUMSS J015657-530157 with our *Suzaku*/XIS, HXD and derived *Swift*/XRT, UVOT data is presented in Figure 9. Since the X-ray fluxes are connected by a straight line with the radio fluxes, these fluxes are seemed to be explained by synchrotron radiation. The peak frequency of the synchrotron spectrum is very high (>10 keV) suggesting that the source could be one a rare type of "extreme" blazar like Mrk 501 in the historical high state (Ghisellini 2004). If this source is an "extreme" blazar, observations at TeV energies or more deep observations with *Fermi*-LAT may detect significant signal in the future.

Finally, we made the similar figure described in Takahashi et al. (2012) for the 1FGL 134 unID objects in which we performed follow-up observations with *Swift*/XRT (Figure 10). This figure presents a comparison of the AGNs (aqua), PSRs (green), and unassociated sources (red) which classified in the 2FGL catalog in the X-ray to gamma-ray flux ratios versus radio to gamma-

ray ratios plane. The three sources we observed with *Suzaku* in this paper are shown in black stars. Apparently, that these sources are situated in the typical AGN region of this diagnostic plane. It is noteworthy that, 1FGL J0157.0-5259 is at the right edge of this typical AGN region, and this means the X-ray and gamma-ray flux ratios of this source is quite high, such that ~ 2 , which is consistent with our speculation that the source is an extreme HBL-type blazar.

6. Summary

In this paper we reported on the results of X-ray follow-up observations of three unID gamma-ray sources detected by *Fermi*-LAT instrument which indicate anomalous SEDs. We have successfully detected X-ray counterparts of 1FGL J0022.2-1850, 1FGL J0038.0+1236 and 1FGL J0157.0-5259 using *Suzaku*. The characteristics of each object are summarized below. We also note that these objects display temporal variability in X-rays, as indicated by the different X-ray fluxes measured by *Suzaku*/XIS and *Swift*/XRT (see, Figure 7, 8, 9). The X-ray spectrum of the discovered *Suzaku* counterpart of 1FGL J0022.2-1850 is well fitted by single power-law model with $\Gamma = 2.43 \pm 0.03$. The spectral shape obtained with *Suzaku* (in X-ray) and *Fermi*-LAT (in gamma ray) suggest the source is typical of a HBL-type blazar, but previous *Swift* observations rather show it was similar to the LBL-type blazar. The source is potentially a TeV emitter that could be detected in the near future. In the case of 1FGL J0038.0+1236, the X-ray spectrum is well fitted by single power-law model with a photon index, $\Gamma = 2.76 \pm 0.17$. At first glance, this source also seems to be classified as a HBL because the X-ray spectrum seen in Figure 8 appear very steep. However, its steep gamma-ray spectrum observed with *Fermi*-LAT favors a FSRQ origin for this source. These results show that this source is difficult to be explained by standard emission models of blazars, i.e., SSC or external Compton models. In the case of 1FGL J0157.0-5259, the *Suzaku* X-ray spectrum obtained from XIS and HXD are well fitted by single power-law model with a photon index, $\Gamma = 1.85 \pm 6.66 \times 10^{-3}$. From the multiwavelength analysis shown in Figure 9, the peak frequency of synchrotron spectrum is very high (~ 10 keV) suggesting that source could be one of "extreme" blazar like Mrk 501 in the historical high state.

We would like to thank C. C. Cheung for useful comments that helped to improve the organization of the manuscript.

REFERENCES

Abdo, A. A., Ackermann, M., Ajello, M., et al. 2009, ApJ, 701, 123

- Abdo, A. A., Ackermann, M., Ajello, M., et al. 2010a, *ApJS*, 187, 460
- Abdo, A. A., Ackermann, M., Ajello, M., et al. 2010b, *ApJS*, 188, 405
- Abdo, A. A., Ackermann, M., Ajello, M., et al. 2010c, *ApJ*, 709, 152
- Abdo, A. A., Ackermann, M., Ajello, M., et al. 2010d, *ApJ*, 710, 92
- Abdo, A. A., Ackermann, M., Ajello, M., et al. 2010e, *ApJ*, 714, 927
- Abdo, A. A., Ackermann, M., Ajello, M., et al. 2010f, *ApJ*, 720, 912
- Ahn, C. P., Alexandroff, R., et al. 2012, *ApJS*, 203, 21
- Atwood, W. B., Abdo, A. A., Ackermann, M., et al. 2009, *ApJ*, 697, 1071
- Burrows, D. N., Hill, J. E., Nousek, J. A., 2005, *Space Sci. Rev.*, 120, 165
- Cardelli, J. A., et al. 1998, *ApJ*, 345, 245
- Cheung, C. C., Donato, D., et al. 2012, *ApJ*, 756, 33
- Cougnard, I., Guillemot, L., et al. 2011, *ApJ*, 732, 47
- Cohen, A. S., Lane, W. M., et al. 2007, *AJ*, 134, 1245
- Condon, J. J., Cotton, W. D., Greisen, E. W., et al. 1998, *AJ*, 115, 1693
- D’Abrusco, R., Massaro, F., Paggi, A., *ApJS*, 206, 12
- Day, C., et al., 1998, *The ASCA Data Reduction Guide*, Tech. Rep., (Greenbelt: NASA GSFC), v.2.0
- De Breuck, C., Tang, Y., et al. 2002, *A&A*, 394, 59
- Dickey, J. M., & Lockman, F. J., 1990, *ARA&A*, 28, 215
- Fossati, G., Maraschi, L., Celotti, A., Comastri, A., & Ghisellini, G. 1998, *MNRAS*, 299, 433
- Gehrels, N., et al. 2004, *ApJ*, 611, 1005
- Ghisellini, G. 2004, *New Astronomy Review*, 48, 375
- Gregory, P. C., Scott, W. K., Douglas, K., Condon, J. J., et al. 1996, *ApJS*, 103, 427
- Hartman, R. C., Bertsch, D. L., Bloom, S. D., et al. 1999, *ApJS*, 123, 79

- Ishisaki, Y., Maeda, Y., Fujimoto, R., et al. 2007, PASJ, 59, 113
- Kataoka, J., Mattox, J. R., Quinn, J., et al. 1999, ApJ, 514, 138
- Kataoka, J., Yatsu, Y., Kawai, N., et al. 2012, ApJ, 757, 176
- Keith, M. J., Johnston, S., et al. 2011, MNRAS, 414, 1292
- Kokubun, M., Makishima, K., Takahashi, T., et al. 2007, PASJ, 59, 53
- Kong, A. K. H., Huang, R. H. H., et al. 2012, ApJ, 747, 3
- Koyama, K., Tsunemi, H., Dotani, T., et al. 2007, PASJ, 59, 23
- Maeda, K., Kataoka, J., Nakamori, T., et al. 2011, ApJ, 729, 103
- Massaro, F., D’Abrusco, R., Paggi, A., et al. 2013, ApJS, 206, 13
- Mauch, T., et al. 2003, MNRAS, 342, 1117
- Mitsuda, K., Bautz, M., Inoue, H., et al. 2007, PASJ, 59, 1
- Murphy, T., Sadler, E. M., et al. 2010, MNRAS, 402, 2403
- Nolan, P., Abdo, A. A., Ackermann, M., et al. 2011, ApJS, 199, 31
- Ransom, S. M., Ray, P. S., et al. 2011, ApJ, 727, 16
- Romani, R. W., & Shaw, M. S. 2011, ApJ, 743, 26
- Romani, R. W. 2012, ApJ, 754, 25
- Roming, P. W. A., Kennedy, T. E., Mason, K. O., et al. 2005, Space Sci. Rev., 120, 95
- Serlemitsos, P. J., Soong, Y., Chan, K.-W., et al. 2007, PASJ, 59, 9
- Takahashi, T., Abe, K., Endo, M., et al. 2007, PASJ, 59, 35
- Takahashi, Y., Kataoka, J., Nakamori, T., et al. 2012, ApJ, 747, 64
- Tawa, N., Hayashida, K., Nagai, M., et al. 2008, PASJ, 60, 11
- Theureau, G., Parent, D., et al. 2011, A&A, 525, 94
- Voges, W., Aschenbach, B., et al. 1999, A&A, 349, 389
- White, R. L., Becker, R. H., Helfand, D. J., & Gregg, M. D. 1997, ApJ, 475, 479

Wright, A. E., Griffith, M. R., et al. 1994, ApJ, 422, 642

Wright, E. L., et al. 2010, AJ, 140, 1868

Table 1: *Suzaku* XIS observation logs.

Target Name	R.A. [deg]	Dec. [deg]	Exposure [ks]	Obs. Start (UT)
1FGL J0022.2-1850	5.5540	-18.9060	34.2	2012-May.30 12:57:00
1FGL J0038.0+1236	9.4627	12.6391	18.8	2012-Jun.29 23:56:00
1FGL J0157.0-5259	29.3640	-53.0280	12.1	2012-May.28 16:19:00

Table 2: Radio counterpart sources for each target.

Target Name	R.A. [deg]	Dec. [deg]	$F_{1.4\text{ GHz}}$ [mJy]	$F_{843\text{ MHz}}$ [mJy]
NVSS J00209-185332	5.5381667	-18.892444	22.1 ± 0.8	-
NVSS J003750+123818	9.461875	12.638556	75.1 ± 2.3	-
SUMSS J015657-530157	29.240833	-53.032778	-	43.4 ± 1.5

Table 3: Fitting parameters for each *Suzaku* target (the power-law model).

Target Name	N_{H} [cm^{-2}]	Γ	$\chi^2/\text{d.o.f}$	$P(\chi^2)$	$F_{0.6-7.5\text{ keV}}$ [$\text{erg cm}^{-2} \text{ s}^{-1}$]
1FGL J0022.2-1850	2.02×10^{20} (fixed)	2.43 ± 0.03	46.81/46	4.39×10^{-1}	2.12×10^{-12}
1FGL J0038.0+1236	5.38×10^{20} (fixed)	2.76 ± 0.17	85.54/70	9.98×10^{-2}	2.11×10^{-13}
1FGL J0157.0-5259	2.70×10^{20} (fixed)	$1.85 \pm 6.66 \times 10^{-3}$	3184.74/2757	1.95×10^{-8}	3.21×10^{-11}

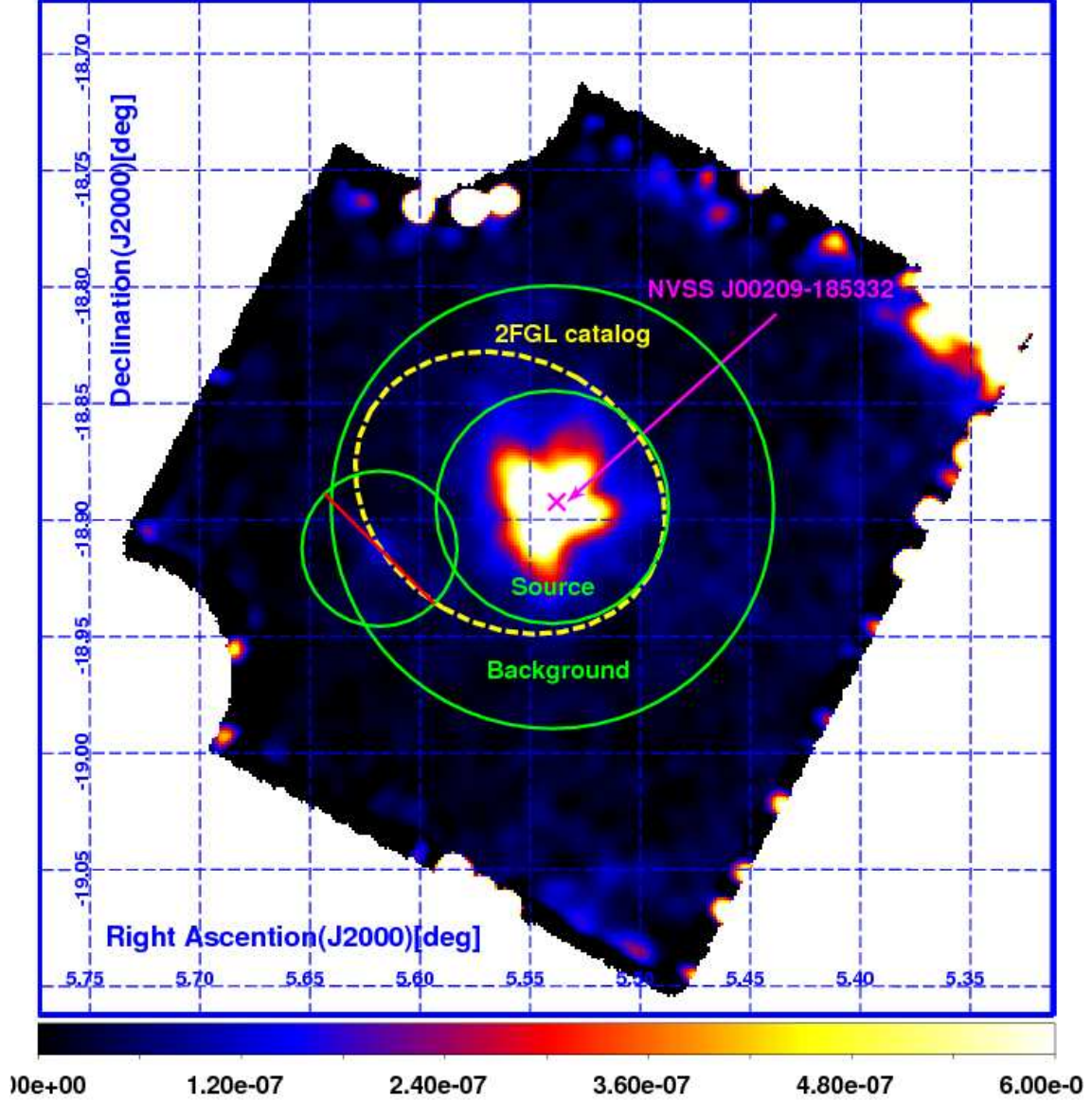


Fig. 1.— *Suzaku* X-ray image of 1FGL J0022.2-1850 (vignetting and exposure corrections applied). Data from XIS 0 and XIS 3 are summed in the 0.4 – 10 keV energy band. The magenta cross denote the position of radio counterpart source NVSS J00209-185332, the yellow dotted ellipse denotes the 95% position error of 2FGL J0022.2-1853, and the inner green ellipse denote the *Suzaku* source extraction region, the outer green ellipse without inner source region denote the *Suzaku* background extraction region.

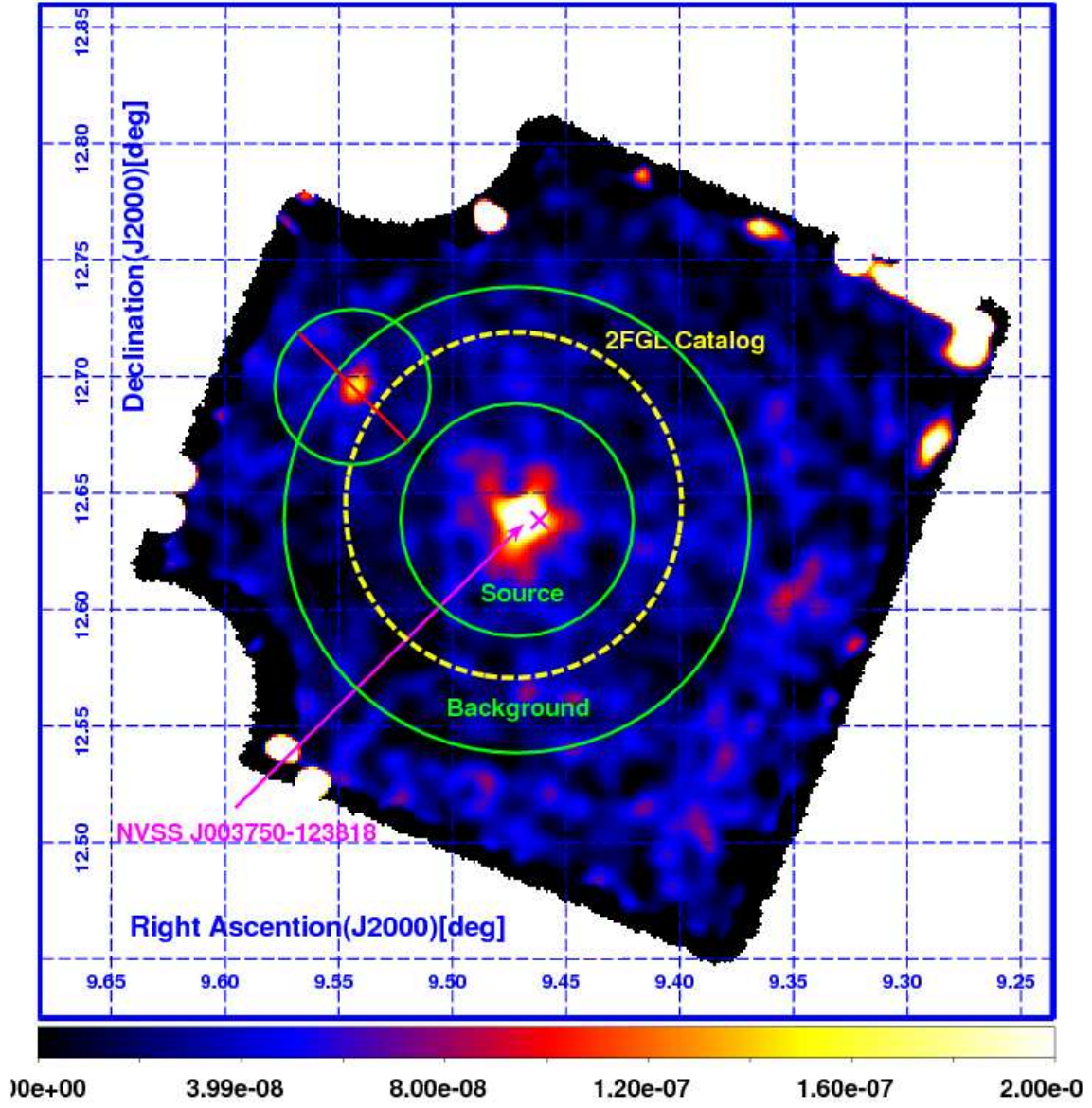


Fig. 2.— Same as Figure 1, but target source is 1FGL J0038.0+1236 and radio counterpart is NVSS J003750+123818.

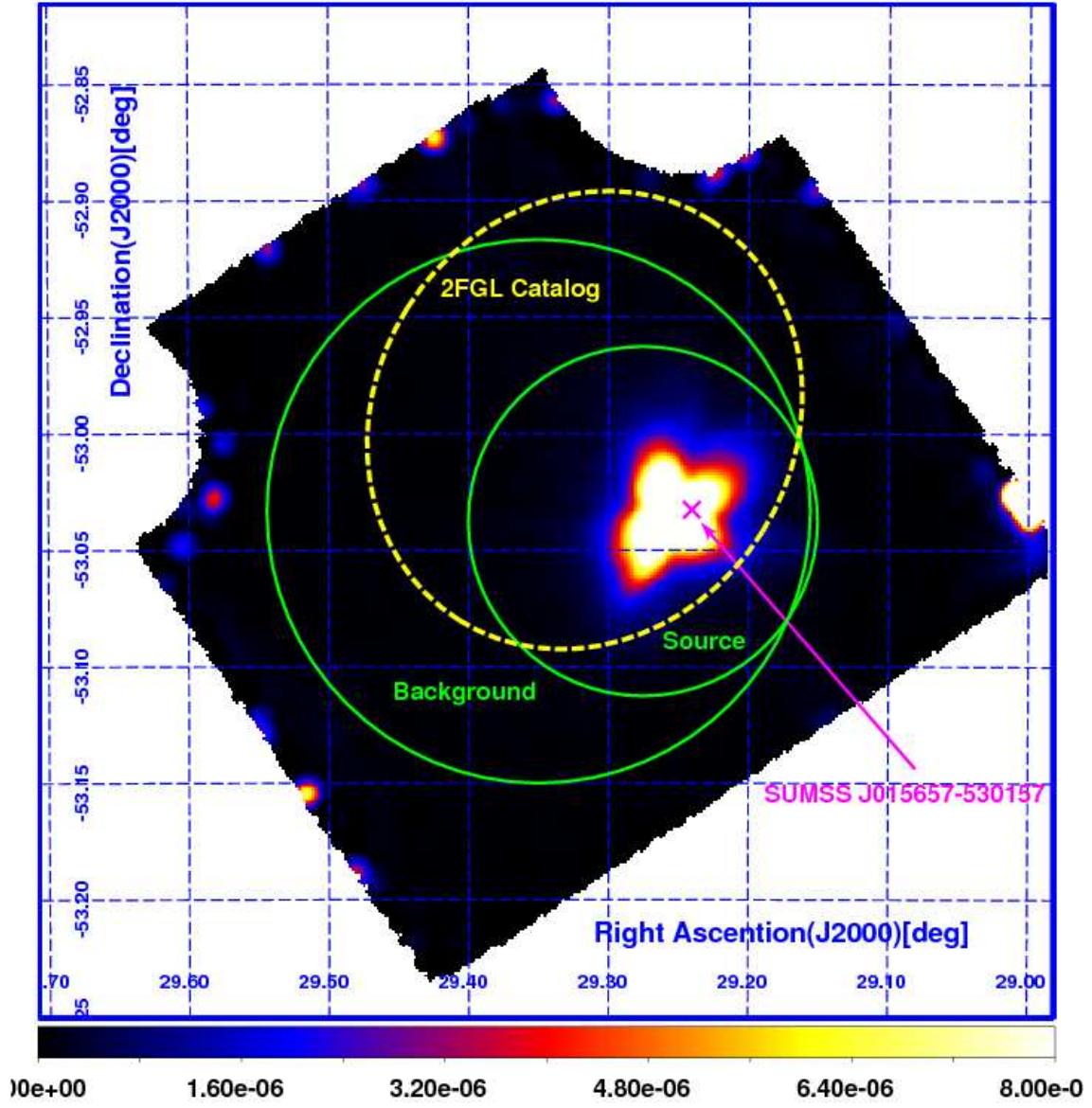


Fig. 3.— Same as Figure 1, but target source is 1FGL J0157.0-5259 and radio counterpart is SUMSS J015657-530157.

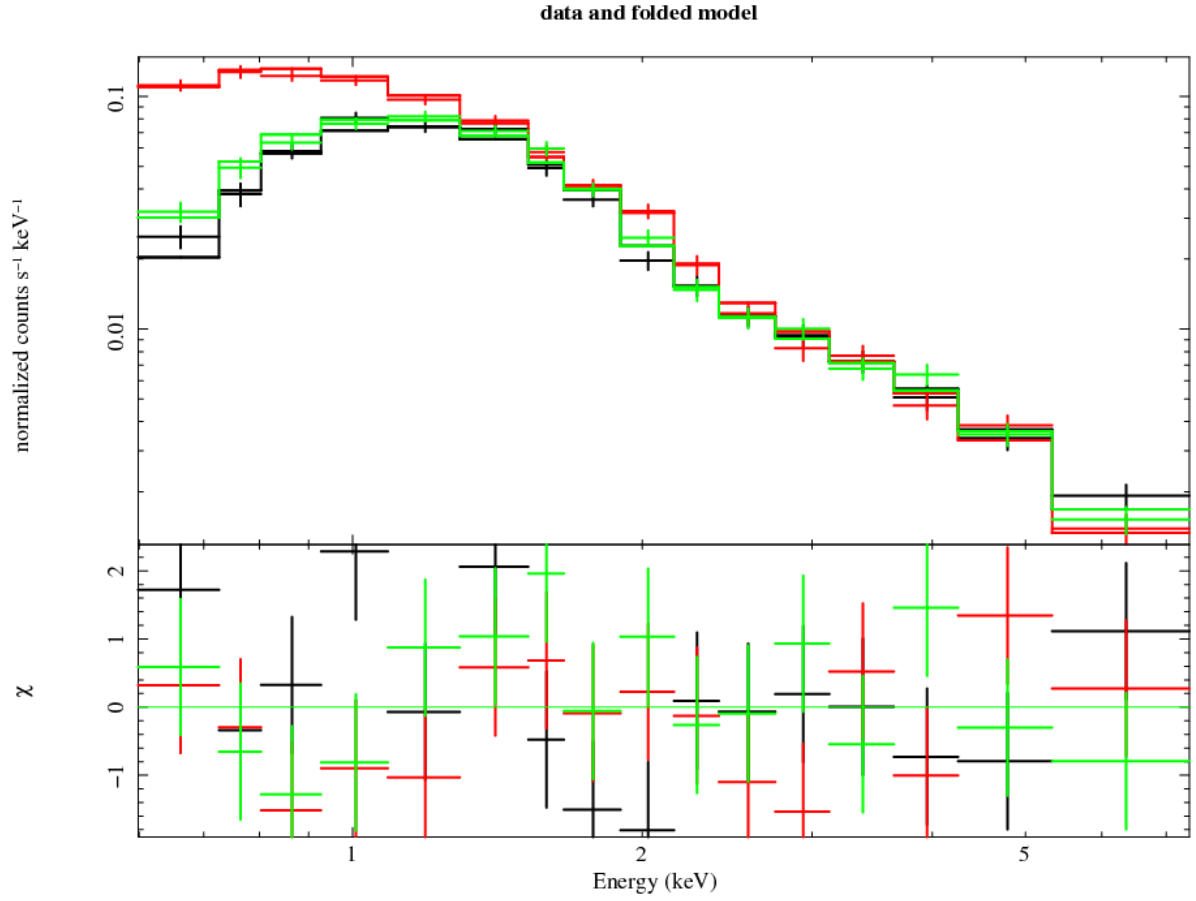


Fig. 4.— *Suzaku* XIS spectra of 1FGL J0022.2-1850 in the photon energy range 0.4 – 10 keV, fitted by the model `wabs + power-law`. Spectra of XIS0, XIS1, XIS3 are shown in black, red, and green, respectively.

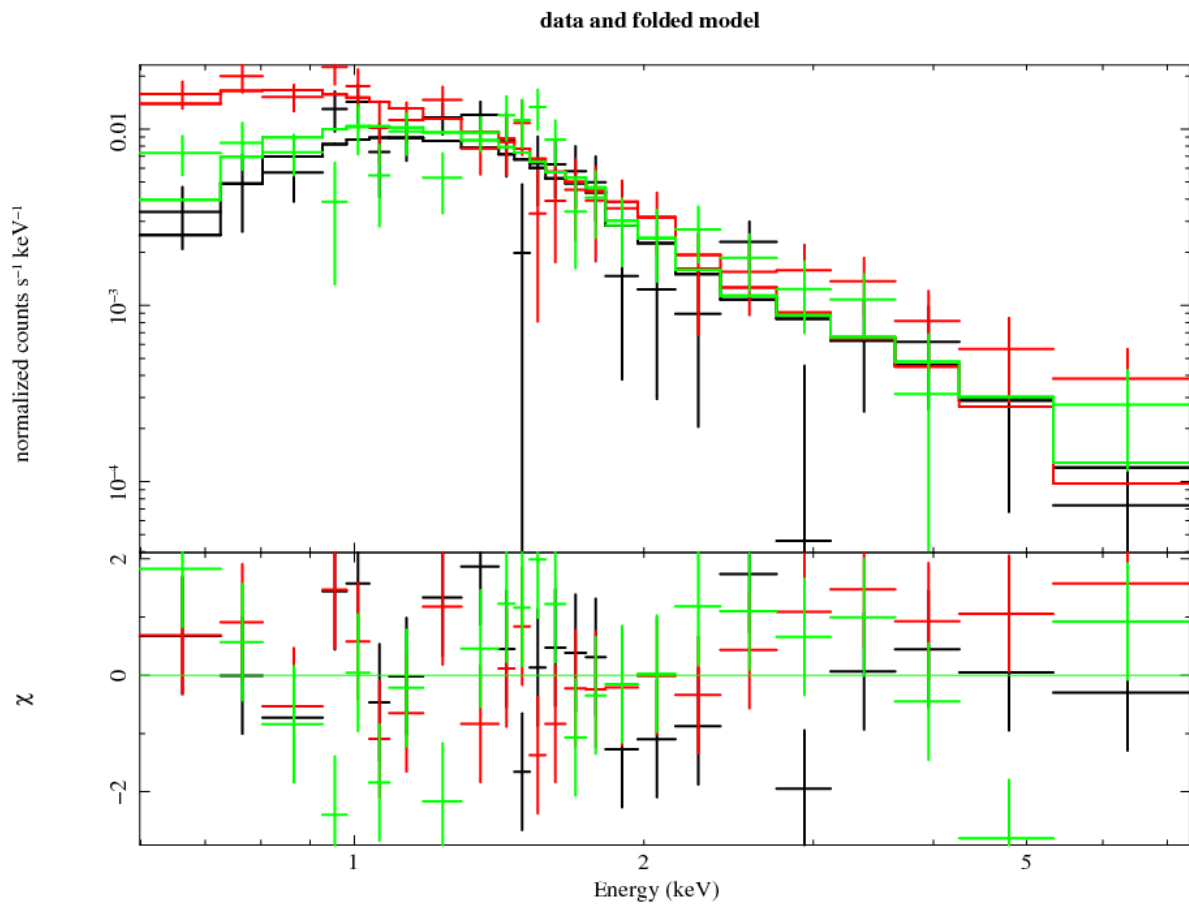


Fig. 5.— *Suzaku* XIS spectra of 1FGL J0038.0+1236 in the photon energy range 0.4 – 10 keV, fitted by the model `wabs + power-law`. Spectra of XIS0, XIS1, XIS3 are shown in black, red, and green, respectively.

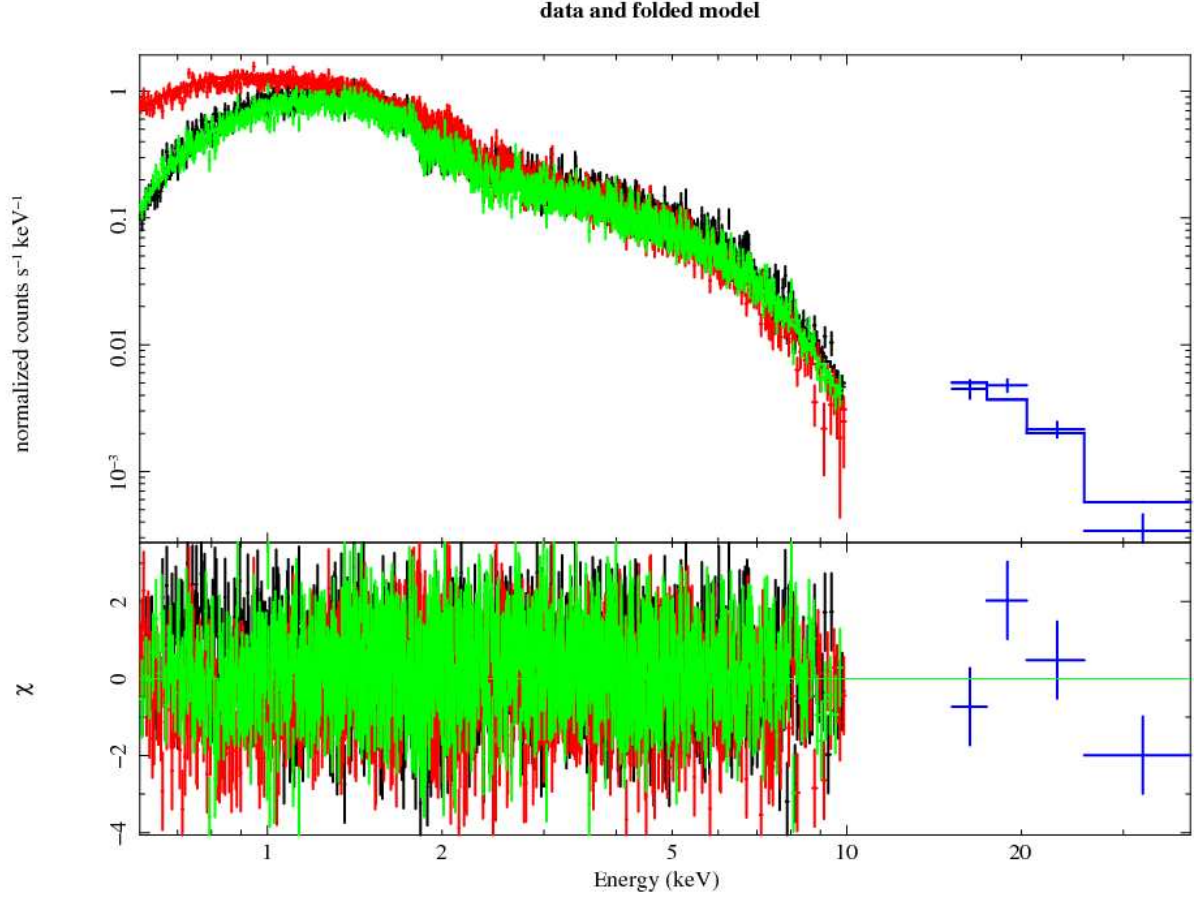


Fig. 6.— *Suzaku* XIS spectra of 1FGL J0157.0-5259 in the photon energy range 0.4 – 40 keV (XIS 0.4 – 10 keV, HXD 15 – 40 keV), fitted by the model `wabs + power-law`. Spectra of XIS0, XIS1, XIS3, HXD are shown in black, red, green, and blue respectively.

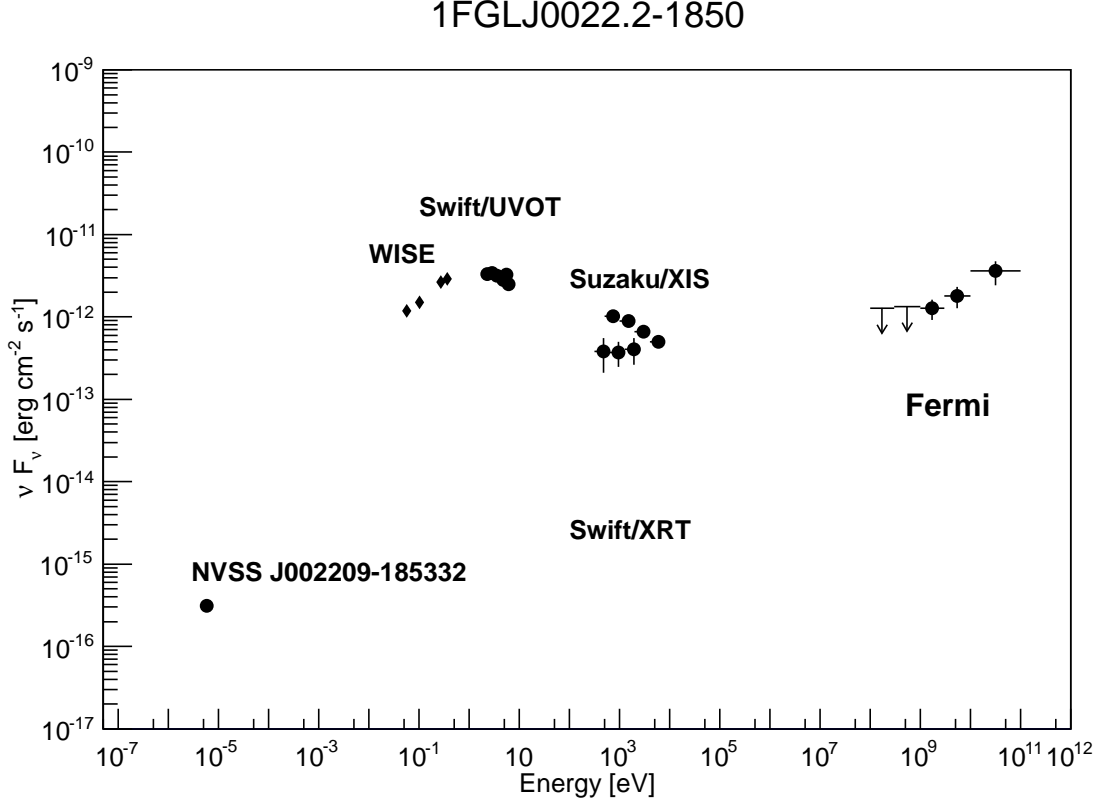


Fig. 7.— Broad-band SEDs of 1FGLJ0022.2-1850. The radio fluxes (1.4 GHz) for this source are taken from NVSS J002209-185332 as radio counterpart. The infrared fluxes ($3.4\mu\text{m}$, $4.6\mu\text{m}$, $12\mu\text{m}$ and $22\mu\text{m}$) are taken from the WISE catalog. The optical/UV fluxes were derived from the *Swift*/UVOT observations (this work). The X-ray are fluxes taken from the *Suzaku*/XIS and *Swift*/XRT observations (this work). Finally, the gamma-ray data points are taken from the 2FGL catalog (Nolan et al. 2012).

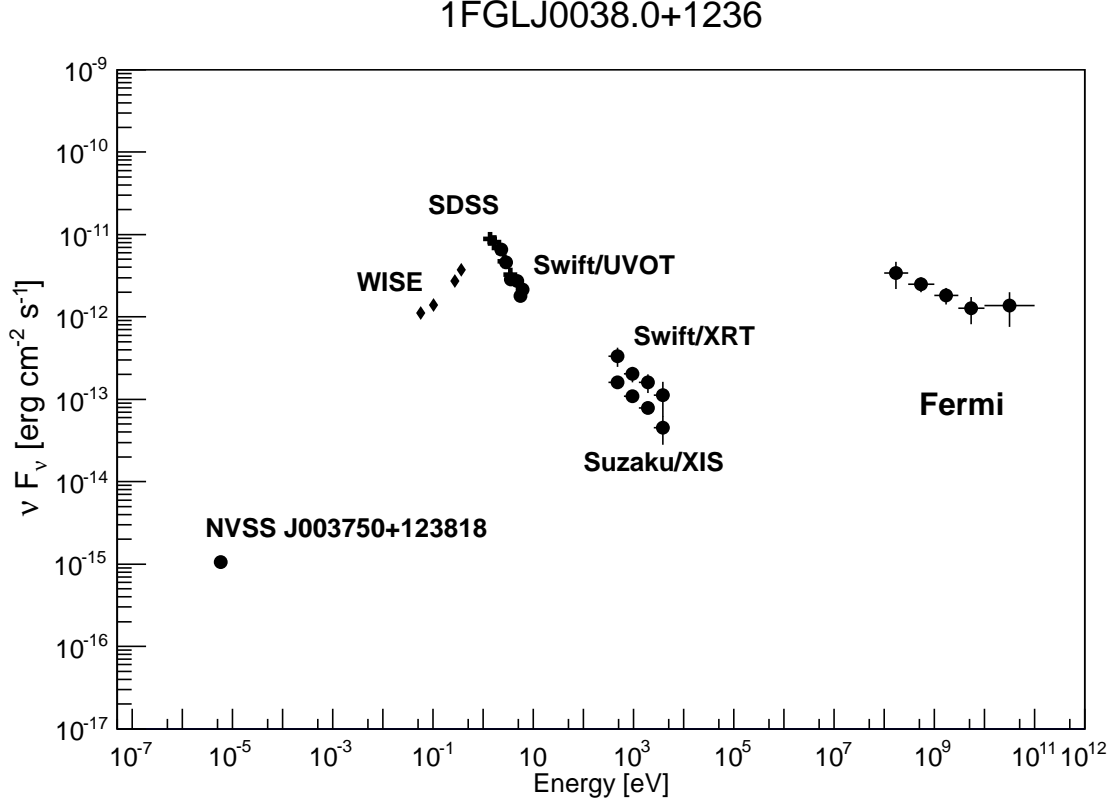


Fig. 8.— Broad-band SEDs of 1FGLJ0038.0+1236. The radio fluxes (1.4 GHz) for this source are taken from NVSS J003750*123818 as radio counterpart. The infrared fluxes ($3.4\mu\text{m}$, $4.6\mu\text{m}$, $12\mu\text{m}$ and $22\mu\text{m}$) are taken from the WISE catalog. The optical/UV fluxes were derived from the *Swift*/UVOT observations (this work) and the SDSS catalog. The X-ray fluxes are taken from the *Suzaku*/XIS and *Swift*/XRT observations (this work). Finally, the gamma-ray data points are taken from the 2FGL catalog (Nolan et al. 2012).

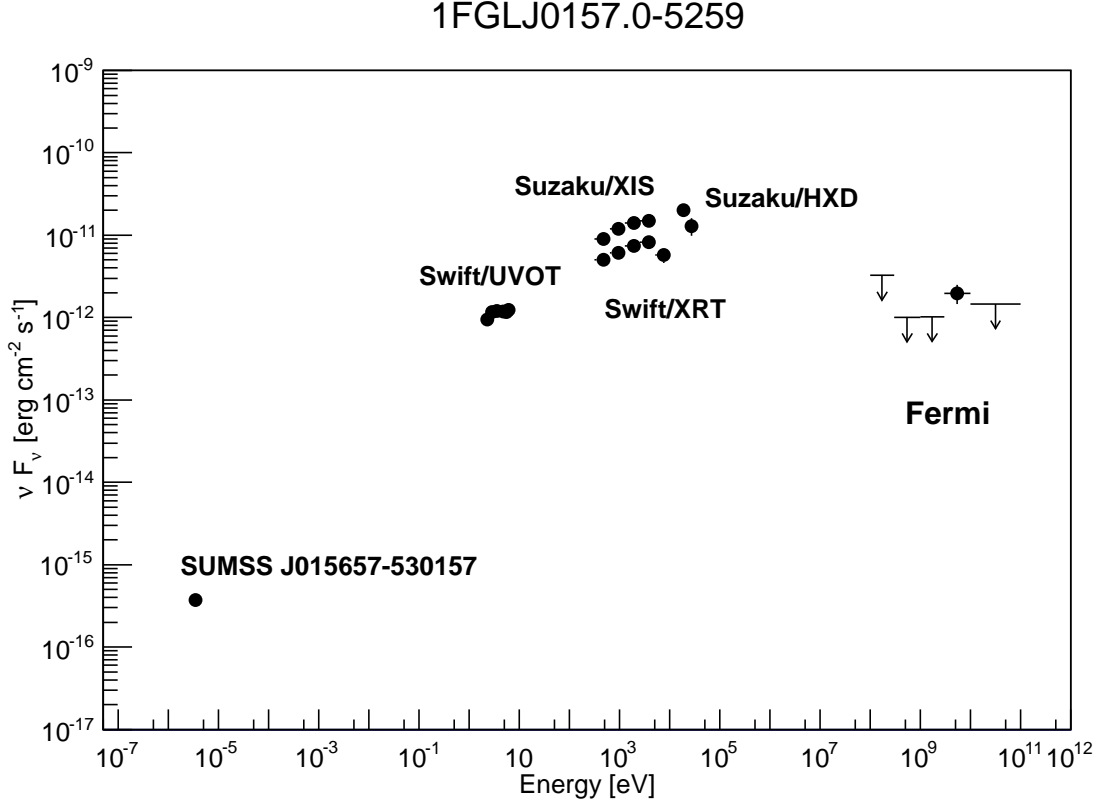


Fig. 9.— Broad-band SEDs of 1FGL J0157.0-5259. The radio fluxes (843 MHz) for this source are taken from SUMSS J015657-530157 as radio counterpart source. The optical/UV fluxes were derived from the *Swift*/UVOT observations. The X-ray fluxes taken from the *Suzaku*/XIS and *Swift*/XRT observations (this work). The hard X-ray fluxes are from the *Suzaku*/HXD observations (this work). Finally, the gamma-ray data points are taken from the 2FGL catalog (Nolan et al. 2012).

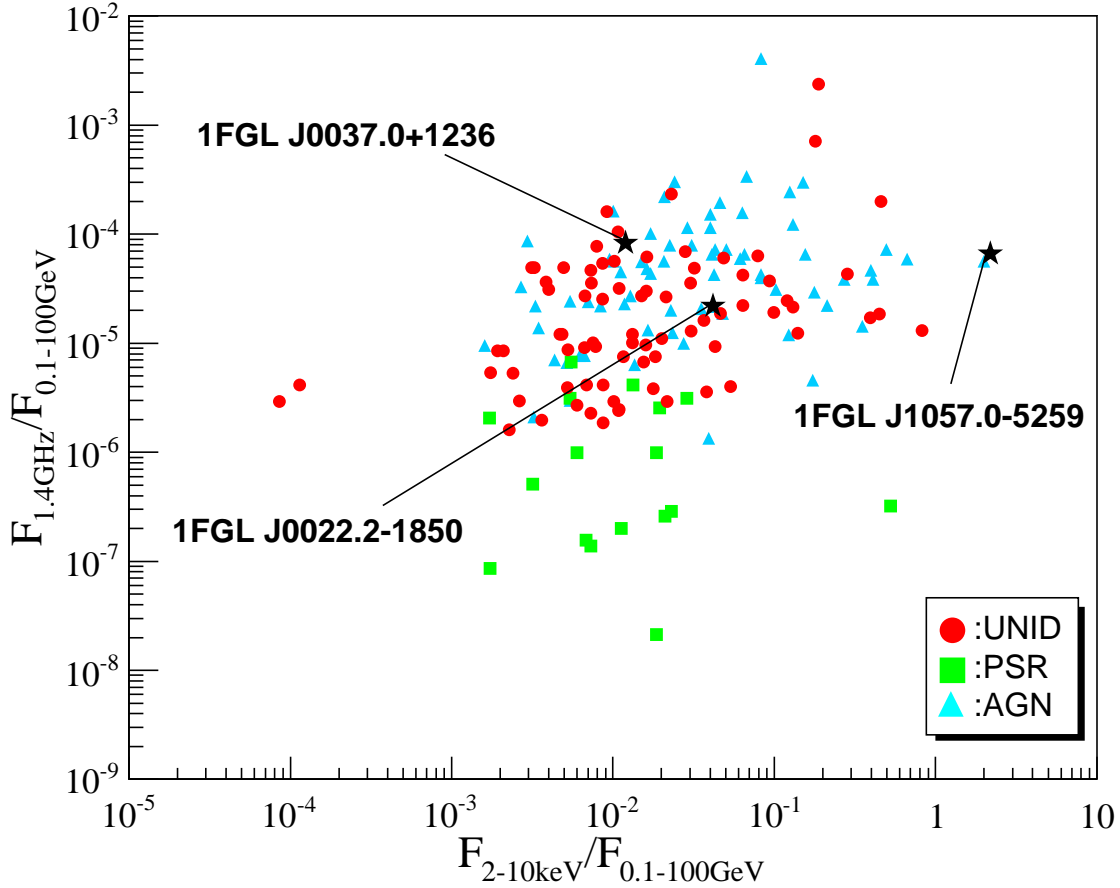
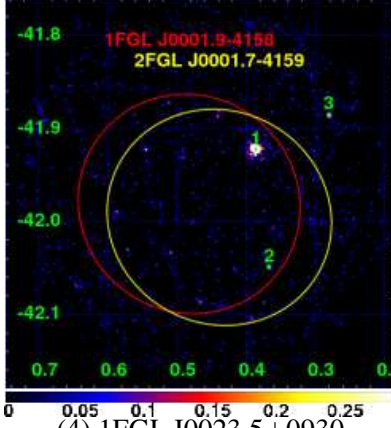


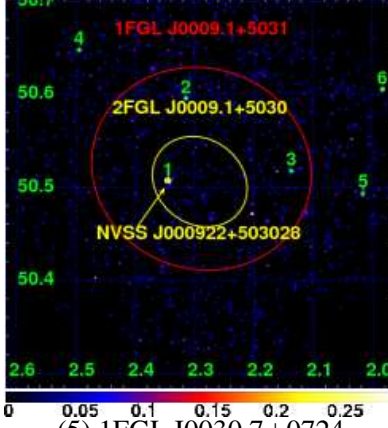
Fig. 10.— X-ray to gamma-ray flux ratios versus radio to gamma-ray ratios for 1FGL 134 unID objects performed follow-up observations with Swift/XRT. Red circles show the flux ratios of the *Fermi*-LAT sources which are still unID in 2FGL catalog. Aqua triangles indicate the data plots of AGN listed in 2FGL catalog. Green squares represent the data points of sources that are associated with PSRs listed in 2FGL catalog. Three black stars show the target sources in this paper, 1FGL J0022.2-1850, 1FGL J0038.0+1236, and 1FGL J0157.0-5259, respectively.

Swift Observed 1FGL unID sources

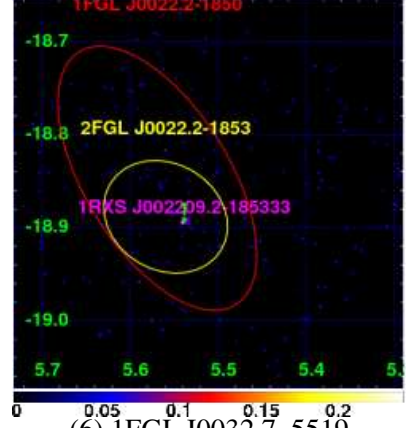
(1) 1FGL J0001.9–4158



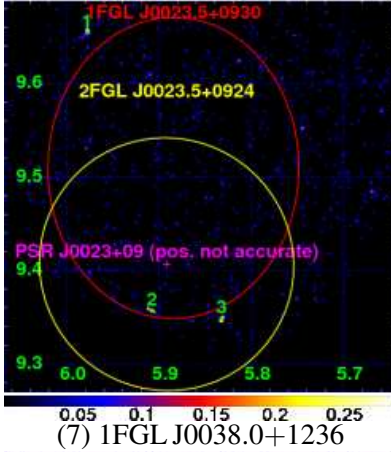
(2) 1FGL J0009.1+5031



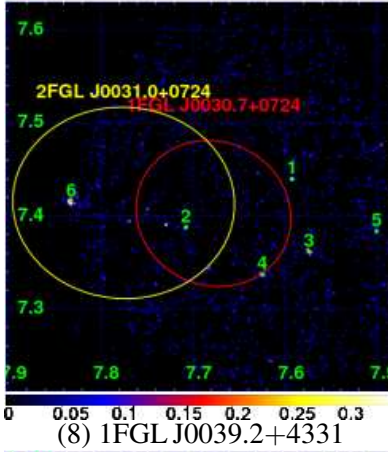
(3) 1FGL J0022.2–1850



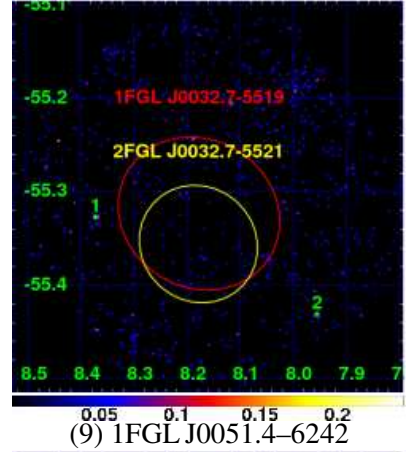
(4) 1FGL J0023.5+0930



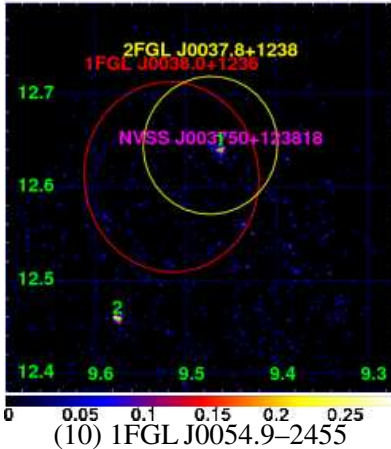
(5) 1FGL J0030.7+0724



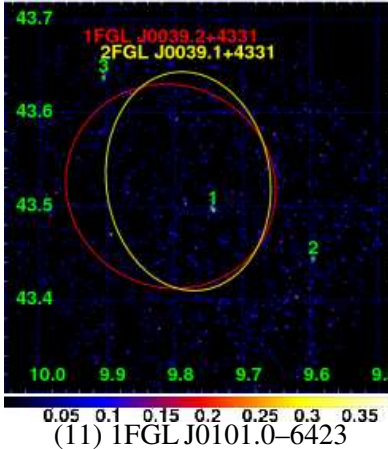
(6) 1FGL J0032.7–5519



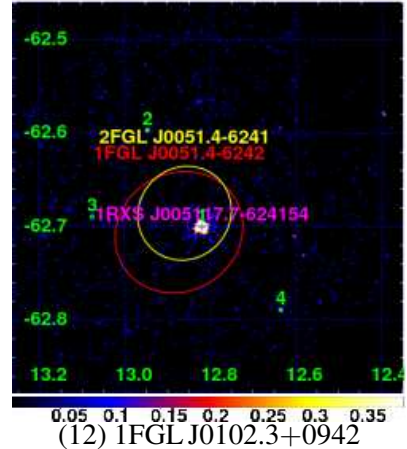
(7) 1FGL J0038.0+1236



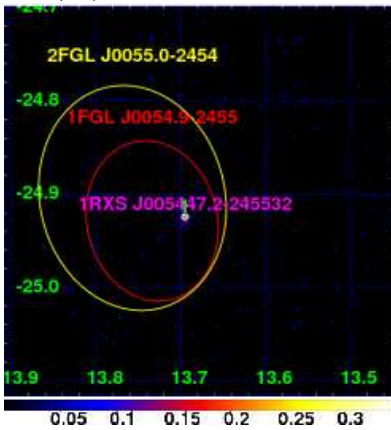
(8) 1FGL J0039.2+4331



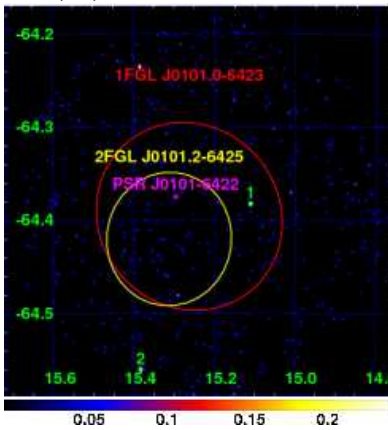
(9) 1FGL J0051.4–6242



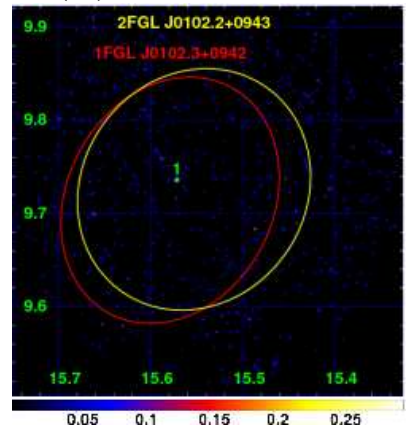
(10) 1FGL J0054.9–2455



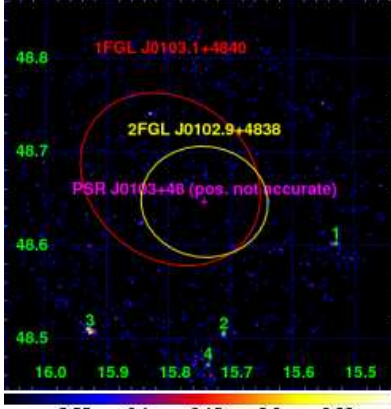
(11) 1FGL J0101.0–6423



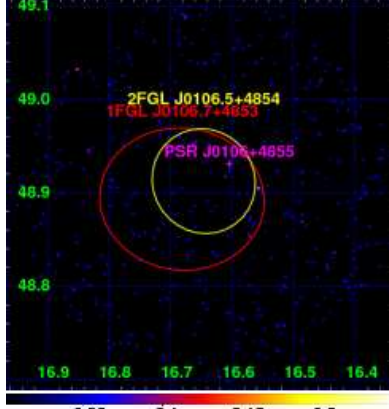
(12) 1FGL J0102.3+0942



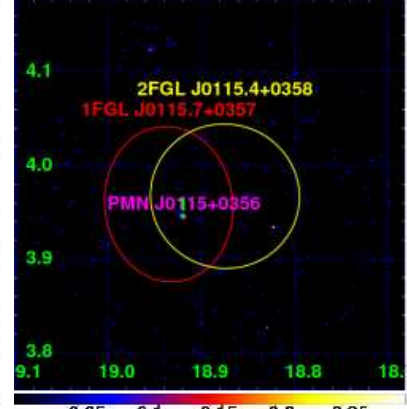
(13) 1FGL J0103.1+4840



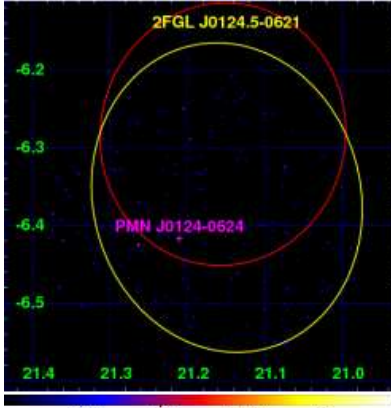
(14) 1FGL J0106.7+4853



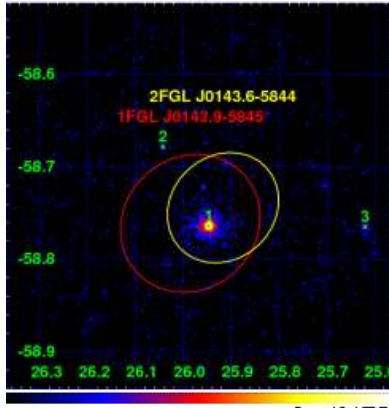
(15) 1FGL J0115.7+0357



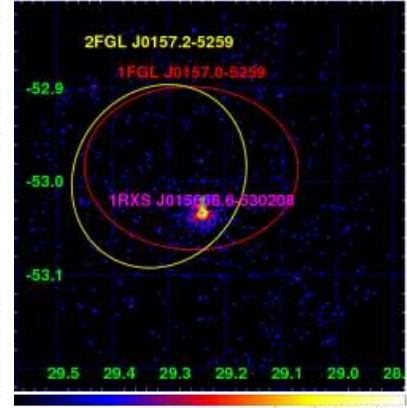
(16) 1FGL J0124.6–0616



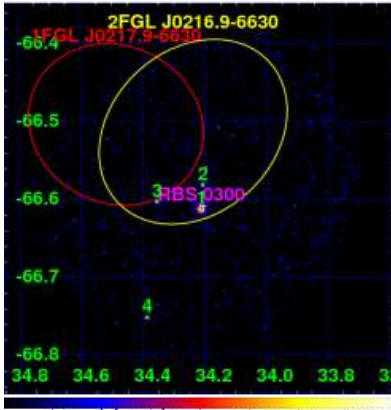
(17) 1FGL J0143.9–5845



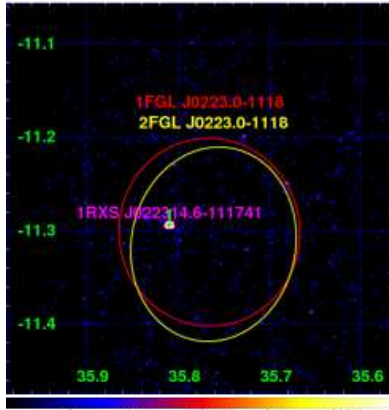
(18) 1FGL J0157.0–5259



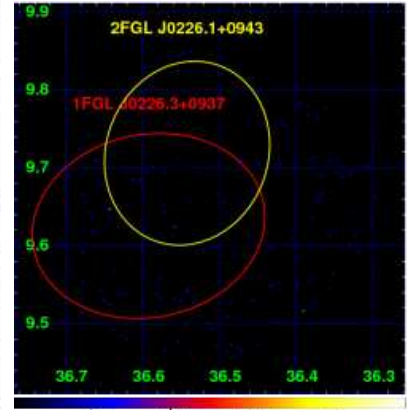
(19) 1FGL J0217.9–6630



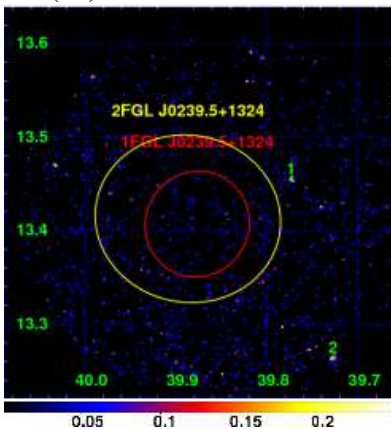
(20) 1FGL J0223.0–1118



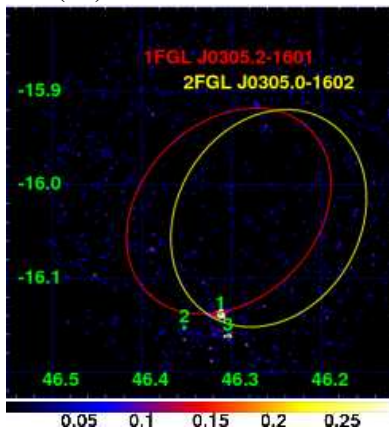
(21) 1FGL J0226.3+0937



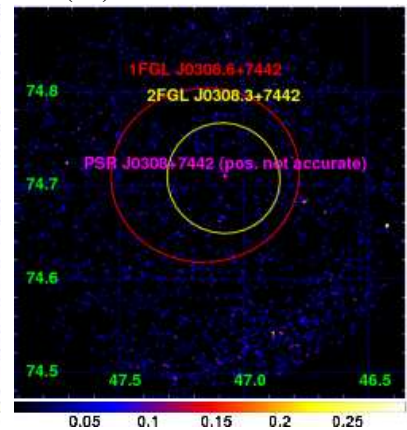
(22) 1FGL J0239.5+1324



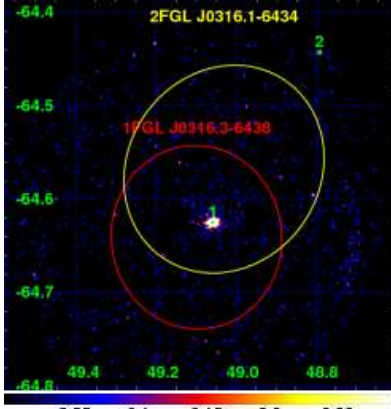
(23) 1FGL J0305.2–1601



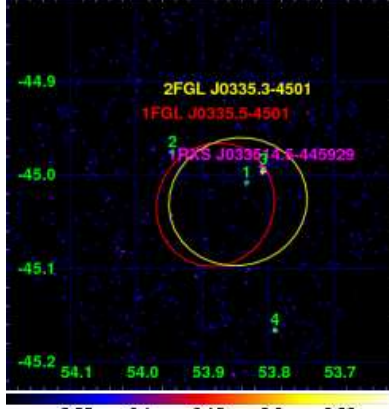
(24) 1FGL J0308.6+7442



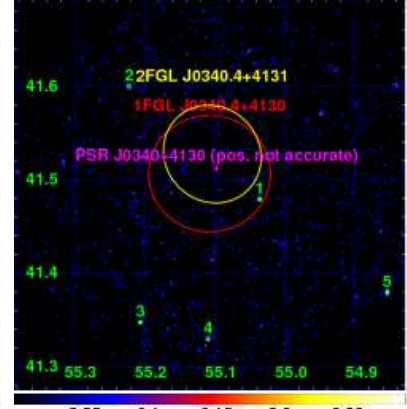
(25) 1FGL J0316.3–6438



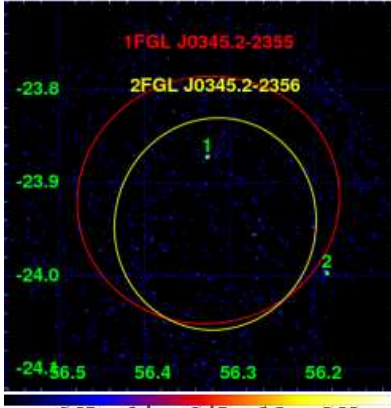
(26) 1FGL J0335.5–4501



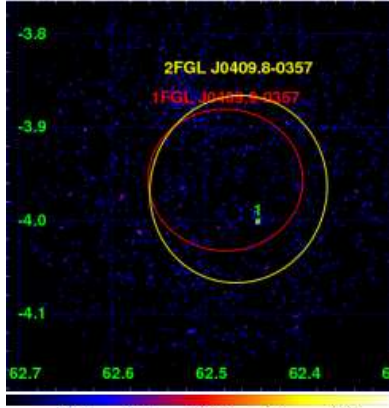
(27) 1FGL J0340.4+4130



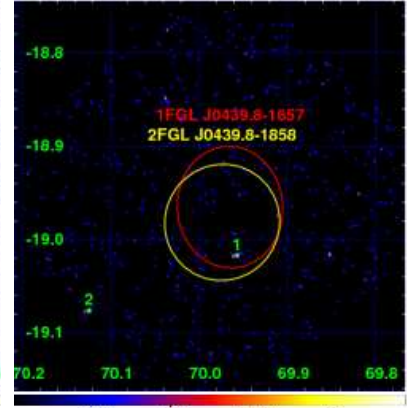
(28) 1FGL J0345.2–2355



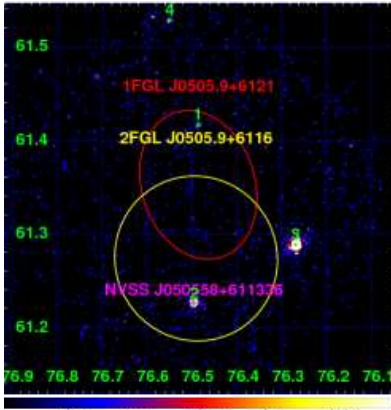
(29) 1FGL J0409.9–0357



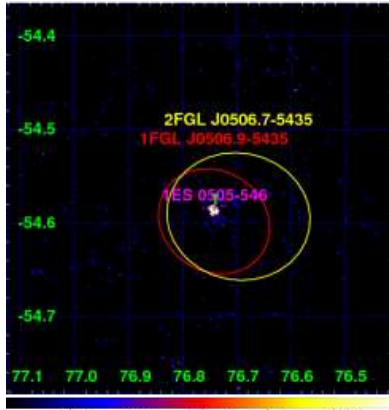
(30) 1FGL J0439.8–1857



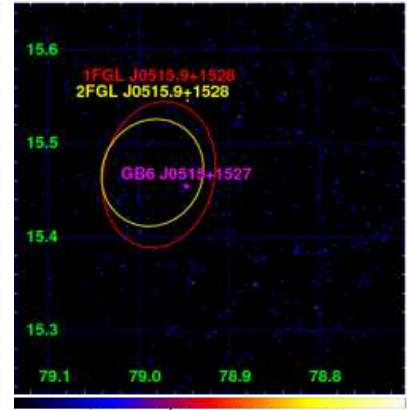
(31) 1FGL J0505.9+6121



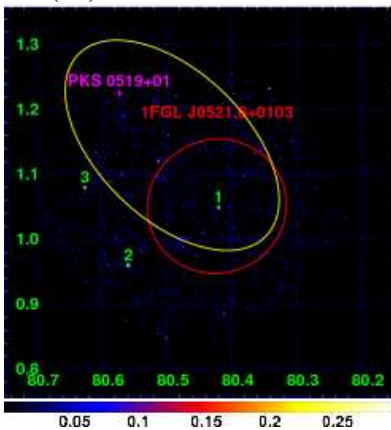
(32) 1FGL J0506.9–5435



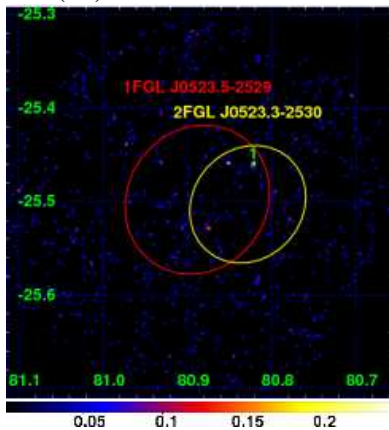
(33) 1FGL J0515.9+1528



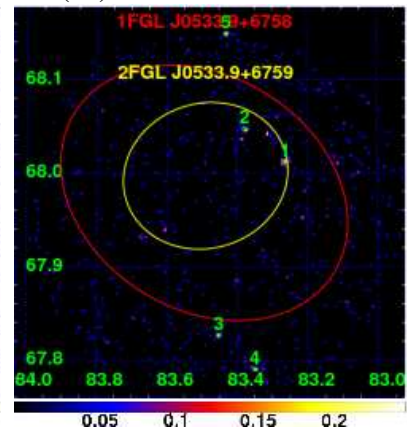
(34) 1FGL J0521.6+0103



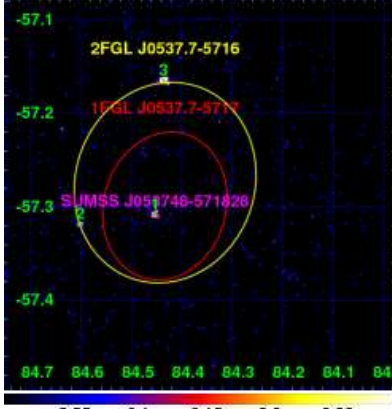
(35) 1FGL J0523.5–2529



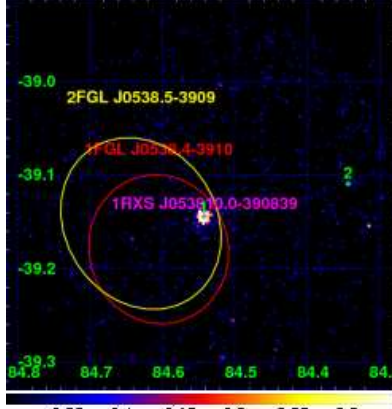
(36) 1FGL J0533.9+6758



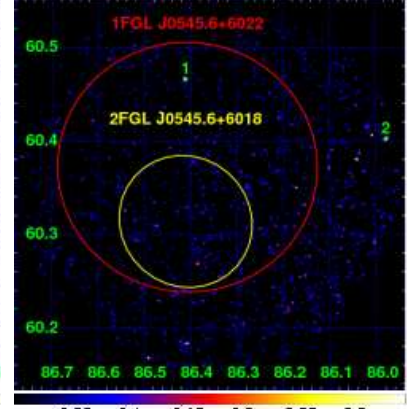
(37) 1FGL J0537.7–5717



(38) 1FGL J0538.4–3910



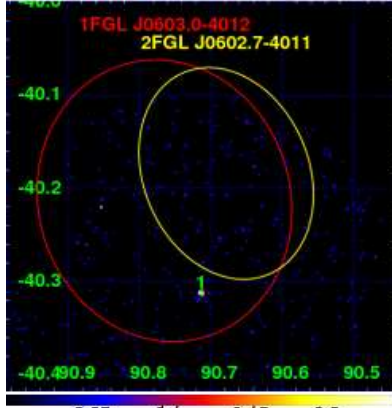
(39) 1FGL J0545.6+6022



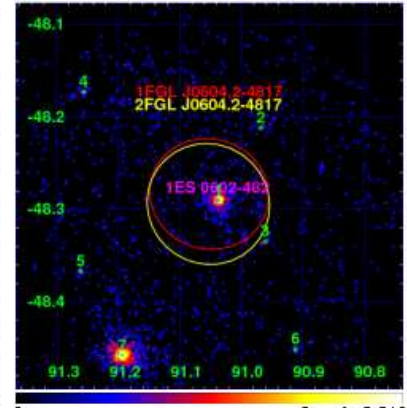
(40) 1FGL J0600.5–2006



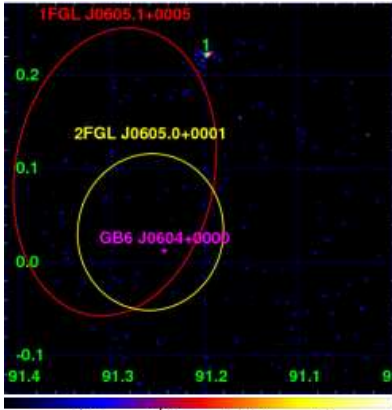
(41) 1FGL J0603.0–4012



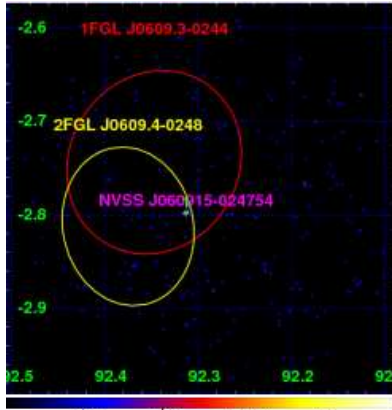
(42) 1FGL J0604.2–4817



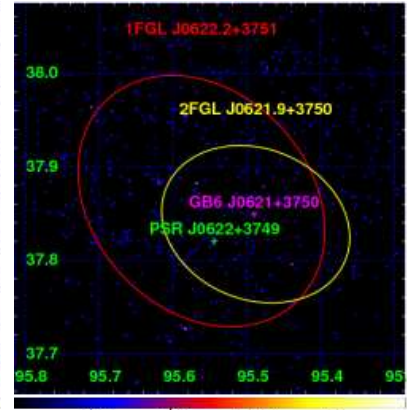
(43) 1FGL J0605.1+0005



(44) 1FGL J0609.3–0244



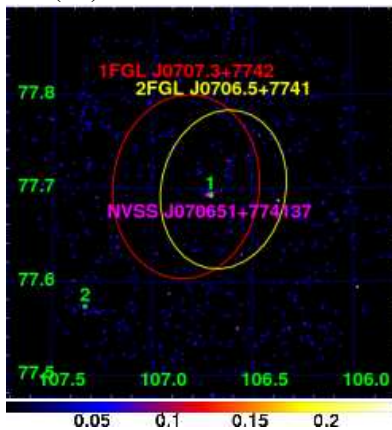
(45) 1FGL J0622.2+3751



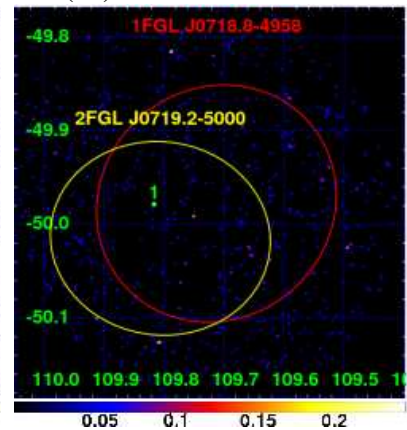
(46) 1FGL J0648.6–6052



(47) 1FGL J0707.3+7742



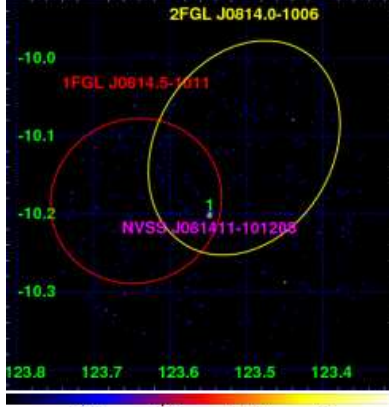
(48) 1FGL J0718.8–4958



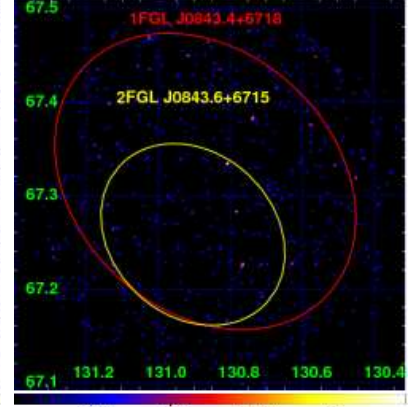
(49) 1FGL J0803.1–0339



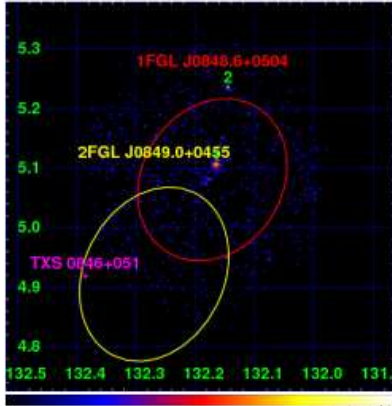
(50) 1FGL J0814.5–1011



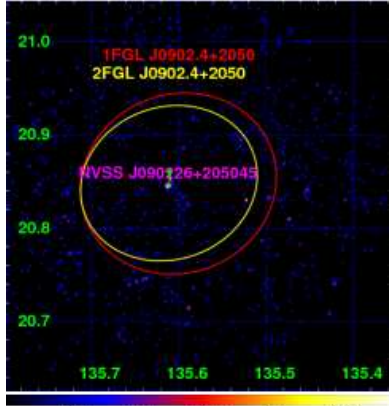
(51) 1FGL J0843.4+6718



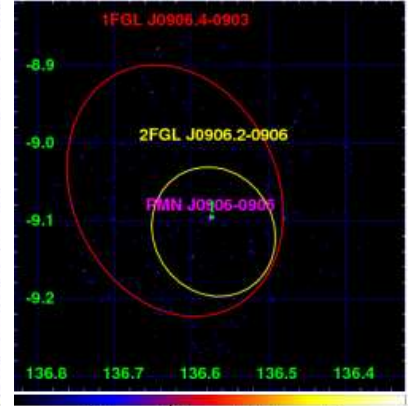
(52) 1FGL J0848.6+0504



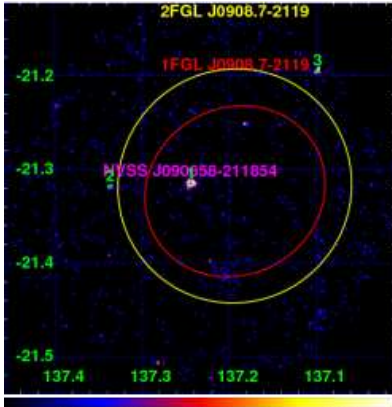
(53) 1FGL J0902.4+2050



(54) 1FGL J0906.4–0903



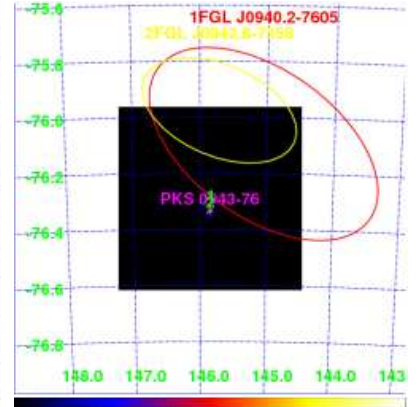
(55) 1FGL J0908.7–2119



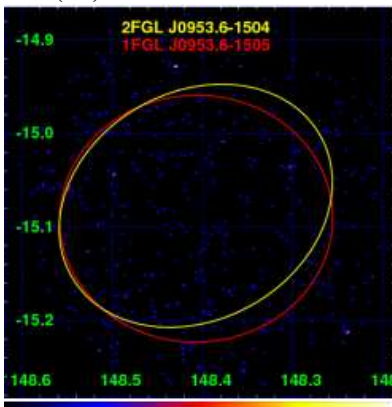
(56) 1FGL J0922.0+2337



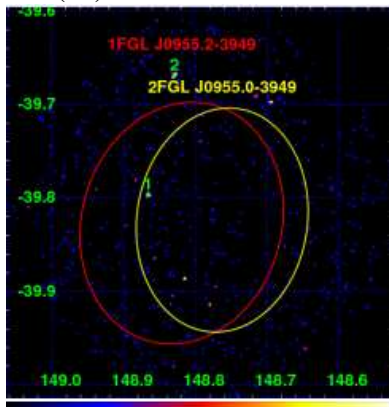
(57) 1FGL J0940.2–7605



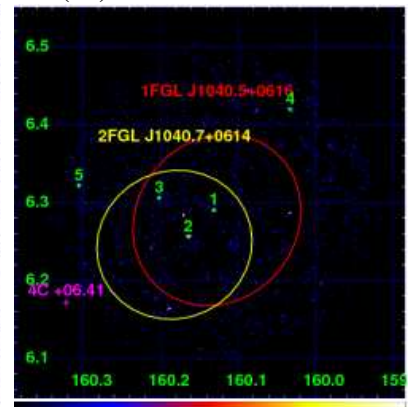
(58) 1FGL J0953.6–1505



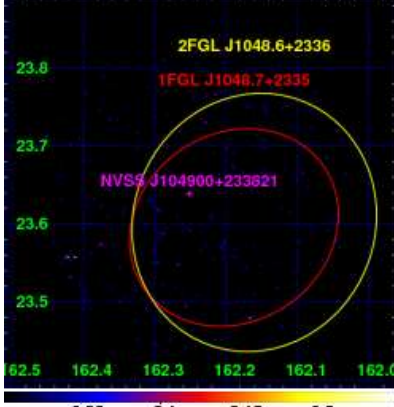
(59) 1FGL J0955.2–3949



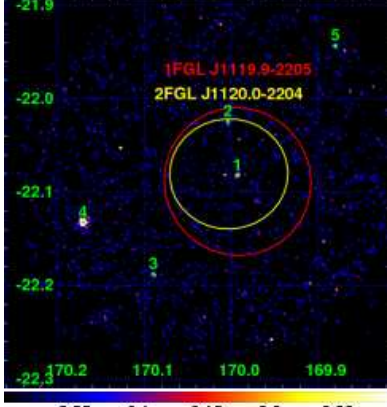
(60) 1FGL J1040.5+0616



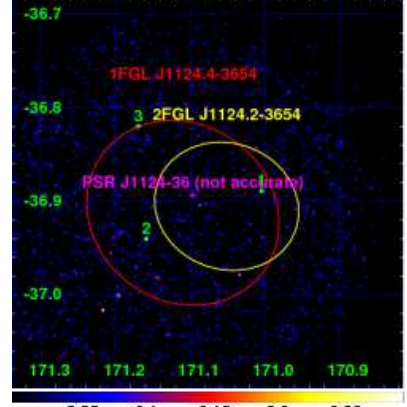
(61) 1FGL J1048.7+2335



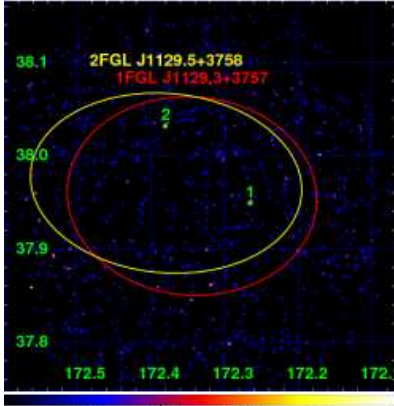
(62) 1FGL J1119.9–2205



(63) 1FGL J1124.4–3654



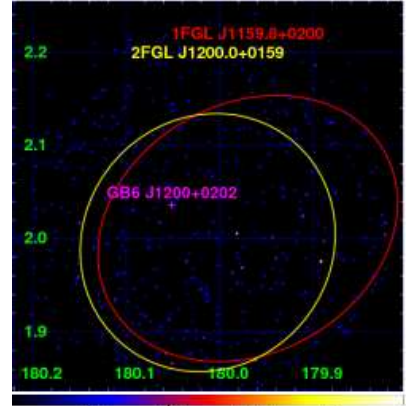
(64) 1FGL J1129.3+3757



(65) 1FGL J1141.8–1403



(66) 1FGL J1159.8+0200



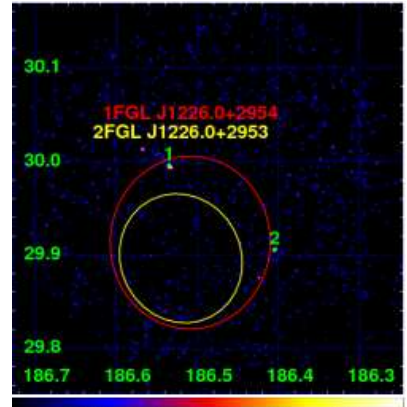
(67) 1FGL J1218.4–0128



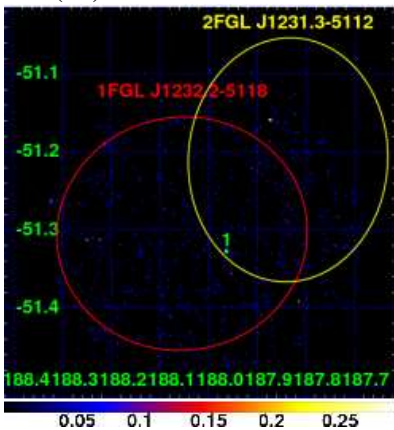
(68) 1FGL J1221.4–0635



(69) 1FGL J1226.0+2954



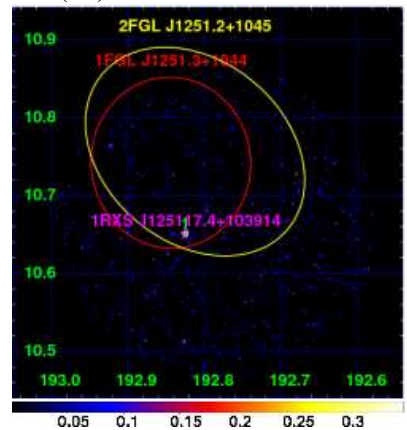
(70) 1FGL J1232.2–5118



(71) 1FGL J1249.3–2812



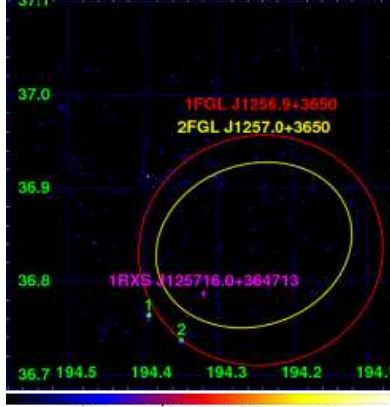
(72) 1FGL J1251.3+1044



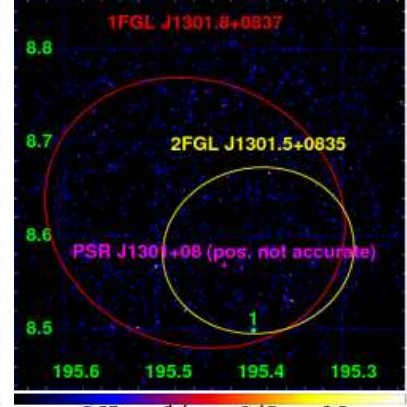
(73) 1FGL J1254.4+2209



(74) 1FGL J1256.9+3650



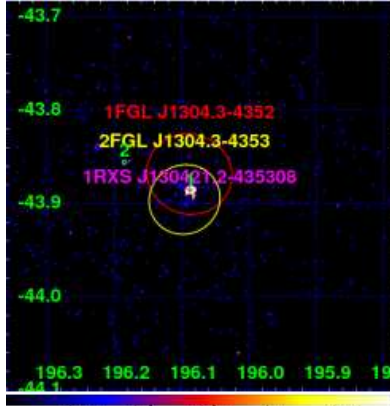
(75) 1FGL J1301.8+0837



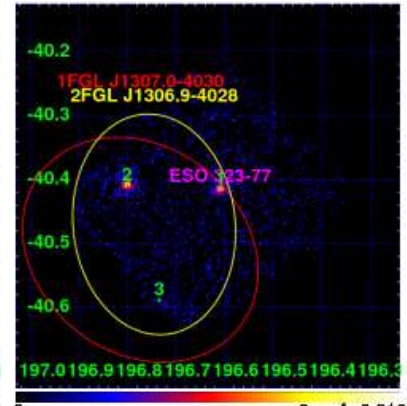
(76) 1FGL J1302.3–3255



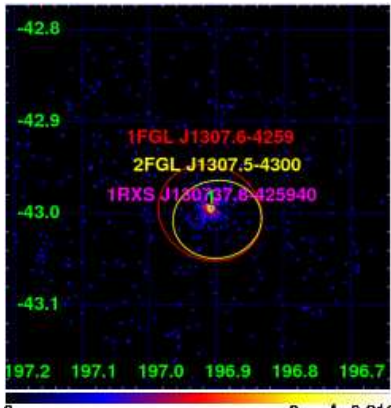
(77) 1FGL J1304.3–4352



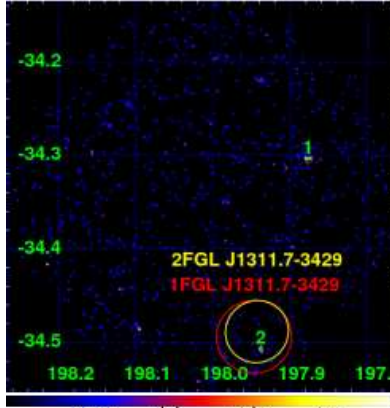
(78) 1FGL J1307.0–4030



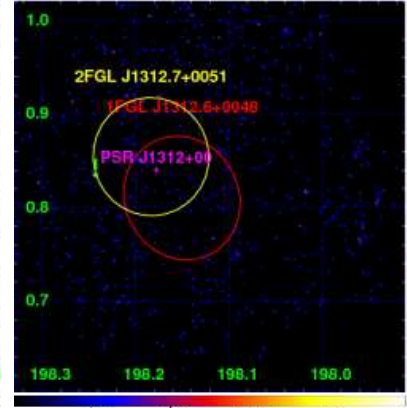
(79) 1FGL J1307.6–4259



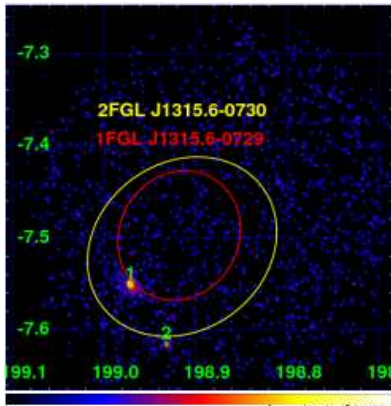
(80) 1FGL J1311.7–3429



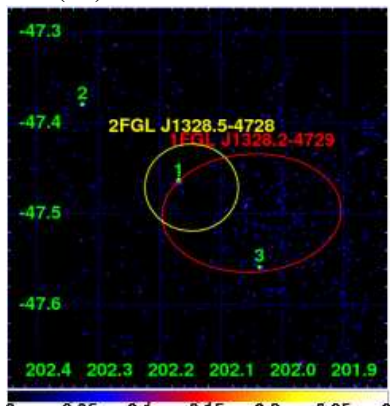
(81) 1FGL J1312.6+0048



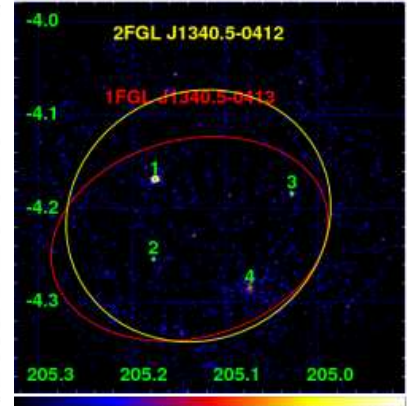
(82) 1FGL J1315.6–0729



(83) 1FGL J1328.2–4729



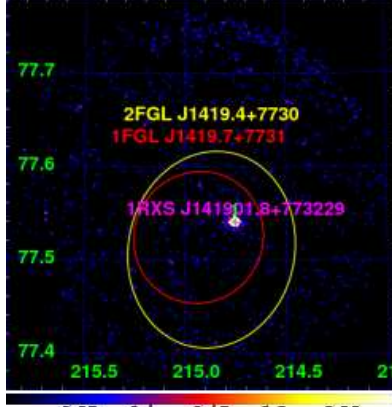
(84) 1FGL J1340.5–0413



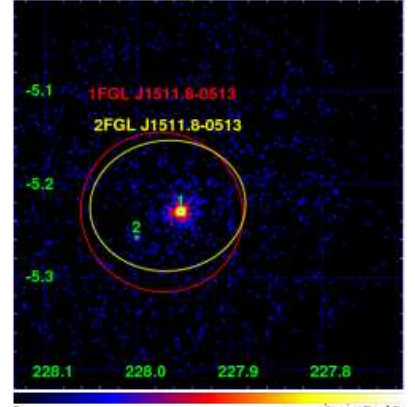
(85) 1FGL J1406.2–2510



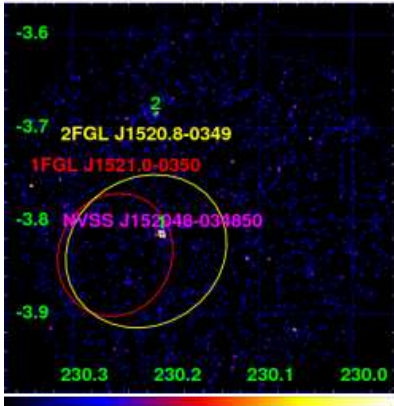
(86) 1FGL J1419.7+7731



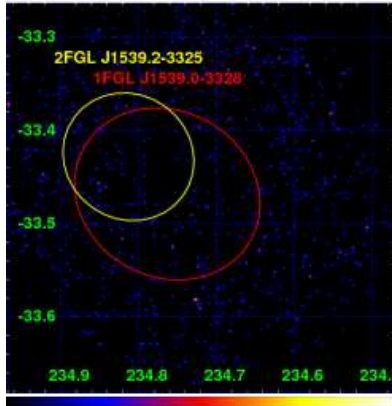
(87) 1FGL J1511.8–0513



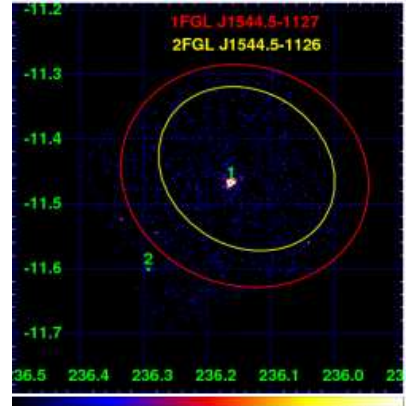
(88) 1FGL J1521.0–0350



(89) 1FGL J1539.0–3328



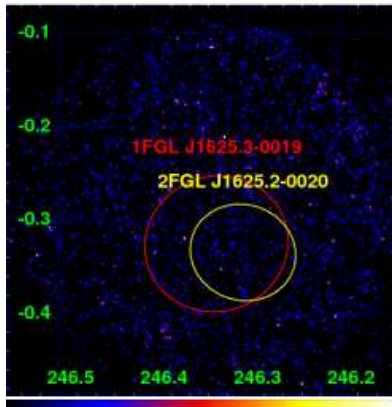
(90) 1FGL J1544.5–1127



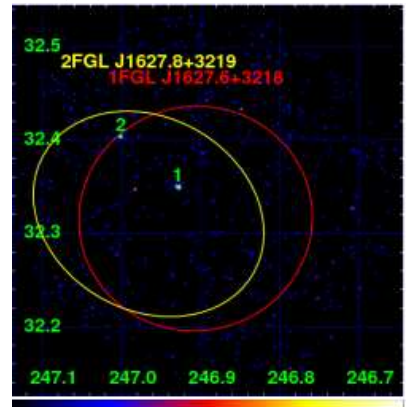
(91) 1FGL J1549.7–0659



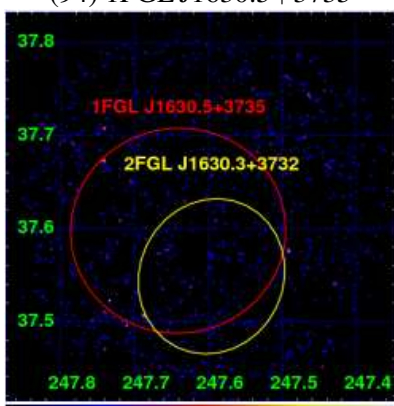
(92) 1FGL J1625.3–0019



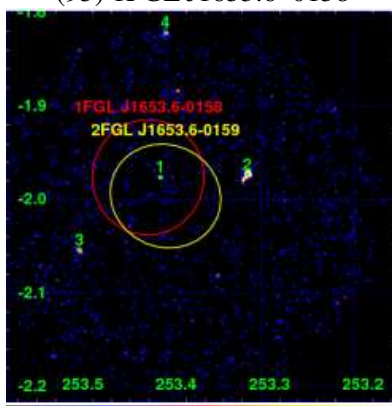
(93) 1FGL J1627.6+3218



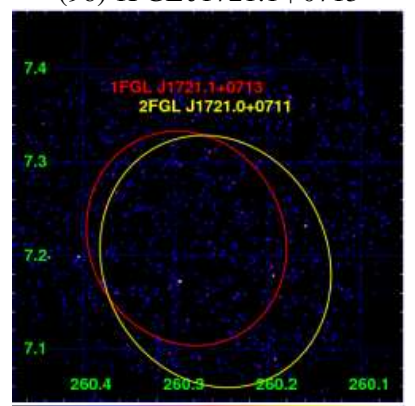
(94) 1FGL J1630.5+3735



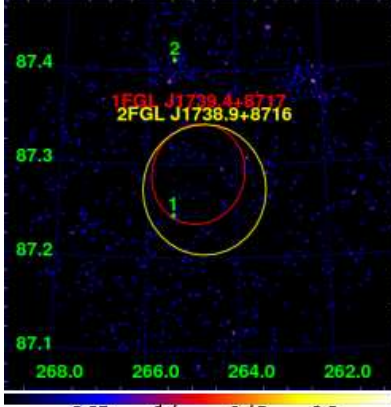
(95) 1FGL J1653.6–0158



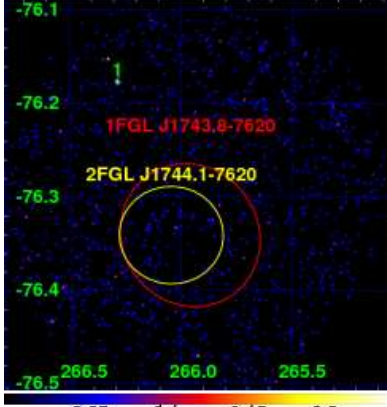
(96) 1FGL J1721.1+0713



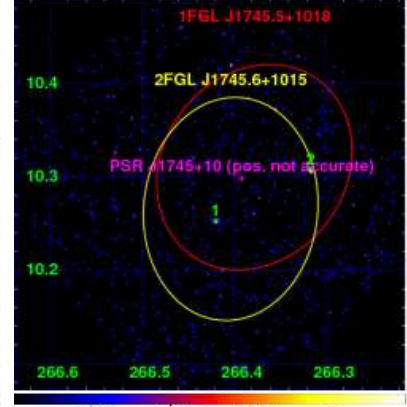
(97) 1FGL J1739.4+8717



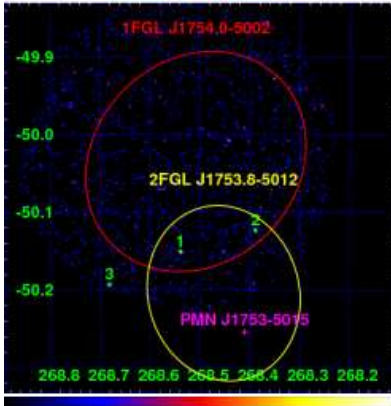
(98) 1FGL J1743.8-7620



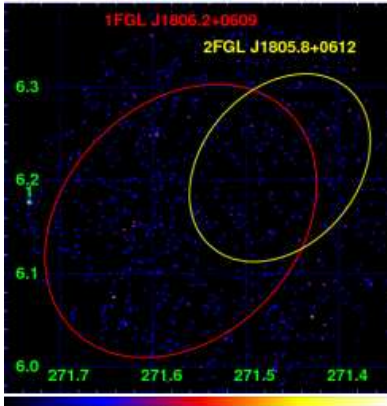
(99) 1FGL J1745.5+1018



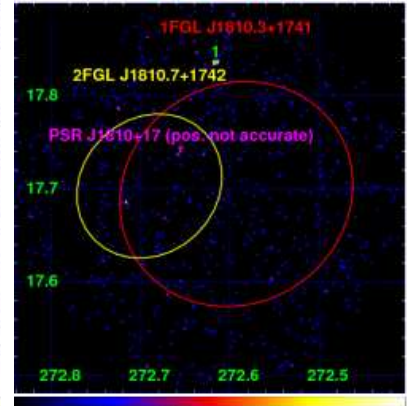
(100) 1FGL J1754.0-5002



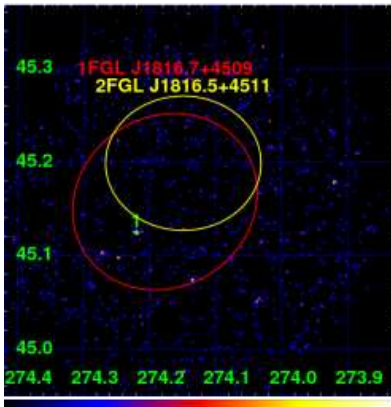
(101) 1FGL J1806.2+0609



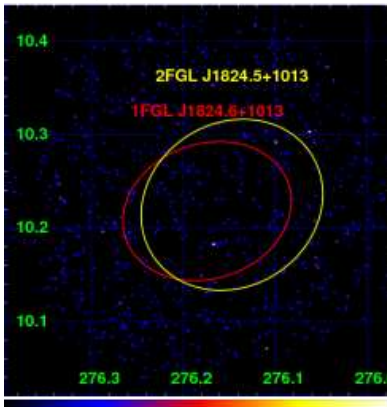
(102) 1FGL J1810.3+1741



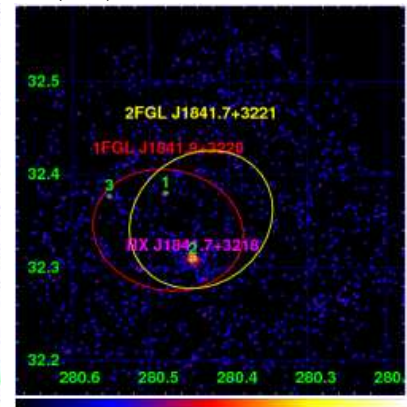
(103) 1FGL J1816.7+4509



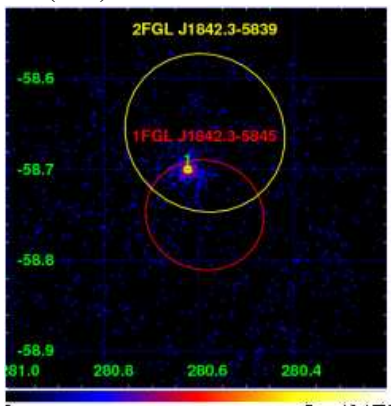
(104) 1FGL J1824.6+1013



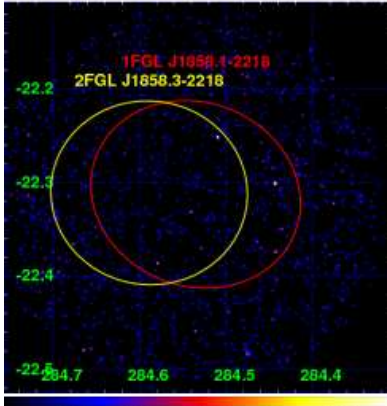
(105) 1FGL J1841.9+3220



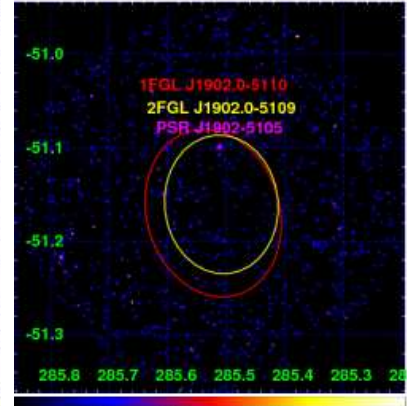
(106) 1FGL J1842.3-5845



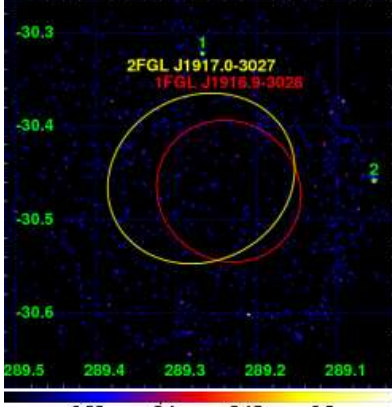
(107) 1FGL J1858.1-2218



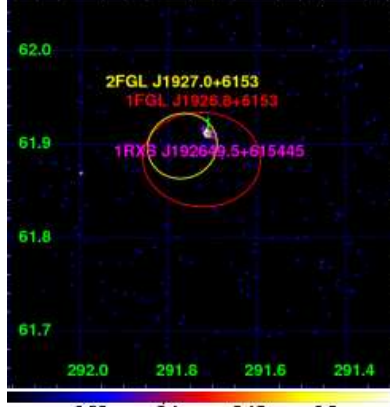
(108) 1FGL J1902.0-5110



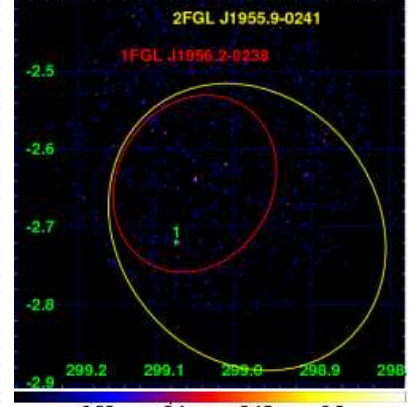
(109) 1FGL J1916.9–3028



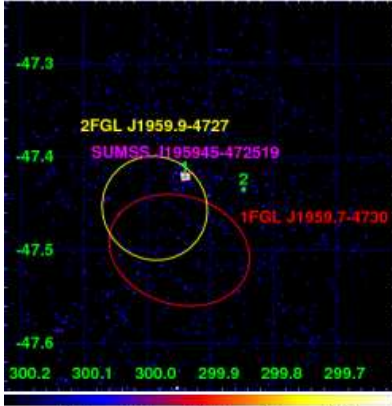
(110) 1FGL J1926.8+6153



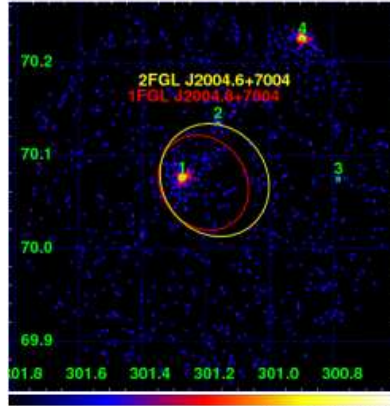
(111) 1FGL J1956.2–0238



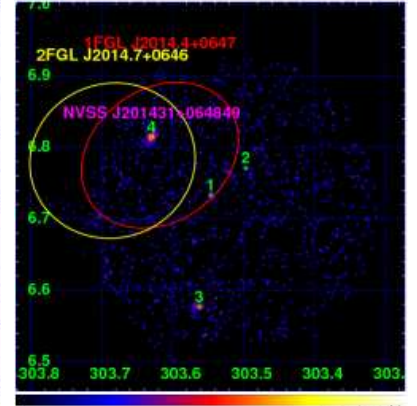
(112) 1FGL J1959.7–4730



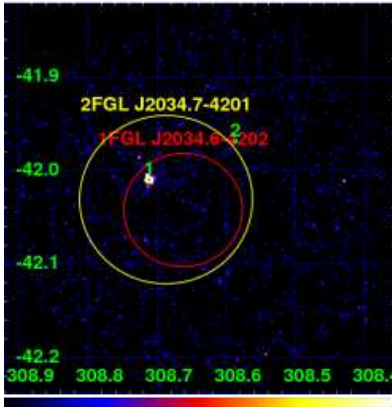
(113) 1FGL J2004.8+7004



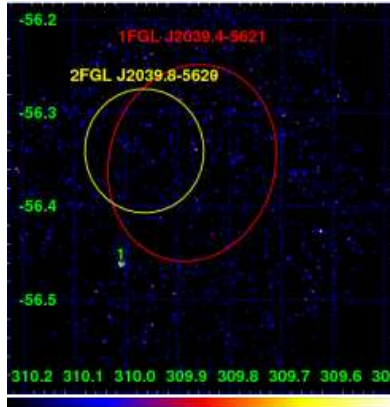
(114) 1FGL J2014.4+0647



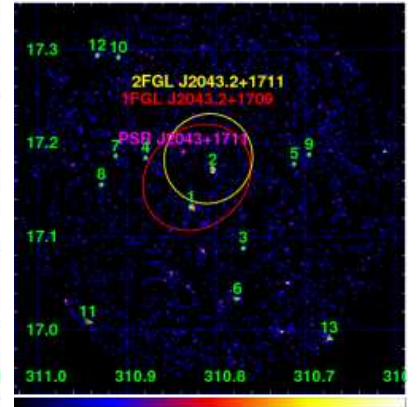
(115) 1FGL J2034.6–4202



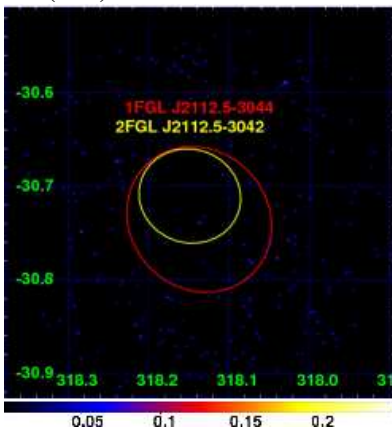
(116) 1FGL J2039.4–5621



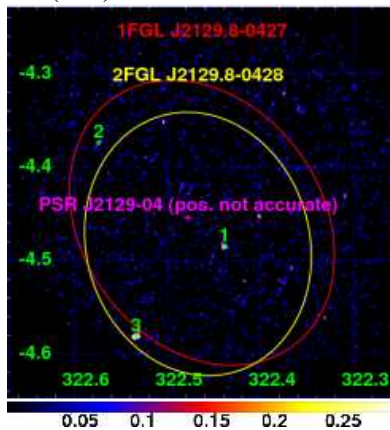
(117) 1FGL J2043.2+1709



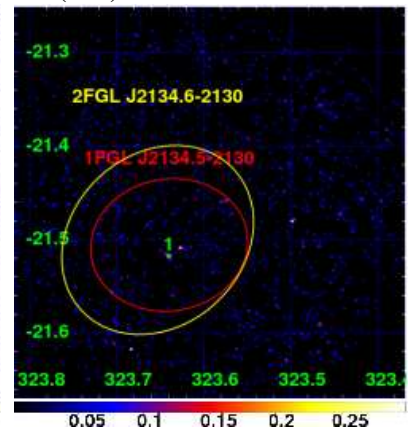
(118) 1FGL J2112.5–3044



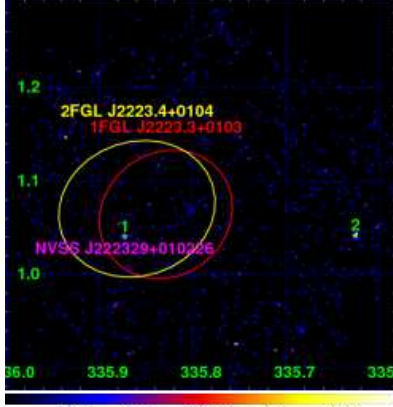
(119) 1FGL J2129.8–0427



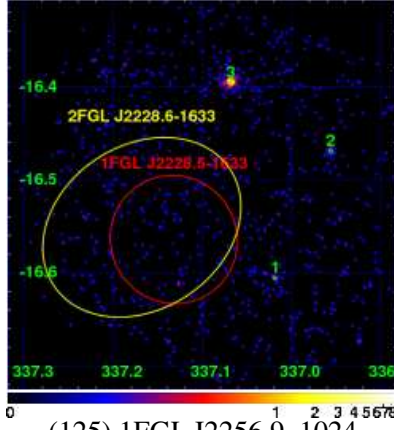
(120) 1FGL J2134.5–2130



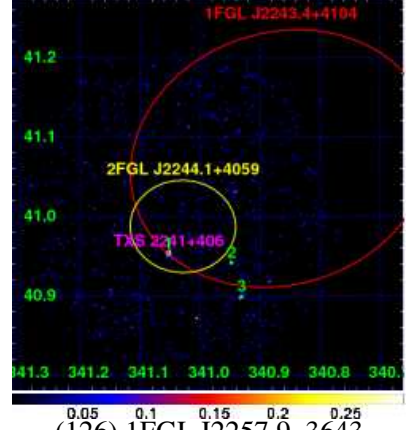
(121) 1FGL J2223.3+0103



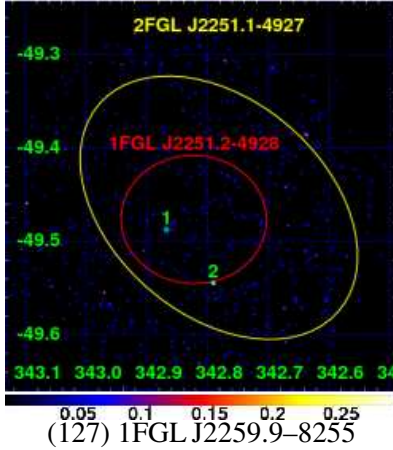
(122) 1FGL J2228.5–1633



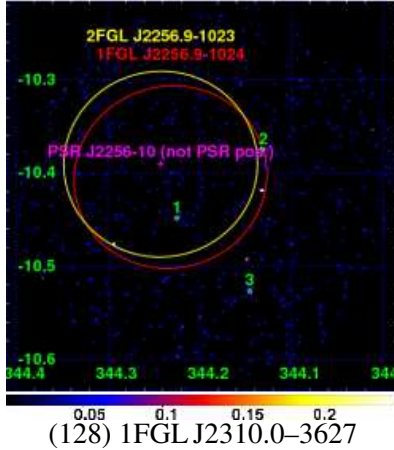
(123) 1FGL J2243.4+4104



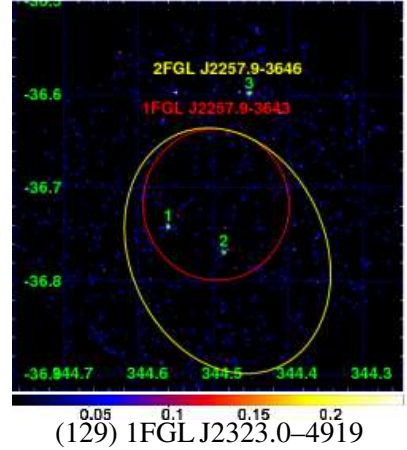
(124) 1FGL J2251.2–4928



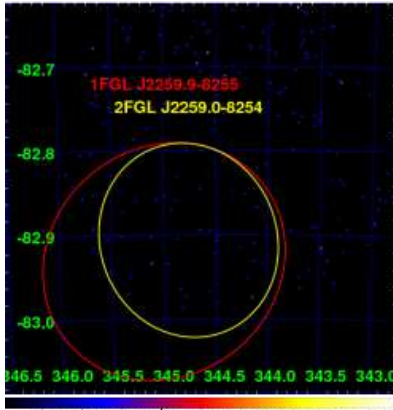
(125) 1FGL J2256.9–1024



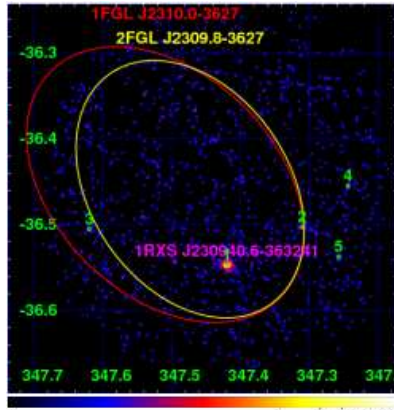
(126) 1FGL J2257.9–3643



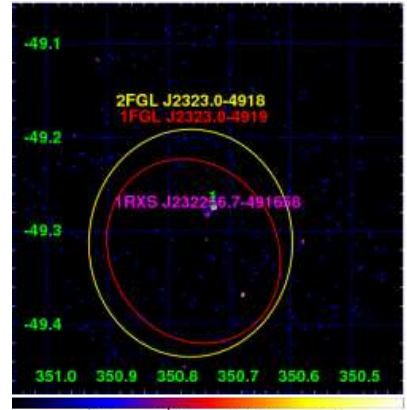
(127) 1FGL J2259.9–8255



(128) 1FGL J2310.0–3627



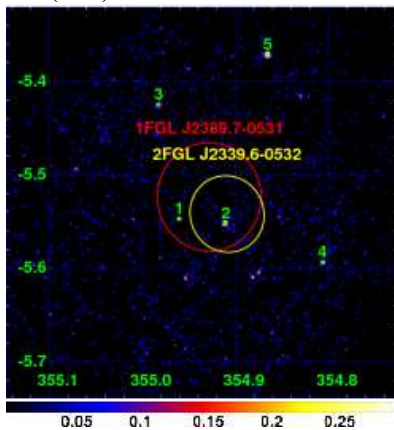
(129) 1FGL J2323.0–4919



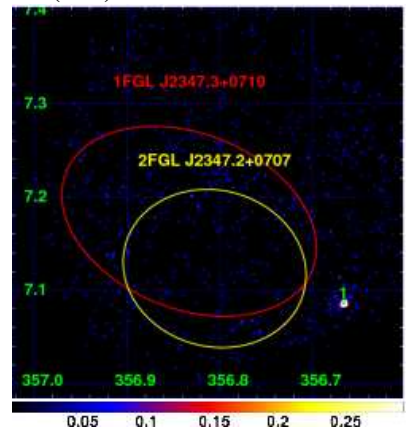
(130) 1FGL J2330.3–4745



(131) 1FGL J2339.7–0531



(132) 1FGL J2347.3+0710



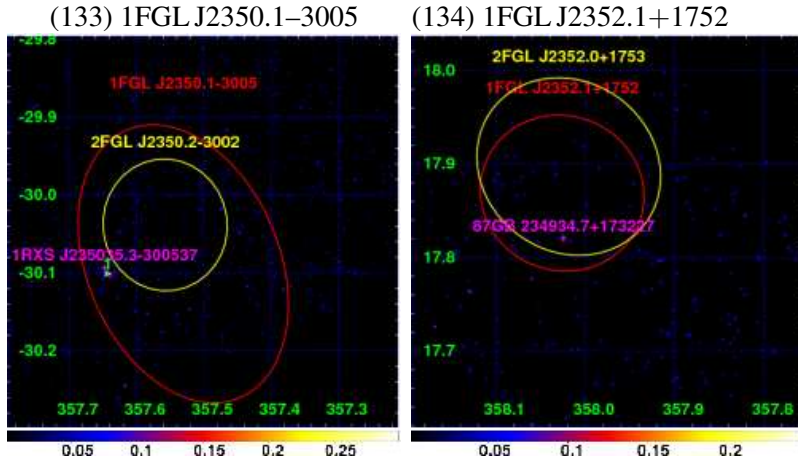


Fig. 11.— *Swift*/XRT images of the 134 1FGL unID catalog sources of the $25' \times 25'$ FoV. One or more sources are detected within the *Swift*/XRT FoV. Unfortunately, 2FGL error regions of some sources run off the edge of *Swift*/XRT FoV. The signal-to-noise acceptance threshold is set to 3σ . The yellow ellipses show 95% error regions of 2FGL catalog gamma-ray sources, and red ellipses show that of 1FGL catalog sources. If there are the radio and bright X-ray sources associated with gamma-ray source, we show those sources as magenta crosses.

Table 4: *Swift*/XRT Results for 1FGL objects. This table only show the details of high signal-to-noise (3σ) sources detected within the *Swift*/XRT FoV. The radius of 90% confidence error circles are described by $r_{90\%}$. Count rates are shown in the energy range of 0.3–10 keV.

1FGL Src	XRT Src#	R.A.(J2000) [deg]	Dec.(J2000) [deg]	$r_{90\%}$ ["]	Count Rates [1E-03 cts/s]	S/N ratio
1FGL J0001.9–4158	1	0.3864	-41.9227	3.73	6.95E+01+/-3.6	19.5
	2	0.3671	-42.0492	6.31	2.22+/-7.3E-01	3.0
	3	0.2813	-41.8854	5.70	3.36+/-9.2E-01	3.7
1FGL J0009.1+5031	1	2.3453	50.5071	4.90	1.00E+01+/-1.6	6.2
	2	2.3150	50.5960	5.64	3.05+/-9.3E-01	3.3
	3	2.1369	50.5176	6.31	2.62+/-8.8E-01	3.0
	4	2.4958	50.6476	6.41	3.16+/-1.0	3.0
	5	2.0160	50.4936	6.12	3.39+/-1.1	3.1
	6	1.9824	50.6048	7.09	4.18+/-1.3	3.2
1FGL J0022.2–1850	1	5.5385	-18.8928	5.53	3.18E+01+/-6.1	5.2
1FGL J0023.5+0930	1	5.9788	9.6547	5.14	6.63+/-1.3	5.0
	2	5.9083	9.3570	5.64	5.42+/-1.2	4.4
	3	5.8325	9.3485	5.05	7.99+/-1.5	5.4
1FGL J0030.7+0724	1	7.5928	7.4397	6.12	1.52+/-4.7E-01	3.2
	2	7.7076	7.3877	6.12	1.37+/-4.6E-01	3.0
	3	7.5743	7.3616	4.88	4.10+/-7.4E-01	5.6
	4	7.6248	7.3369	5.11	3.86+/-7.1E-01	5.4
	5	7.5010	7.3836	5.59	2.04+/-5.6E-01	3.7
	6	7.8316	7.4155	4.64	7.20+/-1.1	6.7
1FGL J0032.7–5519	1	8.3719	-55.3270	6.41	4.49+/-1.3	3.5
	2	7.9552	-55.4314	7.09	3.61+/-1.2	3.0
1FGL J0038.0+1236	1	9.4627	12.6391	4.55	1.46E+01+/-1.9	7.8
	2	9.5753	12.4588	4.51	2.30E+01+/-2.9	7.9
	3	9.4125	12.3414	6.12	7.87+/-2.2	3.5
1FGL J0039.2+4331	1	9.7439	43.4974	5.14	7.46+/-1.6	4.7
	2	9.5962	43.4438	5.35	3.93+/-1.2	3.2
	3	9.9055	43.6382	5.89	5.12+/-1.4	3.5
1FGL J0051.4–6242	1	12.8194	-62.7007	3.60	1.53E-01+/-5.1	30.2
	2	12.9464	-62.5974	6.52	2.71+/-7.7E-01	3.5
	3	13.0755	-62.6899	6.65	2.25+/-7.3E-01	3.1
	4	12.6349	-62.7895	5.82	3.51+/-9.1E-01	3.8
1FGL J0054.9–2455	1	13.6953	-24.9250	4.22	1.04E-01+/-1.0E+01	10.4
1FGL J0101.0–6423	1	15.1107	-64.3823	7.27	3.66+/-1.2	3.0
	2	15.3836	-64.5598	6.41	7.85+/-2.0	4.0
1FGL J0102.3+0942	1	15.5715	9.7362	6.31	3.23+/-1.0	3.1
1FGL J0103.1+4840	1	15.5295	48.6014	5.35	4.83+/-1.3	3.7
	2	15.7110	48.5053	6.04	5.20+/-1.3	3.9
	3	15.9266	48.5087	4.63	2.00E+01+/-2.7	7.5
	4	15.7360	48.4724	4.81	4.93+/-1.4	3.6
1FGL J0115.7+0357	1	18.9199	3.9463	6.65	1.88E+01+/-4.7	4.0
1FGL J0143.9–5845	1	25.9472	-58.7643	3.55	5.30E-01+/-1.1E+01	47.1
	2	26.0424	-58.6789	6.12	5.24+/-1.2	4.2
	3	25.6207	-58.7648	4.56	1.99E+01+/-2.7	7.4
1FGL J0157.0–5259	1	29.2405	-53.0334	3.59	5.11E-01+/-1.5E+01	33.2

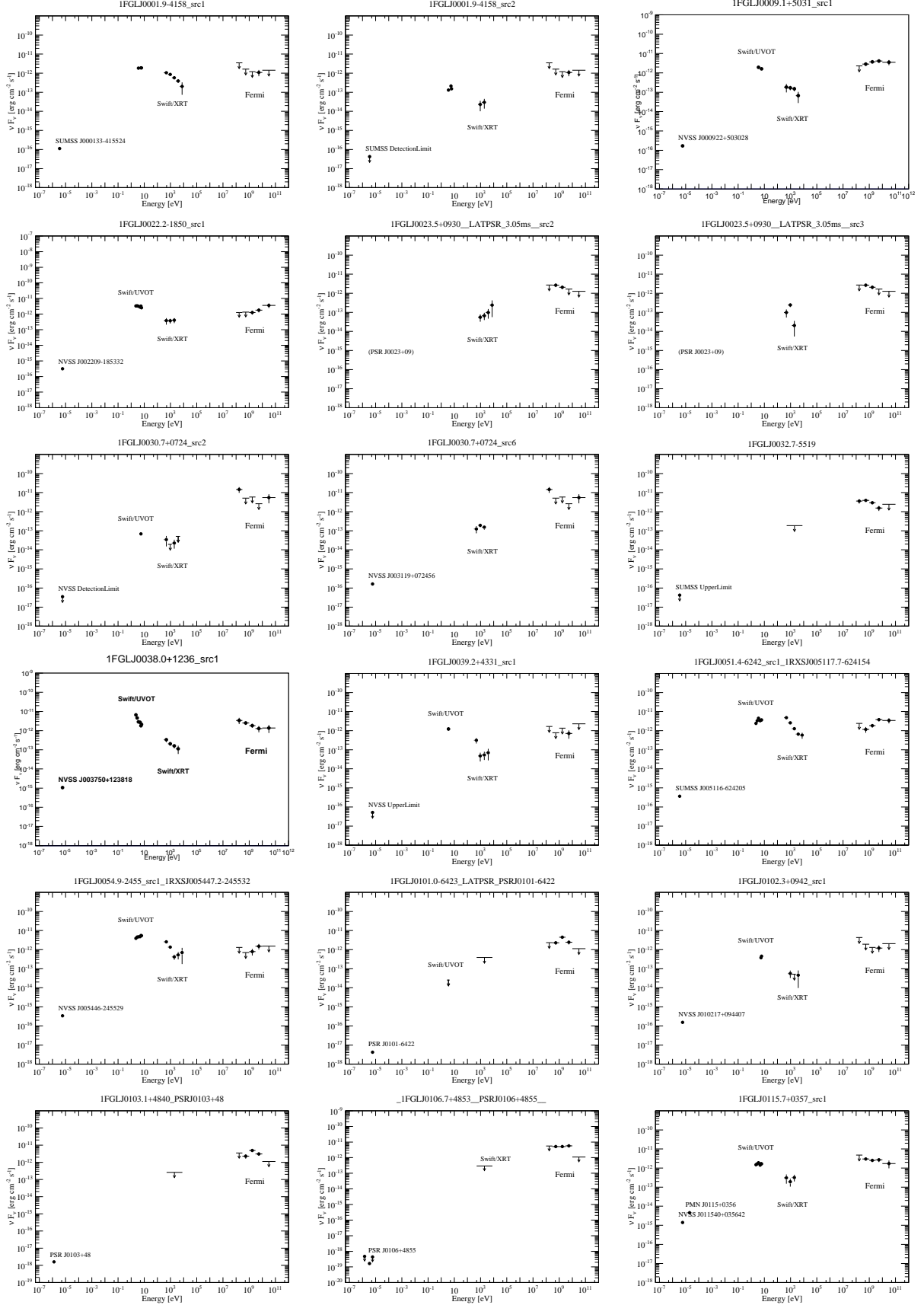
1FGL Src	XRT Src#	R.A.(J2000) [deg]	Dec.(J2000) [deg]	$r_{90\%}$ ["]	Count Rates [1E-03 cts/s]	S/N ratio
1FGL J0217.9–6630	1	34.2113	-66.6116	3.77	5.65E+01+/-3.2	17.5
	2	34.2072	-66.5820	5.08	5.89+/-1.1	5.2
	3	34.3547	-66.6033	4.95	6.40+/-1.2	5.3
	4	34.3879	-66.7521	5.59	5.72+/-1.2	4.7
1FGL J0223.0–1118	1	35.8097	-11.2939	3.98	4.36E+01+/-3.4	12.7
1FGL J0239.5+1324	1	39.7734	13.4551	5.44	5.50+/-1.3	4.2
	2	39.7275	13.2637	5.44	1.11E+01+/-2.2	5.1
1FGL J0305.2–1601	1	46.3123	-16.1387	3.95	5.76E+01+/-4.4	13.2
	2	46.3527	-16.1529	5.96	3.89+/-1.3	3.1
	3	46.3041	-16.1613	4.86	1.15E+01+/-2.1	5.5
1FGL J0316.3–6438	1	49.0593	-64.6252	3.70	1.14E-01+/-5.5	20.8
	2	48.7945	-64.4430	7.27	3.70+/-1.2	3.0
1FGL J0335.5–4501	1	53.8329	-45.0084	5.82	3.90+/-1.2	3.2
	2	53.9449	-44.9757	6.31	3.45+/-1.1	3.0
	3	53.8073	-44.9947	4.81	1.65E+01+/-2.5	6.7
	4	53.7894	-45.1661	6.65	5.41+/-1.5	3.6
1FGL J0340.4+4130	1	55.0355	41.4795	7.09	1.92+/-6.1E-01	3.2
	2	55.2222	41.6003	6.65	2.12+/-6.6E-01	3.2
	3	55.2058	41.3476	6.65	2.44+/-7.1E-01	3.4
	4	55.1090	41.3302	5.53	2.45+/-7.2E-01	3.4
	5	54.8538	41.3795	5.64	5.60+/-1.2	4.6
1FGL J0345.2–2355	1	56.3261	-23.8726	5.76	5.09+/-1.3	4.1
	2	56.1862	-23.9965	5.82	6.88+/-1.6	4.4
1FGL J0409.9–0357	1	62.4433	-4.0006	5.11	7.89+/-1.5	5.3
1FGL J0439.8–1857	1	69.9570	-19.0170	6.52	4.75+/-1.3	3.8
	2	70.1243	-19.0763	7.09	4.09+/-1.3	3.2
1FGL J0505.9+6121	1	76.4858	61.4165	6.41	1.91+/-6.3E-01	3.0
	2	76.4943	61.2259	3.89	3.55E+01+/-2.5	14.3
	3	76.2685	61.2885	3.69	8.08E+01+/-3.7	21.8
	4	76.5497	61.5288	5.64	3.30+/-9.0E-01	3.6
1FGL J0506.9–5435	1	76.7410	-54.5859	3.95	1.84E-01+/-1.3E+01	13.9
1FGL J0521.6+0103	1	80.4198	1.0495	6.12	4.03+/-1.2	3.4
	2	80.5590	0.9602	5.11	1.01E+01+/-1.9	5.3
	3	80.6260	1.0803	6.12	4.03+/-1.3	3.1
1FGL J0523.5–2529	1	80.8216	-25.4604	6.21	3.08+/-9.4E-01	3.3
1FGL J0533.9+6758	1	83.2624	68.0123	5.40	8.03+/-1.5	5.4
	2	83.3788	68.0480	6.41	3.49+/-1.0	3.5
	3	83.4525	67.8272	6.04	4.49+/-1.2	3.8
	4	83.3501	67.7908	5.44	4.90+/-1.3	3.8
	5	83.4313	68.1494	6.31	5.06+/-1.3	3.8
1FGL J0537.7–5717	1	84.4532	-57.3083	4.55	3.13E+01+/-4.0	7.8
	2	84.6011	-57.3187	5.59	1.62E+01+/-3.2	5.1
	3	84.4356	-57.1650	4.17	6.13E+01+/-5.8	10.6
1FGL J0538.4–3910	1	84.5432	-39.1450	3.64	1.35E-01+/-5.3	25.4
	2	84.3436	-39.1091	6.65	3.40+/-1.0	3.3
1FGL J0545.6+6022	1	86.4117	60.4666	6.78	3.57+/-1.2	3.0
	2	85.9778	60.4020	5.82	6.72+/-1.8	3.8

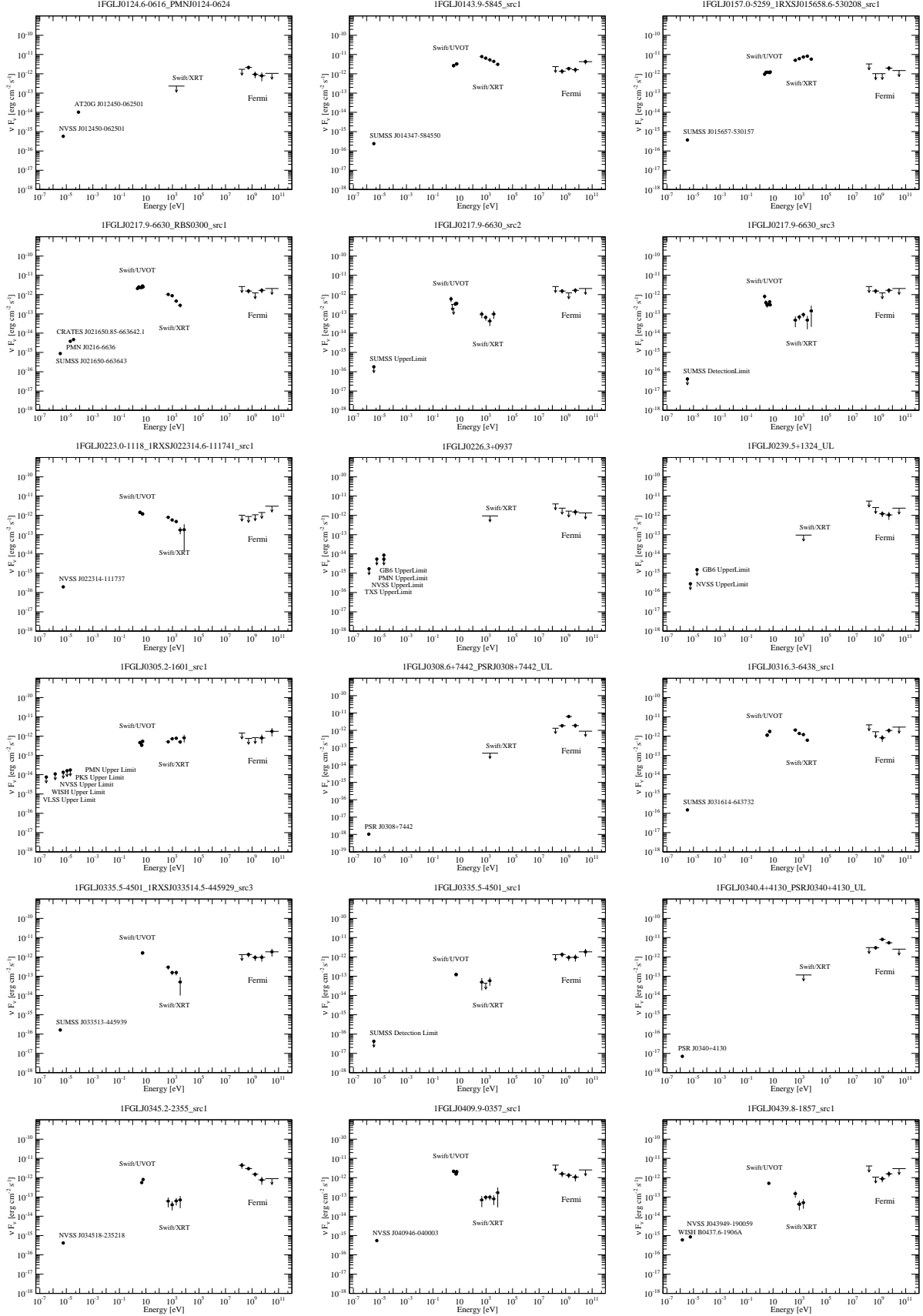
1FGL Src	XRT Src#	R.A.(J2000) [deg]	Dec.(J2000) [deg]	$r_{90\%}$ ["]	Count Rates [1E-03 cts/s]	S/N ratio
1FGL J0600.5–2006	1	90.0660	-20.1167	5.40	2.07E+01+/-5.4	3.9
	2	90.0324	-20.1368	5.02	3.36E+01+/-6.7	5.0
1FGL J0603.0–4012	1	90.7134	-40.3133	5.00	2.54E+01+/-4.0	6.4
1FGL J0604.2–4817	1	91.0367	-48.2904	3.59	1.91E-01+/-6.0	32.1
	2	90.9685	-48.2119	5.59	3.77+/-9.4E-01	4.0
	3	90.9612	-48.3352	6.41	2.25+/-7.5E-01	3.0
	4	91.2562	-48.1729	5.20	6.70+/-1.3	5.1
	5	91.2618	-48.3670	6.04	4.50+/-1.1	4.1
	6	90.9115	-48.4518	6.12	4.13+/-1.1	3.7
	7	91.1940	-48.4578	3.57	3.70E-01+/-9.8	37.6
1FGL J0605.1+0005	1	91.1991	0.2213	4.92	4.97E+01+/-7.2	6.9
1FGL J0609.3–0244	1	92.3127	-2.7977	6.12	1.52E+01+/-3.6	4.2
1FGL J0648.6–6052	1	101.9201	-60.9673	4.88	5.22+/-9.4E-01	5.6
	2	102.1083	-60.9551	6.52	1.90+/-5.8E-01	3.3
	3	101.8282	-60.8258	5.89	2.73+/-6.9E-01	4.0
	4	102.0740	-61.0352	6.12	1.74+/-5.8E-01	3.0
	5	101.6416	-61.0087	6.31	2.56+/-6.9E-01	3.7
	6	101.5771	-60.9332	6.31	1.83+/-6.0E-01	3.0
1FGL J0707.3+7742	1	106.7108	77.6937	5.59	7.04+/-1.5	4.6
	2	107.3337	77.5734	6.12	3.91+/-1.2	3.2
1FGL J0718.8–4958	1	109.8163	-49.9788	7.27	2.89+/-9.5E-01	3.0
1FGL J0803.1–0339	1	120.8008	-3.6000	4.26	2.69E+01+/-2.8	9.6
	2	120.7911	-3.5159	6.65	3.72+/-1.2	3.2
	3	120.7895	-3.8270	5.53	1.10E+01+/-2.2	5.0
1FGL J0814.5–1011	1	123.5479	-10.2019	4.90	3.63E+01+/-5.3	6.8
1FGL J0848.6+0504	1	132.1648	5.1057	3.90	5.29E+01+/-3.7	14.2
	2	132.1449	5.2360	5.31	1.09E+01+/-2.0	5.5
1FGL J0902.4+2050	1	135.6110	20.8456	5.14	6.25+/-1.2	5.4
1FGL J0906.4–0903	1	136.5734	-9.0954	7.09	1.17E+01+/-3.7	3.1
1FGL J0908.7–2119	1	137.2438	-21.3149	4.28	2.72E+01+/-2.8	9.6
	2	137.3365	-21.3181	6.52	4.02+/-1.2	3.4
	3	137.0984	-21.1945	5.14	1.02E+01+/-2.1	5.0
1FGL J0922.0+2337	1	140.4383	23.5963	5.82	6.62+/-1.5	4.3
	2	140.3968	23.5262	7.27	3.87+/-1.3	3.0
	3	140.3262	23.5672	5.96	6.43+/-1.7	3.9
1FGL J0955.2–3949	1	148.8656	-39.7969	5.96	5.08+/-1.4	3.6
	2	148.8290	-39.6696	5.35	9.49+/-1.9	4.9
1FGL J1040.5+0616	1	160.1313	6.2904	5.82	2.99+/-8.0E-01	3.7
	2	160.1639	6.2566	5.20	5.75+/-1.1	5.2
	3	160.2016	6.3061	5.76	3.76+/-8.9E-01	4.2
	4	160.0322	6.4196	6.93	2.32+/-7.7E-01	3.0
	5	160.3053	6.3220	6.65	2.61+/-8.2E-01	3.2
1FGL J1119.9–2205	1	169.9925	-22.0822	5.08	2.67+/-6.1E-01	4.4
	2	170.0034	-22.0245	5.82	1.80+/-5.1E-01	3.5
	3	170.0897	-22.1876	5.49	1.63+/-4.8E-01	3.4
	4	170.1708	-22.1321	3.97	1.89E+01+/-1.5	12.4
	5	169.8795	-21.9436	6.04	1.88+/-6.0E-01	3.1

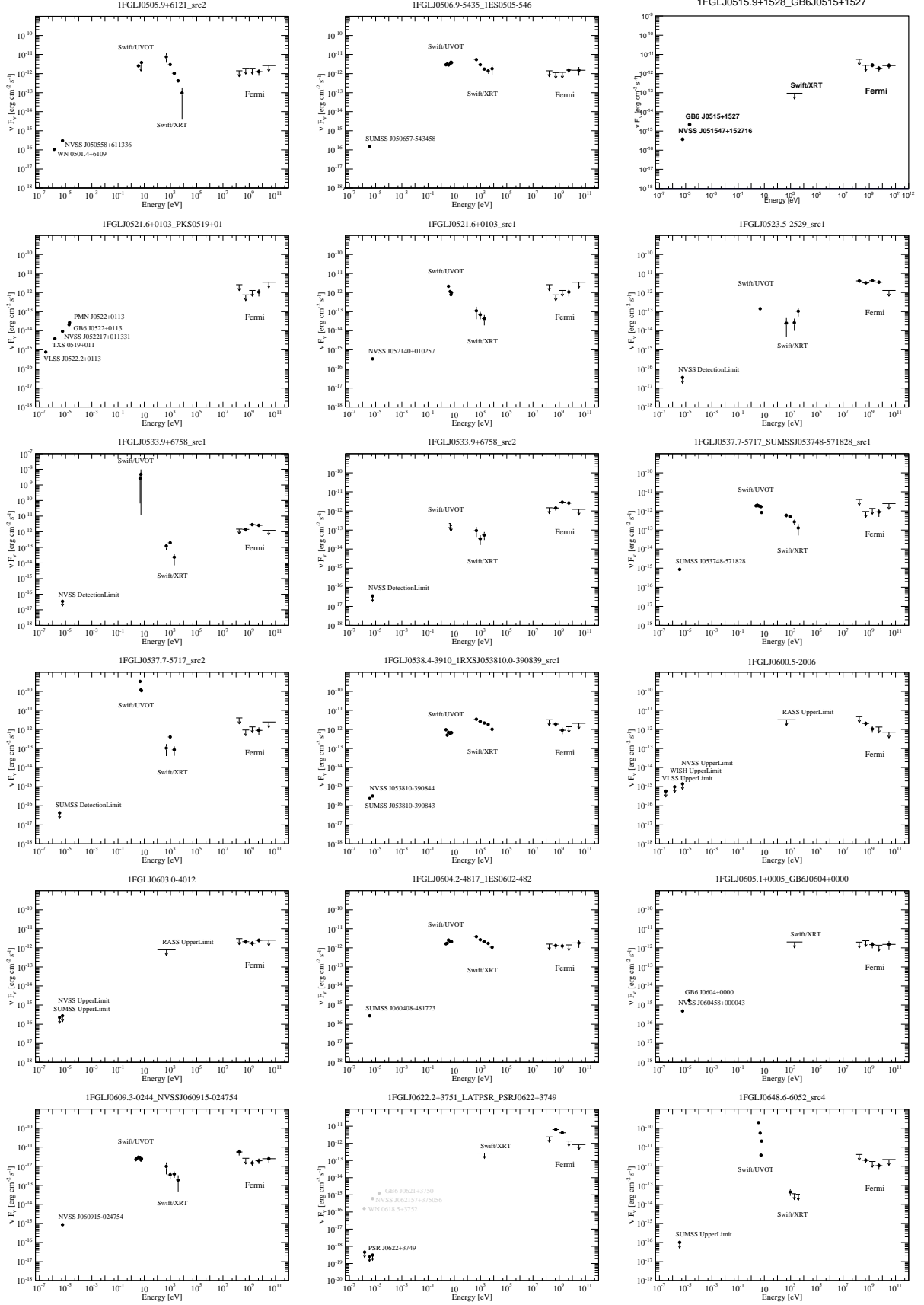
1FGL Src	XRT Src#	R.A.(J2000) [deg]	Dec.(J2000) [deg]	$r_{90\%}$ ["]	Count Rates [1E-03 cts/s]	S/N ratio
1FGL J1124.4–3654	1	171.0039	-36.8891	6.21	1.71+/-5.5E-01	3.1
	2	171.1585	-36.9404	5.76	2.51+/-6.5E-01	3.8
	3	171.1690	-36.8199	5.40	2.23+/-6.3E-01	3.5
1FGL J1129.3+3757	1	172.2650	37.9494	6.65	3.07+/-9.5E-01	3.2
	2	172.3798	38.0324	6.52	2.74+/-9.1E-01	3.0
1FGL J1141.8–1403	1	175.4239	-14.1322	3.74	7.76E+01+/-4.1	19.0
	2	175.3233	-14.0799	6.78	2.88+/-9.1E-01	3.1
1FGL J1218.4–0128	1	184.6469	-1.3324	8.27	9.26+/-3.1	3.0
1FGL J1221.4–0635	1	185.3635	-6.4784	4.78	8.44+/-1.5	5.7
	2	185.2748	-6.6540	5.59	3.69+/-1.0	3.5
	3	185.4747	-6.5225	5.96	2.93+/-9.4E-01	3.1
	4	185.3609	-6.4182	5.14	4.90+/-1.2	4.1
	5	185.4733	-6.6844	4.97	9.29+/-1.7	5.5
1FGL J1226.0+2954	1	186.5352	29.9957	5.00	9.19+/-1.7	5.4
	2	186.4046	29.9057	5.59	5.17+/-1.4	3.8
1FGL J1232.2–5118	1	187.9632	-51.3279	6.21	4.83+/-1.3	3.6
1FGL J1249.3–2812	1	192.3304	-28.1422	3.95	4.76E+01+/-3.6	13.1
	2	192.2482	-28.2060	6.12	5.05+/-1.3	3.8
	3	192.5229	-28.2054	4.74	1.67E+01+/-2.4	7.1
1FGL J1251.3+1044	1	192.8250	10.6513	4.09	5.94E+01+/-5.3	11.1
1FGL J1254.4+2209	1	193.6389	22.1844	5.59	1.94E+01+/-3.7	5.2
	2	193.6657	22.1065	4.92	3.42E+01+/-5.0	6.8
1FGL J1256.9+3650	1	194.3924	36.7638	6.52	2.24E+01+/-5.4	4.1
	2	194.3487	36.7376	6.52	2.02E+01+/-5.2	3.9
1FGL J1301.8+0837	1	195.3958	8.4991	6.93	3.76+/-1.2	3.0
1FGL J1302.3–3255	1	195.6096	-33.0154	6.12	1.55+/-4.9E-01	3.2
	2	195.5295	-32.7874	5.59	1.85+/-5.4E-01	3.5
	3	195.7604	-32.8232	5.17	2.32+/-6.0E-01	3.8
1FGL J1304.3–4352	1	196.0869	-43.8864	3.86	1.22E-01+/-8.0	15.3
	2	196.1849	-43.8558	7.27	5.79+/-1.9	3.0
1FGL J1307.0–4030	1	196.6086	-40.4145	3.64	1.23E-01+/-4.9	25.2
	2	196.8008	-40.4080	3.61	1.74E-01+/-6.1	28.6
	3	196.7351	-40.5895	5.31	3.65+/-1.1	3.4
1FGL J1307.6–4259	1	196.9083	-42.9943	3.65	5.46E-01+/-2.1E+01	25.5
1FGL J1311.7–3429	1	197.8769	-34.3037	5.08	8.00+/-1.8	4.3
	2	197.9380	-34.5076	5.96	4.90+/-1.6	3.1
1FGL J1312.7+0051	1	198.2429	0.8348	6.78	3.72+/-1.2	3.0
1FGL J1315.6–0729	1	198.9712	-7.5508	3.69	8.16E+01+/-3.9	21.2
	2	198.9320	-7.6155	4.71	8.51+/-1.4	6.2
1FGL J1328.2–4729	1	202.1693	-47.4641	5.49	5.77+/-1.1	5.1
	2	202.3257	-47.3795	5.82	4.94+/-1.1	4.6
	3	202.0373	-47.5586	6.21	3.76+/-9.8E-01	3.8
	4	201.7203	-47.4907	5.53	1.02E+01+/-2.7	3.8
1FGL J1340.5–0413	1	205.1756	-4.1685	3.97	2.48E+01+/-2.0	12.4
	2	205.1773	-4.2541	5.59	2.79+/-7.6E-01	3.7
	3	205.0287	-4.1842	5.49	3.75+/-8.7E-01	4.3
	4	205.0739	-4.2852	4.41	6.19+/-1.1	5.6
1FGL J1406.2–2510	1	211.5423	-25.1342	5.96	2.49E+01+/-5.4	4.6
1FGL J1419.7+7731	1	214.7543	77.5418	3.77	7.17E+01+/-4.1	17.7

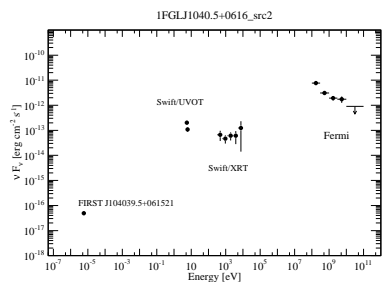
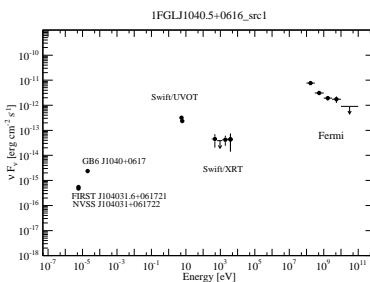
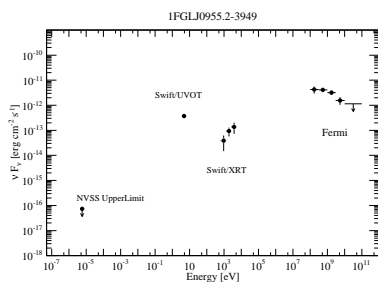
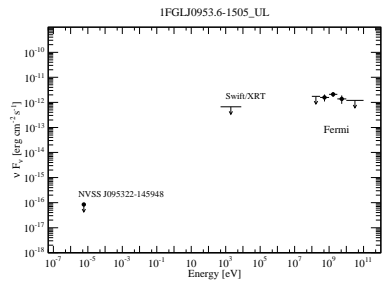
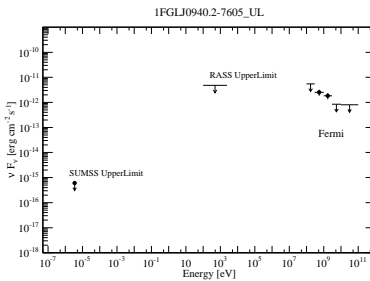
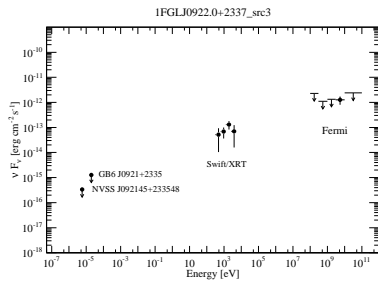
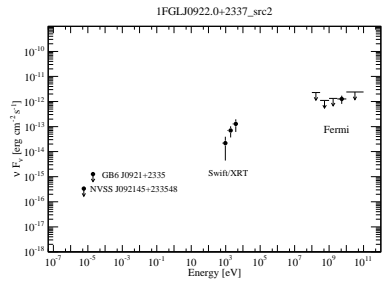
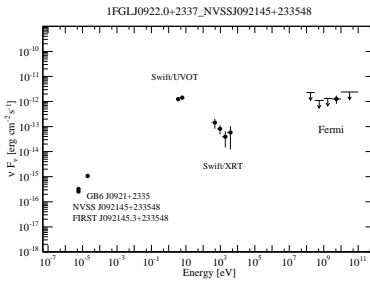
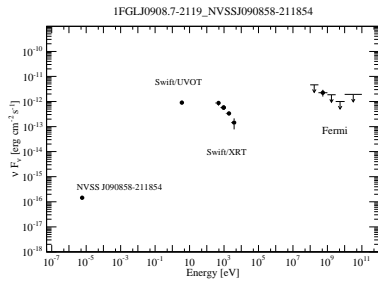
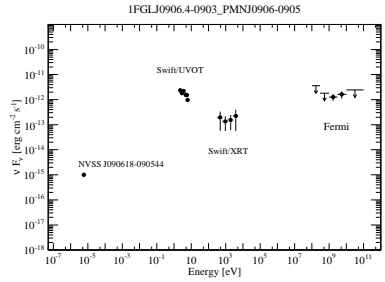
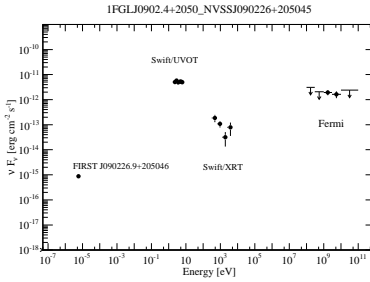
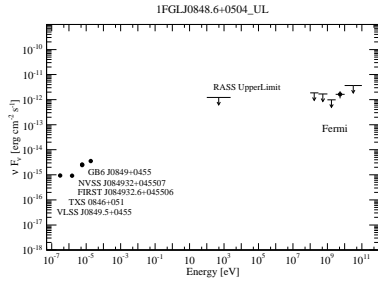
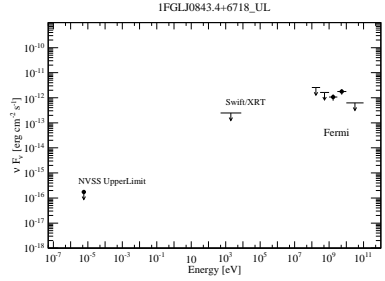
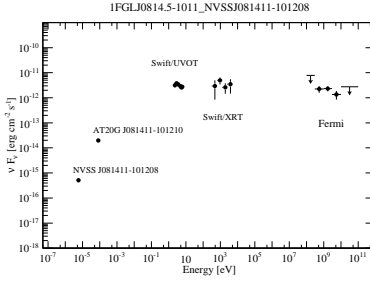
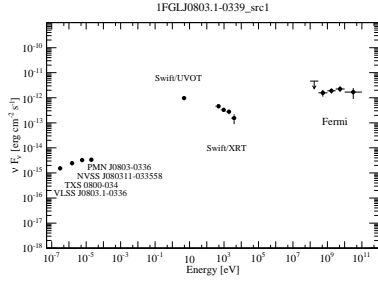
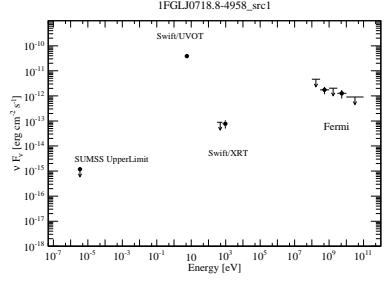
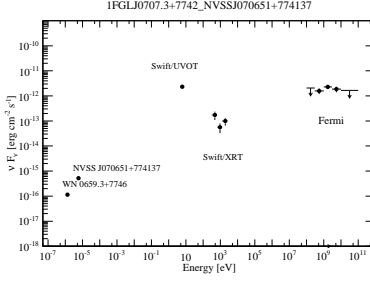
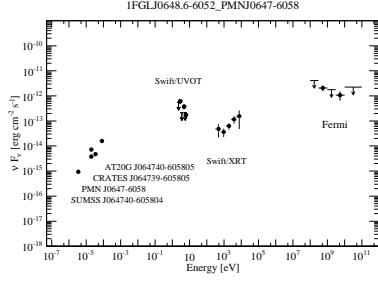
1FGL Src	XRT Src#	R.A.(J2000) [deg]	Dec.(J2000) [deg]	$r_{90\%}$ ["]	Count Rates [1E-03 cts/s]	S/N ratio
1FGL J1511.8–0513	1	227.9530	-5.2297	3.55	4.50E-01+/-1.1E+01	42.5
	2	228.0008	-5.2577	5.02	9.17+/-1.7	5.5
1FGL J1521.0–0350	1	230.2047	-3.8140	4.01	1.94E+01+/-1.7	11.6
	2	230.2114	-3.6863	4.92	2.31+/-6.6E-01	3.5
1FGL J1544.5–1127	1	236.1636	-11.4676	3.70	7.55E+01+/-3.6	20.9
	2	236.2932	-11.6010	5.96	3.57+/-9.2E-01	3.9
1FGL J1549.7–0659	1	237.4678	-6.9857	3.70	1.17E-01+/-5.6	20.8
1FGL J1627.6+3218	1	246.9290	32.3502	5.49	1.00E+01+/-1.9	5.3
	2	247.0013	32.4037	5.96	7.85+/-1.8	4.4
1FGL J1653.6–0158	1	253.4077	-1.9764	6.04	2.84+/-9.5E-01	3.0
	2	253.3149	-1.9732	4.11	2.93E+01+/-2.7	10.8
	3	253.4946	-2.0543	5.02	9.17+/-1.7	5.4
	4	253.4024	-1.8221	5.49	6.99+/-1.6	4.4
1FGL J1738.9+8716	1	265.4297	87.2447	6.93	3.23+/-1.0	3.1
	2	265.4339	87.4113	5.76	4.98+/-1.4	3.7
1FGL J1744.1+7620	1	266.2855	-76.1771	6.12	3.73+/-9.2E-01	4.0
1FGL J1745.5+1018	1	266.4193	10.2526	6.65	4.03+/-1.2	3.2
	2	266.3164	10.3072	5.64	7.42+/-1.7	4.4
1FGL J1754.0–5002	1	268.5392	-50.1507	5.49	6.18+/-1.5	4.0
	2	268.3887	-50.1235	5.70	5.30+/-1.4	3.7
	3	268.6812	-50.1930	7.27	4.14+/-1.4	3.0
1FGL J1806.2+0609	1	271.7333	6.1765	5.96	7.81+/-2.1	3.8
1FGL J1810.3+1741	1	272.6161	17.8358	5.44	8.85+/-1.8	4.8
1FGL J1816.7+4509	1	274.2201	45.1247	6.04	5.57+/-1.3	4.4
1FGL J1841.9+3220	1	280.4803	32.3805	5.82	4.01+/-9.7E-01	4.2
	2	280.4459	32.3103	3.75	6.11E+01+/-3.4	18.2
	3	280.5522	32.3770	5.82	2.66+/-8.0E-01	3.3
1FGL J1842.3–5845	1	280.6243	-58.7002	3.58	4.37E-01+/-1.3E+01	34.1
1FGL J1916.9–3028	1	289.2676	-30.3227	6.31	9.91+/-2.8	3.5
	2	289.0549	-30.4573	5.76	1.78E+01+/-4.0	4.4
1FGL J1926.8+6153	1	291.7104	61.9111	4.18	1.27E-01+/-1.2E+01	10.6
1FGL J1956.2–0238	1	299.0734	-2.7197	6.21	4.68+/-1.3	3.7
1FGL J1959.7–4730	1	299.9399	-47.4216	3.94	5.51E+01+/-4.1	13.5
	2	299.8476	-47.4352	6.52	3.32+/-1.1	3.0
1FGL J2004.8+7004	1	301.2739	70.0766	3.69	1.09E-01+/-5.0	22.0
	2	301.1617	70.1349	5.11	7.68+/-1.4	5.4
	3	300.7818	70.0746	7.27	3.32+/-1.0	3.2
	4	300.8928	70.2259	3.73	1.15E-01+/-5.9	19.4
1FGL J2014.4+0647	1	303.5461	6.7328	5.76	4.85+/-1.1	4.4
	2	303.4967	6.7707	6.41	2.44+/-8.1E-01	3.0
	3	303.5626	6.5772	4.39	1.79E+01+/-2.1	8.3
	4	303.6298	6.8144	3.78	7.48E+01+/-4.3	17.4
1FGL J2034.6–4202	1	308.7116	-42.0101	3.93	4.18E+01+/-3.2	13.0
	2	308.5874	-41.9693	5.89	4.20+/-1.1	3.7
1FGL J2039.4–5621	1	310.0106	-56.4619	4.97	1.12E+01+/-1.8	6.2
1FGL J2129.8–0427	1	322.4393	-4.4849	4.90	4.25+/-7.6E-01	5.6
	2	322.5741	-4.3742	5.76	1.60+/-4.9E-01	3.3
	3	322.5339	-4.5812	4.38	1.05E+01+/-1.3	8.3
1FGL J2134.5–2130	1	323.6404	-21.5176	5.64	3.01+/-8.2E-01	3.7

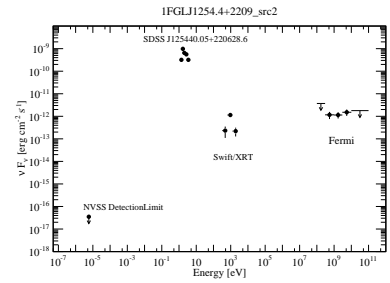
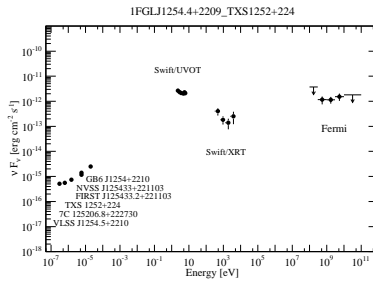
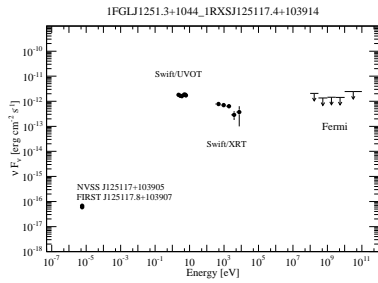
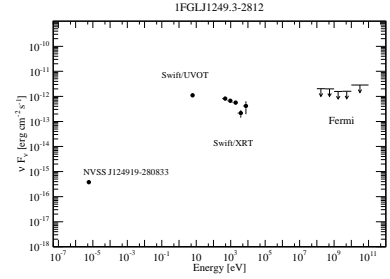
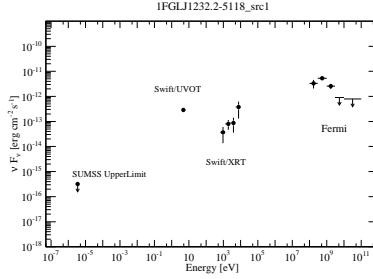
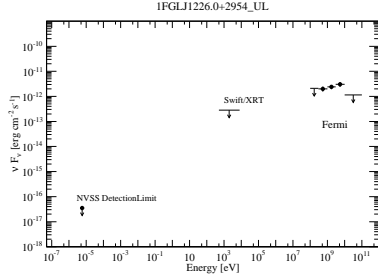
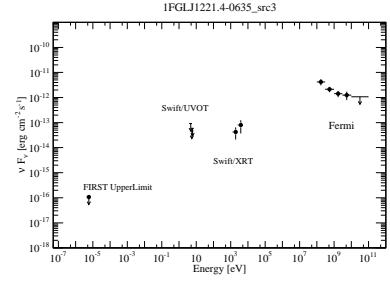
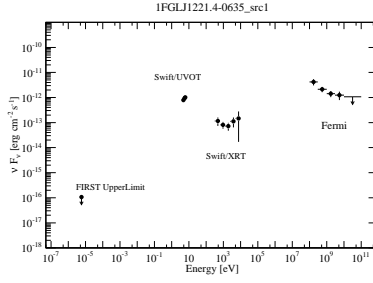
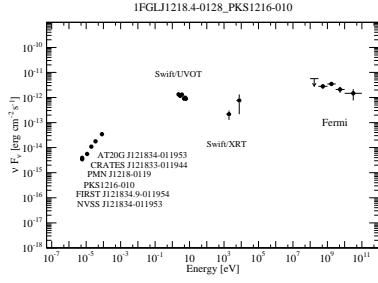
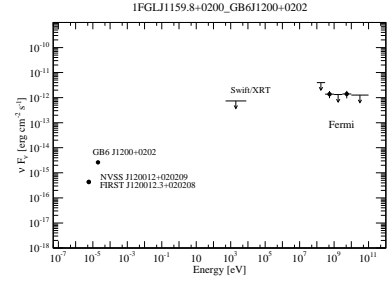
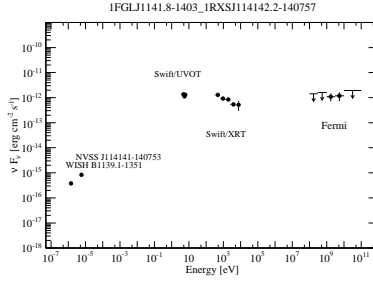
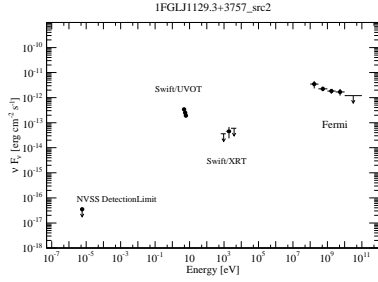
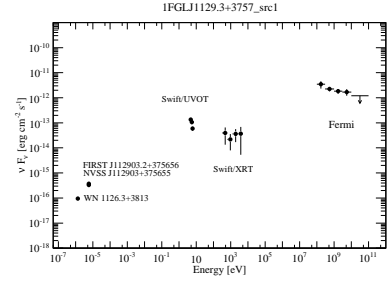
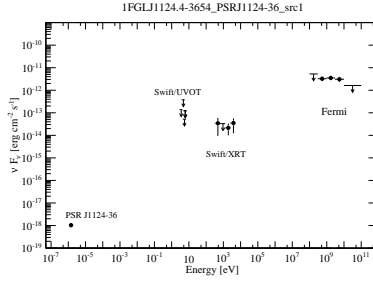
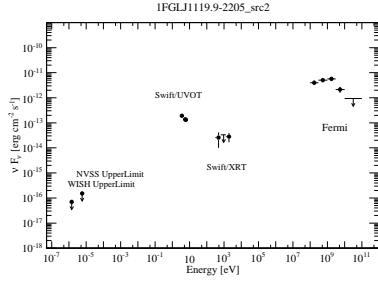
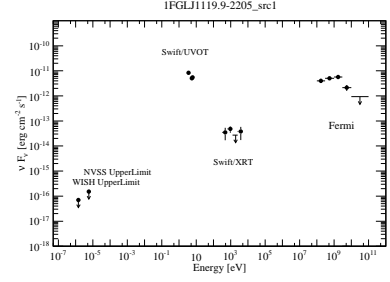
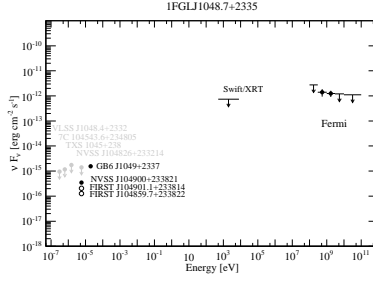
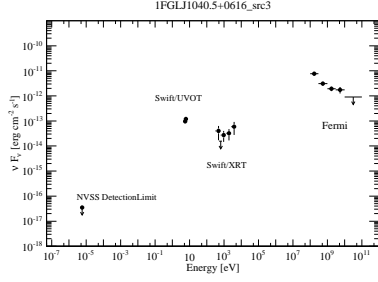
1FGL Src	XRT Src#	R.A.(J2000) [deg]	Dec.(J2000) [deg]	$r_{90\%}$ ["]	Count Rates [1E-03 cts/s]	S/N ratio
1FGL J2223.3+0103	1	335.8724	1.0403	5.82	3.93+/-1.1	3.6
	2	335.6256	1.0416	5.31	9.29+/-1.8	5.2
1FGL J2228.5–1633	1	337.0186	-16.6058	5.59	4.19+/-1.2	3.6
	2	336.9564	-16.4692	6.21	5.33+/-1.3	4.0
	3	337.0684	-16.3948	3.73	1.07E+01+/-5.6	19.3
1FGL J2243.4+4104	1	341.0528	40.9538	4.57	1.52E+01+/-2.0	7.5
	2	340.9480	40.9421	6.04	3.60+/-1.0	3.5
	3	340.9314	40.8992	5.96	5.16+/-1.2	4.2
1FGL J2251.2–4928	1	342.8677	-49.4876	6.93	3.65+/-1.1	3.2
	2	342.7909	-49.5447	5.96	4.44+/-1.3	3.5
1FGL J2256.9–1024	1	344.2248	-10.4482	6.65	3.80+/-1.2	3.2
	2	344.1310	-10.3750	5.44	9.14+/-1.8	5.1
	3	344.1457	-10.5265	6.65	3.89+/-1.2	3.2
1FGL J2257.9–3643	1	344.5606	-36.7415	6.04	5.85+/-1.5	3.9
	2	344.4865	-36.7684	6.52	5.28+/-1.4	3.7
	3	344.4524	-36.5985	5.17	1.11E+01+/-2.1	5.3
1FGL J2310.0–3627	1	347.4192	-36.5466	3.73	7.12E+01+/-3.7	19.4
	2	347.3100	-36.5028	5.31	5.10+/-1.1	4.7
	3	347.6192	-36.5051	6.12	3.31+/-9.1E-01	3.6
	4	347.2436	-36.4546	6.12	3.20+/-9.4E-01	3.4
	5	347.2568	-36.5376	6.21	2.56+/-8.4E-01	3.0
1FGL J2323.0–4919	1	350.7275	-49.2745	4.92	4.03E+01+/-6.0	6.8
1FGL J2330.3–4745	1	352.4761	-47.6597	6.21	1.63+/-5.5E-01	3.0
	2	352.3234	-47.5036	3.94	7.65E+01+/-5.8	13.1
1FGL J2339.7–0531	1	354.9608	-5.5473	5.31	4.19+/-7.9E-01	5.3
	2	354.9106	-5.5524	4.90	4.58+/-8.1E-01	5.6
	3	354.9828	-5.4250	5.76	2.48+/-6.5E-01	3.8
	4	354.8064	-5.5937	5.82	2.17+/-6.3E-01	3.5
	5	354.8657	-5.3717	4.81	8.36+/-1.3	6.5
1FGL J2347.3+0710	1	356.6665	7.0863	4.13	3.03E+01+/-2.9	10.3
1FGL J2350.1–3005	1	357.6430	-30.1017	4.60	2.39E+01+/-3.1	7.7

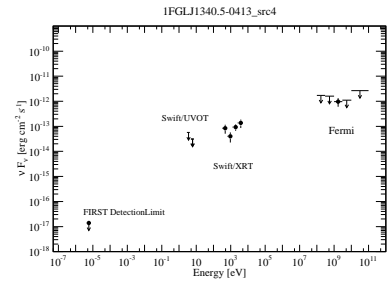
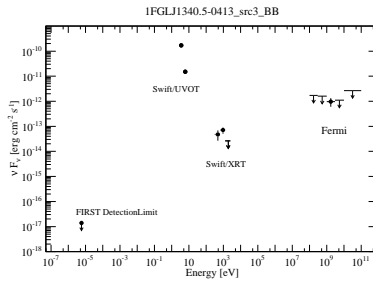
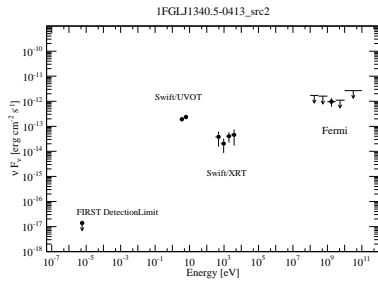
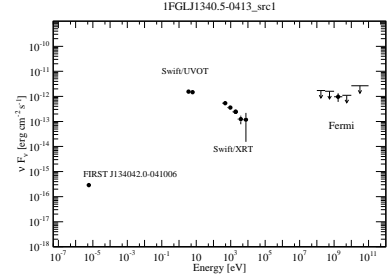
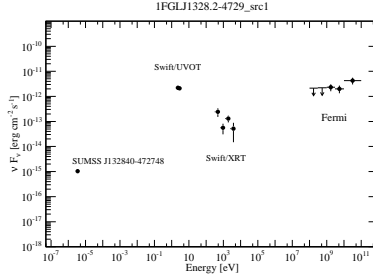
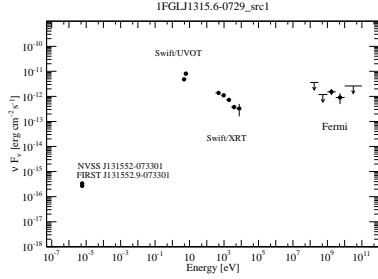
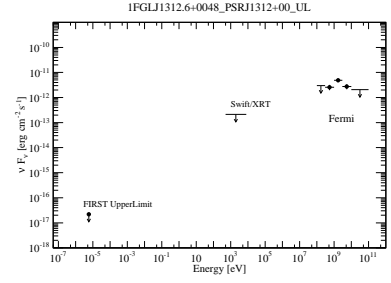
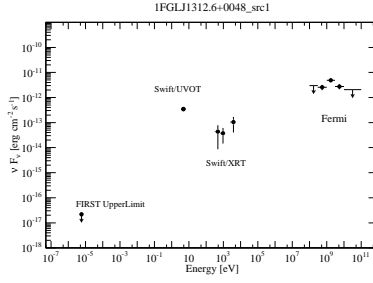
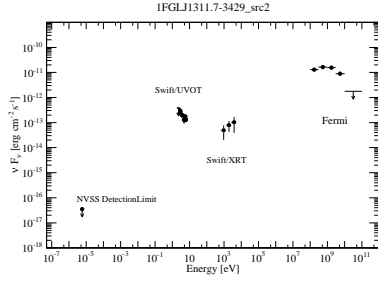
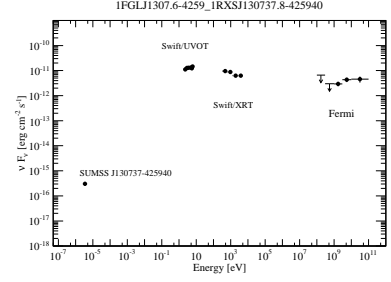
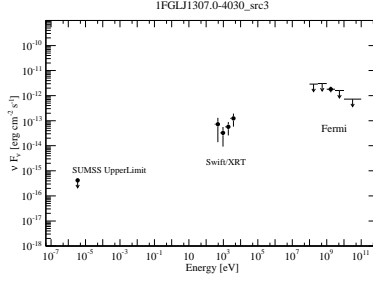
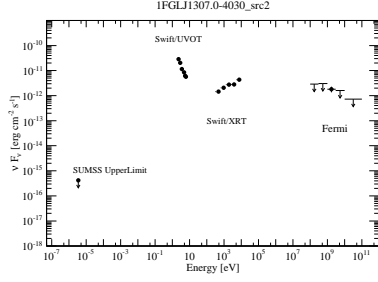
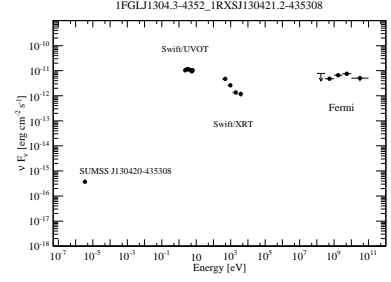
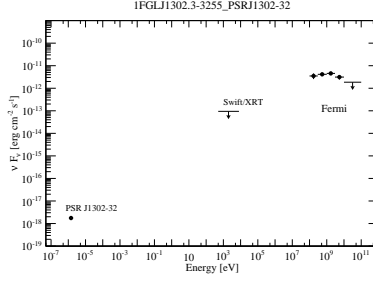
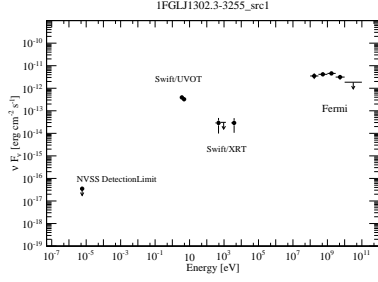
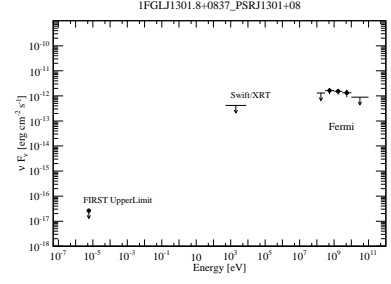
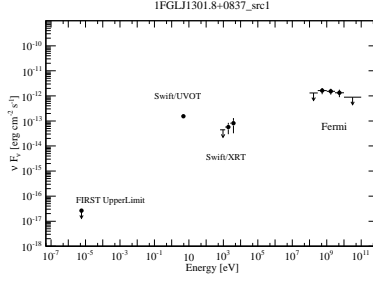
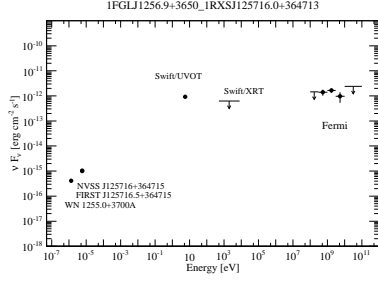


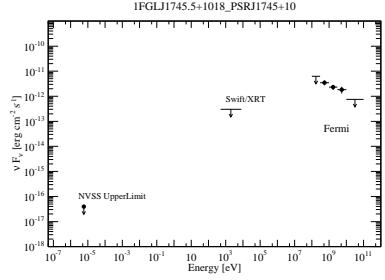
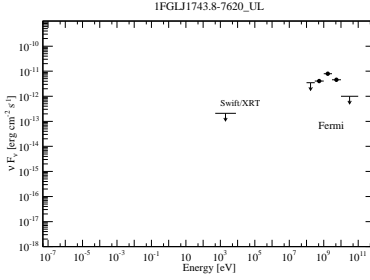
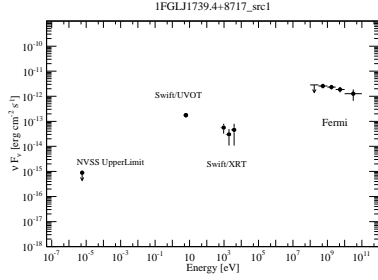
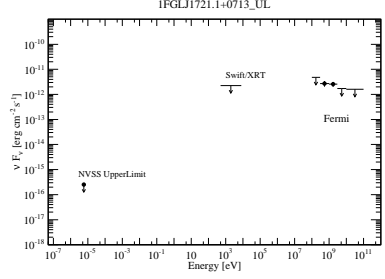
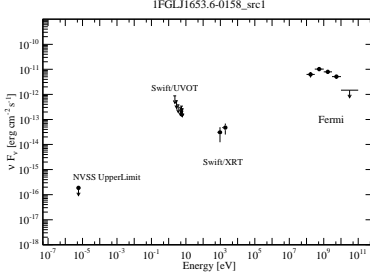
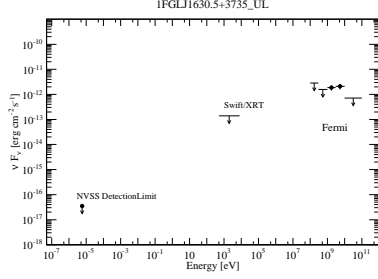
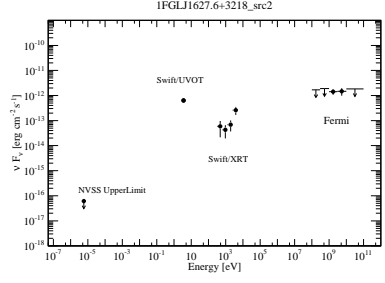
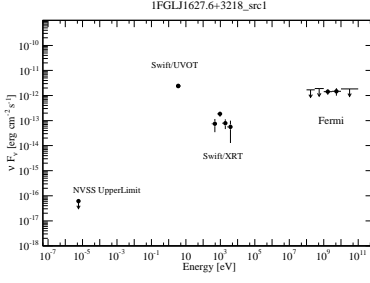
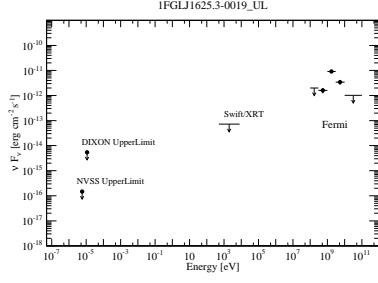
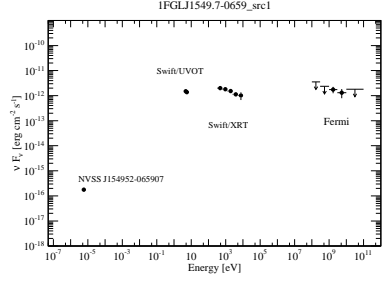
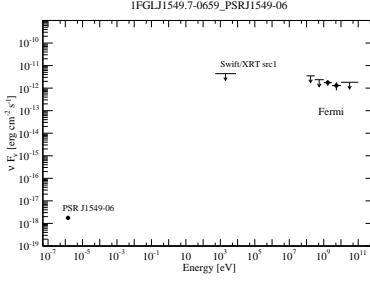
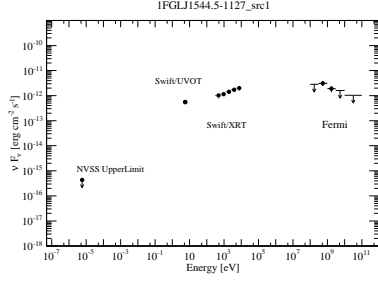
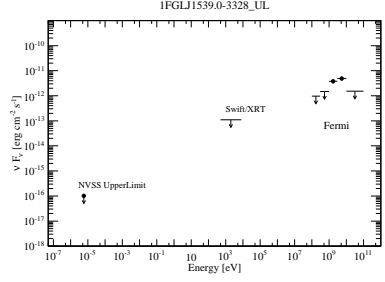
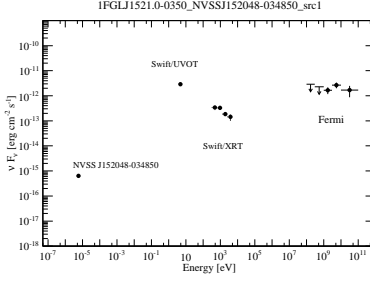
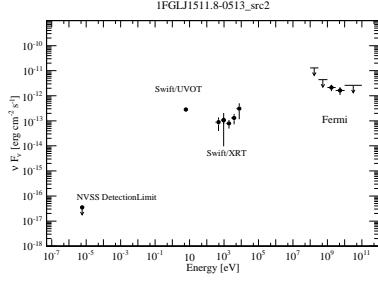
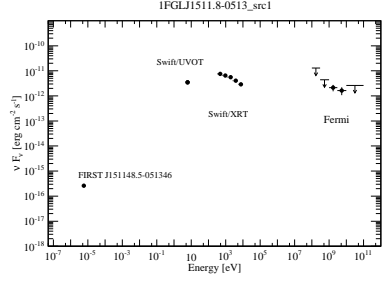
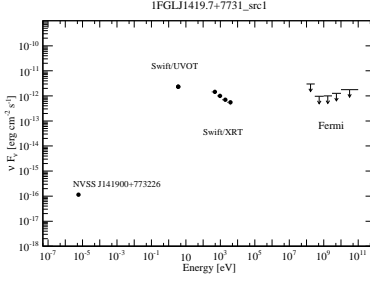
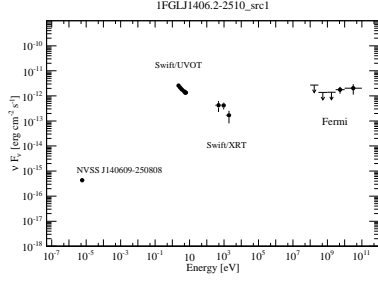


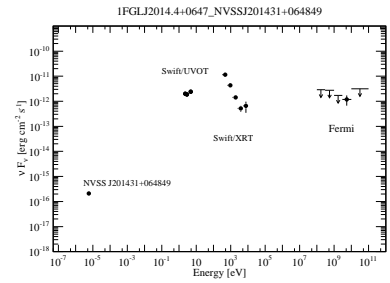
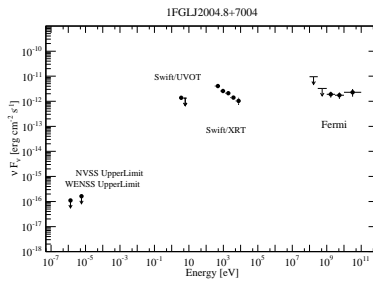
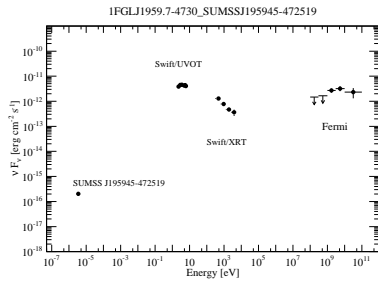
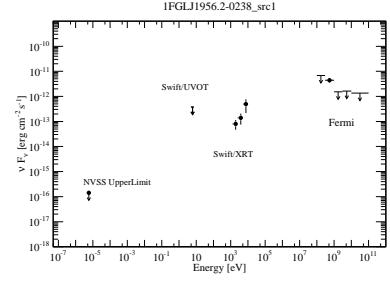
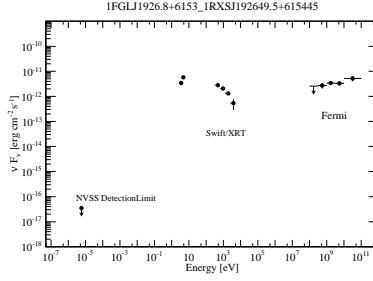
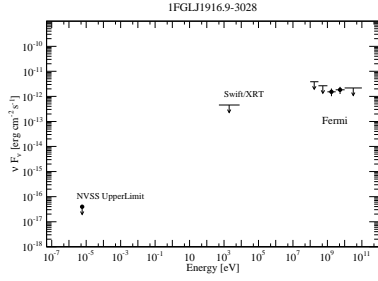
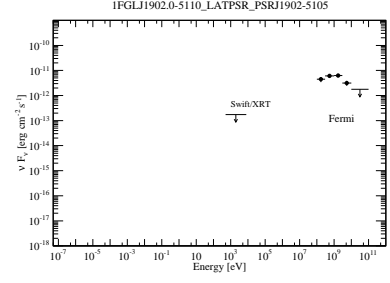
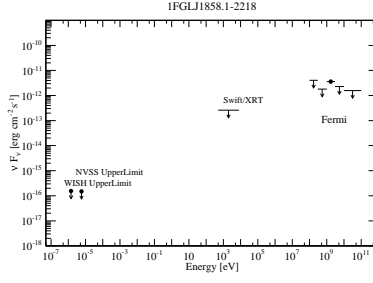
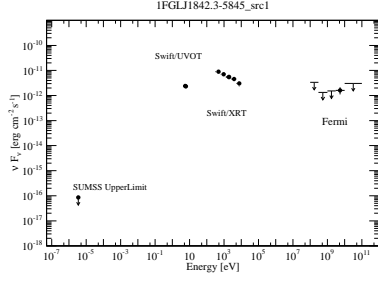
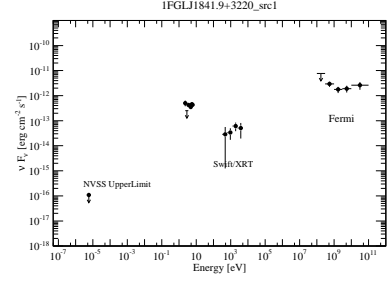
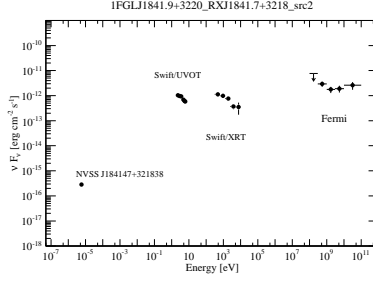
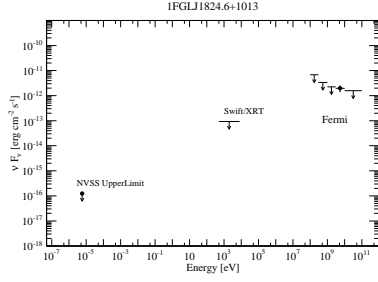
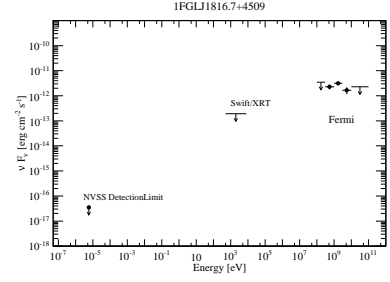
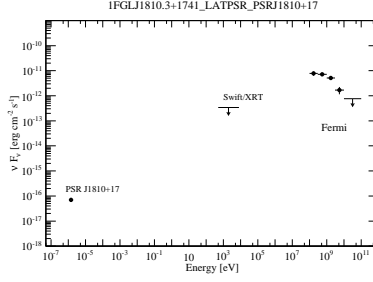
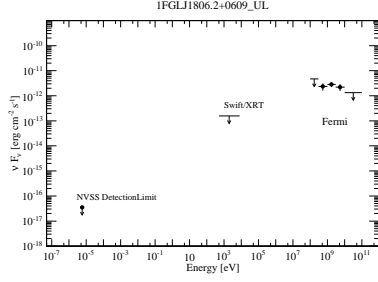
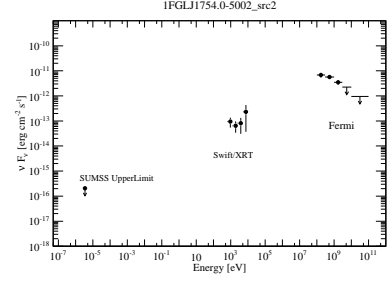
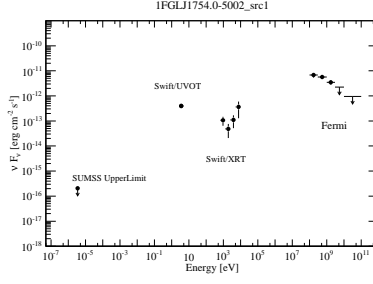
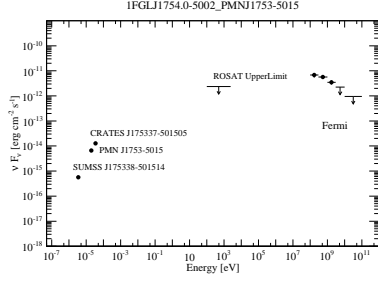


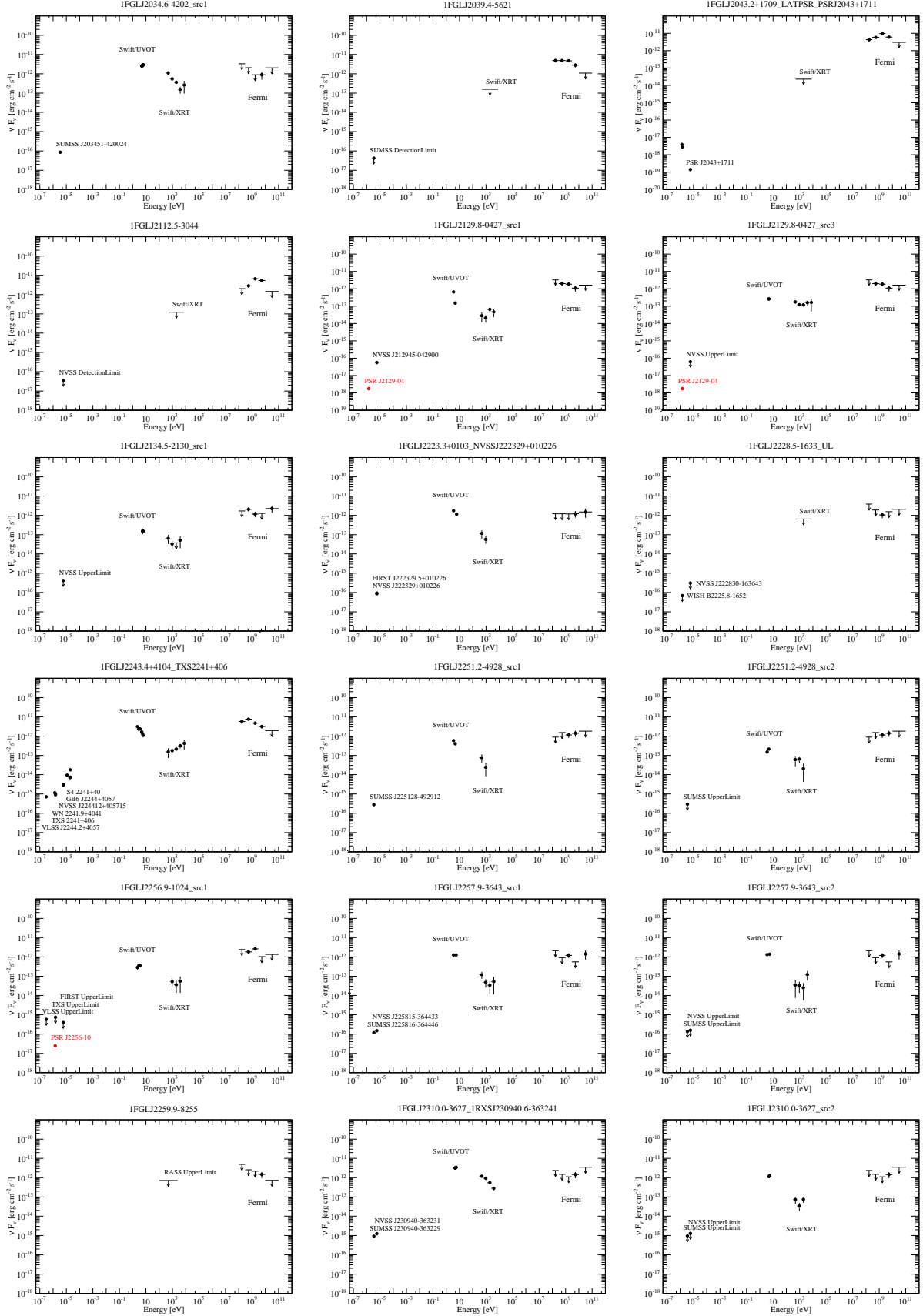












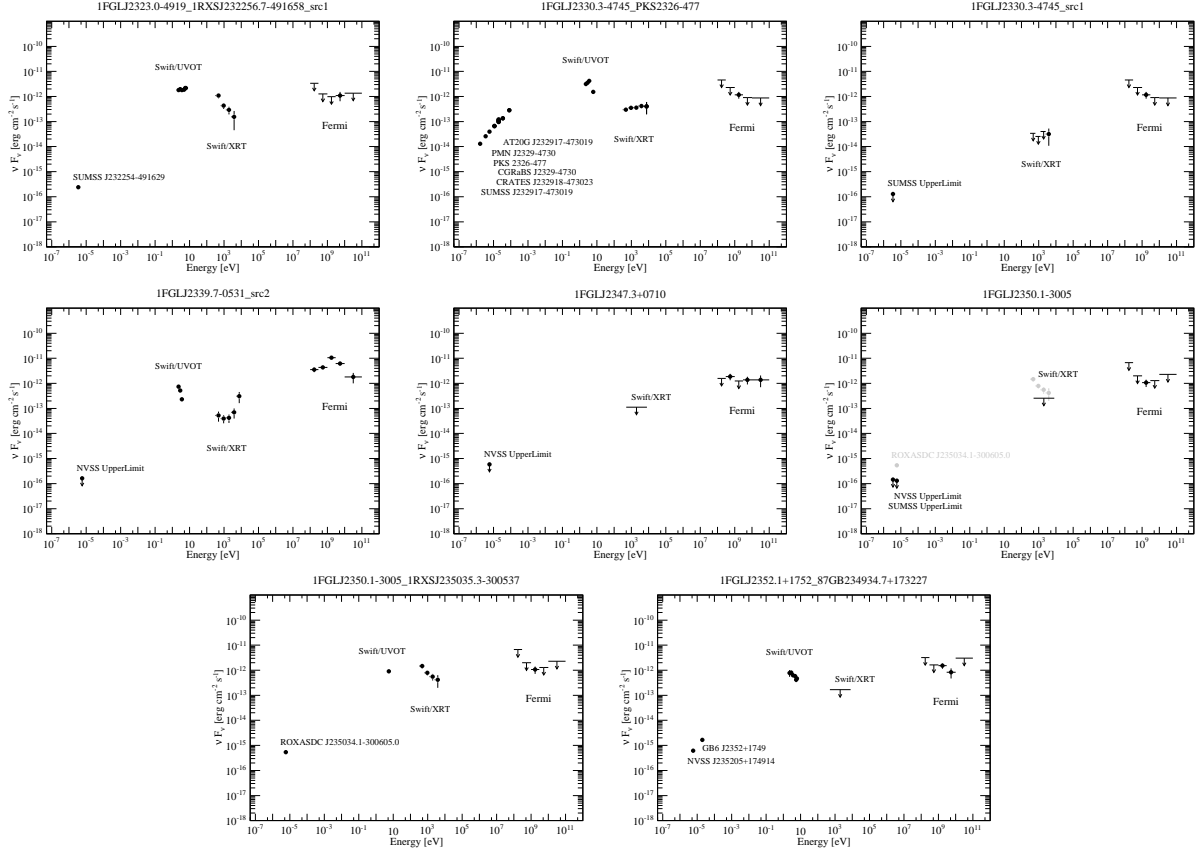


Fig. 12.— Broadband SEDs of the 134 1FGL unidentified sources we selected in this paper. The radio fluxes of these sources are described in Section 2.3. The X-ray fluxes for these sources are given from *Swift*/XRT analysis (see Section 2.1). Finally, the LAT fluxes of these sources are taken from the 2FGL catalog (Nolan et al. 2012).

Table 5: All Radio fluxes and *Swift*/UVOT fluxes plotted in SEDs(Figure 12) are listed here.

Name	Radio [mJy]				UV (Swift/UVOT) [E-12 erg/cm ² /s]					
	F_{350MHz}	F_{843MHz}	$F_{1.4GHz}$	$F_{4.85GHz}$	V-band	B-band	U-band	UVW1-band	UVM2-band	UVW2-band
J0001.9-4158_src1	-	13.2 ± 1.2	-	-	-	-	-	-	-	-
J0001.9-4158_src2	-	< 5	-	-	-	-	0.131 ± 0.017	-	0.213 ± 0.030	0.152 ± 0.010
J0009.1+5031	-	-	12.1 ± 0.6	-	-	-	1.94 ± 0.06	-	-	1.61 ± 0.063
J0022.2-1850	-	-	22.4 ± 0.8	-	3.31 ± 0.33	3.39 ± 0.23	3.19 ± 0.19	2.83 ± 0.17	3.26 ± 0.21	2.51 ± 0.12
J0023.5+0930_PSRJ0023+48_src2	2.00 ± 0.01	-	-	-	-	-	-	-	-	-
J0023.5+0930_PSRJ0023+48_src3	2.00 ± 0.01	-	-	-	-	-	-	-	-	-
J0030.7+0724_src2	-	-	< 2.5	-	-	-	-	-	0.0685 ± 0.0067	-
J0030.7+0724_src6	-	-	12.2	-	-	-	-	-	-	-
J0032.7-5519	-	< 5	-	-	-	-	-	-	-	-
J0038.0+1236	-	-	75.6 ± 2.3	-	6.63 ± 0.51	4.59 ± 0.31	2.87 ± 0.22	2.71 ± 0.21	1.79 ± 0.18	2.14 ± 0.15
J0039.2+4331	-	-	< 3.7	-	-	-	1.21 ± 0.04	-	-	-
J0051.4-6242	-	43.2 ± 1.5	-	-	2.39 ± 0.19	3.31 ± 0.16	4.45 ± 0.10	3.29 ± 0.13	3.53 ± 0.13	3.67 ± 0.12222
J0054.9-2455	-	-	24.3 ± 0.9	-	3.92 ± 0.32	4.55 ± 0.23	4.70 ± 0.21	4.75 ± 0.20	5.51 ± 0.26	5.43 ± 0.18
J0101.0-6423_PSRJ0101-6422	-	-	0.20 ± 0.01	-	-	-	< 0.0253	-	-	-
J0102.3+0942	-	-	11.0 ± 0.5	-	-	-	-	-	0.375 ± 0.028	0.454 ± 0.026
J0103.1+4840	0.50 ± 0.01	-	-	-	-	-	-	-	-	-
J0106.7+4853	-	-	-	-	-	-	-	-	-	-
J0115.7+0357	-	-	99.4 ± 3.0	-	1.51 ± 0.27	1.65 ± 0.18	1.90 ± 0.15	1.42 ± 0.12	1.68 ± 0.14	1.65 ± 0.10
J0124.6-0616_PMNJ0124-0624	-	-	40.9 ± 1.3	-	-	-	-	-	-	-
J0143.9-5845	-	28.3 ± 1.2	-	-	-	-	2.66 ± 0.07	-	-	3.27 ± 0.08
J0157.0-5259	-	44.2 ± 1.6	-	-	0.946 ± 0.139	1.17 ± 0.10	1.21 ± 0.08	1.19 ± 0.07	1.17 ± 0.08	1.24 ± 0.06
J0217.9-6630_RBS0300_src1	-	-	-	78.0 ± 8.0	2.05 ± 0.25	2.48 ± 0.18	2.32 ± 0.15	2.31 ± 0.10	2.79 ± 0.20	2.50 ± 0.05
J0217.9-6630_src2	-	< 21.4	-	-	0.592 ± 0.185	< 0.307	< 0.194	0.319 ± 0.047	0.347 ± 0.079	0.348 ± 0.015
J0217.9-6630_src3	-	< 5	-	-	0.807 ± 0.192	0.383 ± 0.106	0.282 ± 0.069	0.318 ± 0.045	0.424 ± 0.085	0.292 ± 0.014
J0223.0-1118_IRXSJ022314.6-111741	-	-	14.0 ± 0.6	-	-	-	1.43 ± 0.04	-	1.18 ± 0.06	-
J0226.3+0937	-	-	< 385.8	-	-	-	-	-	-	-
J0239.5+1324	-	-	< 20.4	-	-	-	-	-	-	-
J0305.2-1601	-	-	< 951.6	-	-	-	0.464 ± 0.046	0.342 ± 0.051	0.538 ± 0.046	-
J0308.6+7442	0.30 ± 0.01	-	-	-	-	-	-	-	-	-
J0316.3-6438	-	17.8 ± 1.3	-	-	-	-	1.13 ± 0.04	-	1.74 ± 0.06	-
J0335.5-4501_src1	-	< 20.5	-	-	-	-	-	-	0.122 ± 0.012	-
J0335.5-4501_src3	-	19.3 ± 1.2	-	-	-	-	-	-	1.61 ± 0.05	-
J0340.4+4130_PSRJ0340+4130	2.0 ± 0.1	-	-	-	-	-	-	-	-	-
J0345.2-2355	-	-	29.2 ± 1.0	-	-	-	-	0.552 ± 0.023	-	0.805 ± 0.031
J0409.9-0357	-	-	39.1 ± 1.2	-	-	-	2.12 ± 0.08	-	1.57 ± 0.07	2.02 ± 0.09
J0439.8-1857	-	-	60 ± 2.3	-	-	-	-	0.513 ± 0.020	-	-
J0505.9+6121_NVSSJ050558+611336	-	-	21.8 ± 0.8	-	-	-	2.53 ± 0.36	-	< 2.74	3.79 ± 0.87
J0506.9-5435_1ES0505-546	-	18.0 ± 1.1	-	-	2.91 ± 0.28	3.16 ± 0.20	2.80 ± 0.17	3.29 ± 0.16	3.89 ± 0.20	3.72 ± 0.15
J0515.9+1528_GB6J0515+1527	-	-	26.5 ± 0.9	-	5.91 ± 0.95	6.47 ± 0.95	6.41 ± 0.93	4.78 ± 1.36	< 4.53	< 6.36
J0521.6+0103_src1	-	-	24.1 ± 0.8	-	-	-	2.12 ± 0.17	1.13 ± 0.064	0.778 ± 0.082	1.01 ± 0.15

Name	Radio [mJy]				UV (Swift/UVOT) [E-12 erg/cm ² /s]					
	F_{350MHz}	F_{843MHz}	$F_{1.4GHz}$	$F_{4.85GHz}$	V-band	B-band	U-band	UVW1-band	UVM2-band	UVW2-band
J0523.5-2529	-	-	< 2.5	-	-	-	-	0.142 ± 0.010	-	-
J0533.9+6758_src1	-	-	< 2.5	-	-	-	-	2615 ± 2550	4886 ± 4874	-
J0533.9+6758_src2	-	-	< 2.5	-	-	-	-	< 0.219	< 0.176	-
J0537.7-5717_src2	-	< 5	-	-	1.87 ± 0.18	2.05 ± 0.13	1.88 ± 0.11	1.75 ± 0.10	1.70 ± 0.11	0.829 ± 0.053
J0537.7-5717_SUMSSJ053748-571828	-	102.6 ± 3.3	-	-	-	-	-	327 ± 7	120 ± 3	108 ± 2
J0538.4-3910_1RXSJ053810.0-390839	-	-	23 ± 0.8	-	0.970 ± 0.157	0.503 ± 0.087	0.699 ± 0.023	0.610 ± 0.060	0.691 ± 0.065	0.669 ± 0.073
J0600.5-2006	-	-	< 100	-	-	-	-	-	-	-
J0603.0-4012	-	-	< 19.6	-	-	-	-	-	-	-
J0604.2-4817_1ES0602-482	-	32.3 ± 1.3	-	-	1.64 ± 0.17	1.75 ± 0.12	2.57 ± 0.06	2.16 ± 0.11	2.23 ± 0.13	2.12 ± 0.07
J0605.1+0005_GB6J0604+0000	-	-	34.4 ± 1.1	-	-	-	-	-	-	-
J0609.3-0244_NVSSJ060915-024754	-	-	61.3 ± 1.9	-	2.30 ± 0.49	2.67 ± 0.41	3.00 ± 0.28	2.87 ± 0.31	2.17 ± 0.46	2.46 ± 0.38
J0622.2+3751_LATPSR_PSRJ0622+3749	-	-	< 0.022	-	-	-	-	-	-	-
J0648.6-6052_PMNJ0647-6058	-	-	-	78.0 ± 4.0	< 0.552	0.610 ± 0.122	< 0.213	0.372 ± 0.073	< 0.216	0.173 ± 0.030
J0648.6-6052_src4	-	< 12	-	-	-	-	193 ± 4	54.6 ± 1.2	3.75 ± 0.21	20.9 ± 0.4
J0707.3+7742_NVSSJ070651+774137	-	-	37.0 ± 1.2	-	-	-	-	-	-	2.32 ± 0.05
J0718.8-4958_src1	-	< 141.4	-	-	-	-	-	-	38.9 ± 0.88	-
J0803.1-0339_src1	-	-	231.1 ± 8.2	-	-	-	-	0.971 ± 0.031	-	-
J0814.5-1011_NVSSJ081411-101208	-	-	36.4 ± 1.2	-	3.13 ± 0.36	3.75 ± 0.28	3.42 ± 0.23	2.90 ± 0.23	2.56 ± 0.22	2.77 ± 0.18
J0843.4+6718	-	-	< 12.5	-	-	-	-	-	-	57
J0848.6+0504_TXS0846+051	-	-	174.09 ± 0.14	-	-	-	-	-	-	57
J0902.4+2050_NVSSJ090226+205045	-	-	62.85 ± 0.15	-	5.03 ± 0.34	5.79 ± 0.25	4.86 ± 0.11	5.29 ± 0.21	5.17 ± 0.23	4.94 ± 0.16
J0906.4-0903_PMNJ0906-0905	-	-	71.3 ± 2.2	-	2.38 ± 0.30	1.83 ± 0.19	2.20 ± 0.16	1.56 ± 0.13	1.51 ± 0.15	0.960 ± 0.079
J0908.7-2119_NVSSJ090858-211854	-	-	10.4 ± 0.6	-	-	-	0.909 ± 0.040	-	-	-
J0922.0+2337_NVSSJ092145+233548	-	-	18.4 ± 0.14	-	-	-	1.25 ± 0.05	-	-	1.42 ± 0.05
J0922.0+2337_src2	-	-	< 23.8	-	-	-	-	-	-	-
J0922.0+2337_src3	-	-	< 23.8	-	-	-	-	-	-	-
J0940.2-7605_UL	-	< 71.7	-	-	-	-	-	-	-	-
J0953.6-1505	-	-	< 6	-	-	-	-	-	-	-
J0955.2-3949_src1	-	-	< 5.3	-	-	-	-	0.373 ± 0.045	-	-
J1040.5+0616_src1	-	-	39.02 ± 0.17	-	-	-	-	-	0.316 ± 0.019	0.234 ± 0.024
J1040.5+0616_src2	-	-	3.53 ± 0.19	-	-	-	-	-	0.201 ± 0.016	0.109 ± 0.020
J1040.5+0616_src3	-	-	< 2.5	-	-	-	-	-	0.0960 ± 0.0134	0.120 ± 0.020
J1048.7+2335	-	-	-	-	-	-	-	-	-	-
J1119.9-2205_src1	-	-	< 10.9	-	-	-	8.42 ± 0.19	-	5.04 ± 0.12	5.52 ± 0.13
J1119.9-2205_src2	-	-	< 10.9	-	-	-	0.193 ± 0.024	-	0.136 ± 0.013	0.132 ± 0.019
J1124.4-3654_PSRJ1124-36	< 0.3	-	-	-	-	-	< 0.137	< 0.377	< 0.0523	< 0.124
J1129.3+3757_src1	-	-	26.5 ± 1.2	-	-	-	-	0.136 ± 0.017	0.107 ± 0.018	0.0595 ± 0.0109
J1129.3+3757_src2	-	-	< 2.5	-	-	-	-	0.343 ± 0.023	0.249 ± 0.023	0.192 ± 0.016
J1141.8-1403_1RXSJ114142.2-140757	-	-	59.2 ± 2.2	-	-	-	-	1.36 ± 0.11	1.13 ± 0.04	1.30 ± 0.04
J1159.8+0200_GB6J1200+0202	-	-	30.82 ± 0.14	-	-	-	-	-	-	-
J1218.4-0128_PKS1216-010	-	-	280.11 ± 0.15	-	1.34 ± 0.25	1.16 ± 0.15	1.30 ± 0.12	0.897 ± 0.090	0.982 ± 0.098	0.896 ± 0.067
J1221.4-0635_src1	-	-	< 7.59	-	-	-	-	0.788 ± 0.042	0.936 ± 0.038	1.02 ± 0.04
J1221.4-0635_src3	-	-	< 7.59	-	-	-	-	< 0.0913	< 0.0464	< 0.0588

Name	Radio [mJy]				UV (Swift/UVOT) [E-12 erg/cm ² /s]					
	F_{350MHz}	F_{843MHz}	$F_{1.4GHz}$	$F_{4.85GHz}$	V-band	B-band	U-band	UVW1-band	UVM2-band	UVW2-band
J1226.0+2954_UL	-	-	< 2.5	-	-	-	-	-	-	-
J1232.2-5118_src1	-	< 37.5	-	-	-	-	-	0.288 ± 0.040	-	-
J1249.3-2812	-	-	26.8 ± 0.9	-	-	-	-	-	-	1.11 ± 0.03
J1251.3+1044_1RXSJ125117.4+103914	-	-	4.21 ± 0.15	-	1.79 ± 0.18	1.66 ± 0.11	1.60 ± 0.10	1.83 ± 0.09	1.82 ± 0.10	1.71 ± 0.07
J1254.4+2209_src2	-	-	< 2.5	-	-	-	-	-	-	-
J1254.4+2209_TXSJ1252+224	-	-	83.43 ± 0.15	-	2.66 ± 0.32	2.30 ± 0.14	2.13 ± 0.12	2.04 ± 0.11	2.30 ± 0.18	2.11 ± 0.09
J1256.9+3650_1RXSJ125716.0+364713	-	-	73.86 ± 0.17	-	-	-	-	-	0.914 ± 0.052	-
J1301.8+0837_PSRJ1301+08	-	-	< 1.87	-	-	-	-	-	-	-
J1301.8+0837_src1	-	-	< 1.87	-	-	-	-	0.153 ± 0.018	-	-
J1302.3-3255_PSRJ1302-32	0.500 ± 0.001	-	-	-	-	-	-	-	-	-
J1302.3-3255_src1	-	-	< 2.5	-	-	-	0.389 ± 0.016	0.325 ± 0.024	-	-
J1304.3-4352_1RXSJ130421.2-435308	-	43.8 ± 1.7	-	-	10.5 ± 0.5	11.5 ± 0.4	11.2 ± 0.4	10.5 ± 0.3	9.39 ± 0.38	10.4 ± 0.3
J1307.0-4030_ESO323-77	-	48.0 ± 1.9	-	-	83.2 ± 1.9	57.9 ± 1.1	32.7 ± 0.7	15.6 ± 0.3	7.20 ± 0.22	7.40 ± 0.23
J1307.0-4030_src2	-	< 49.9	-	-	28.6 ± 0.7	20.3 ± 0.5	11.4 ± 0.3	8.46 ± 0.22	6.16 ± 0.21	5.71 ± 0.21
J1307.0-4030_src3	-	< 49.9	-	-	-	-	-	-	-	-
J1307.6-4259_1RXSJ130737.8-425940	-	36.2 ± 1.6	-	-	11.1 ± 0.56	12.7 ± 0.4	12.9 ± 0.5	13.1 ± 0.5	12.3 ± 0.5	14.5 ± 0.4
J1311.7-3429	-	-	-	-	-	-	-	-	-	-
J1312.6+0048	-	-	-	-	-	-	-	-	-	-
J1315.6-0729_src1	-	-	19.21 ± 0.15	-	-	-	-	4.76 ± 0.10	-	8.03 ± 0.17
J1328.2-4729_src1	-	123.6 ± 3.8	-	-	2.20 ± 0.33	2.09 ± 0.23	-	-	-	-
J1340.5-0413_src1	-	-	20.74 ± 0.14	-	-	-	1.56 ± 0.04	-	-	1.48 ± 0.04
J1340.5-0413_src2	-	-	< 1	-	-	-	0.190 ± 0.022	-	-	0.233 ± 0.016
J1340.5-0413_src3	-	-	< 1	-	-	-	170 ± 4	-	-	15.1 ± 0.3
J1340.5-0413_src4	-	-	< 1	-	-	-	< 0.0567	-	-	< 0.0313
J1406.2-2510_NVSSJ140609-250808	-	-	30.7 ± 1.0	-	2.57 ± 0.34	2.13 ± 0.21	1.81 ± 0.16	1.53 ± 0.14	1.36 ± 0.15	1.36 ± 0.10
J1419.7+7731_1RXSJ141901.8+773229	-	-	8.1 ± 0.5	-	-	-	2.32 ± 0.05	-	-	-
J1511.8-0513_src1	-	-	18.72 ± 0.14	-	-	-	-	-	-	3.45 ± 0.08
J1511.8-0513_src2	-	-	< 2.5	-	-	-	-	-	-	0.284 ± 0.021
J1521.0-0350_NVSSJ152048-034850	-	-	45.4 ± 1.4	-	-	-	-	2.91 ± 0.06	-	-
J1539.0-3328_UL	-	-	< 7.3	-	-	-	-	-	-	-
J1544.5-1127_src1	-	-	< 31	-	-	-	-	-	0.556 ± 0.090	-
J1549.7-0659_PSRJ1549-06	< 0.5	-	-	-	-	-	-	-	-	-
J1549.7-0659_src1	-	-	-	-	-	-	-	1.50 ± 0.08	1.39 ± 0.07	-
J1625.3-0019_UL	-	-	< 10.5	-	-	-	-	-	-	-
J1627.6+3218_src1	-	-	< 4.4	-	-	-	2.41 ± 0.06	-	-	-
J1627.6+3218_src2	-	-	< 4.4	-	-	-	0.629 ± 0.020	-	-	-
J1630.5+3735_UL	-	-	< 2.5	-	-	-	-	-	-	-
J1653.6-0158_src1	-	-	< 13.2	-	< 0.875	< 0.554	< 0.382	< 0.290	< 0.342	< 0.262
J1721.1+0713_UL	-	-	< 17.9	-	-	-	-	-	-	-
J1739.4+8717	-	-	-	-	-	-	-	-	-	-
J1221.4-0635_src1	-	-	< 7.59	-	-	-	-	0.788 ± 0.042	0.936 ± 0.038	1.02 ± 0.04
J1743.8-7620	-	-	-	-	-	-	-	-	-	-
J1745.5+1018_PSRJ1745+10	-	-	< 2.8	-	-	-	-	-	-	-

Name	Radio [mJy]				UV (Swift/UVOT) [E-12 erg/cm ² /s]					
	F_{350MHz}	F_{843MHz}	$F_{1.4GHz}$	$F_{4.85GHz}$	V-band	B-band	U-band	UVW1-band	UVM2-band	UVW2-band
J1754.0-5002.PMNJ1753-5015	-	-	137.0 ± 11.0	-	-	-	-	-	-	-
J1754.0-5002_src1	-	< 14.8	-	-	-	-	0.394 ± 0.038	-	-	-
J1754.0-5002_src2	-	< 14.8	-	-	-	-	-	-	-	-
J1806.2+0609_UL	-	-	< 2.5	-	-	-	-	-	-	-
J1810.3+1741.LATPSR.PSRJ1810+17	20.0 ± 0.1	-	-	-	-	-	-	-	-	-
J1816.7+4509	-	-	< 2.5	-	-	-	-	-	-	-
J1824.6+1013	-	-	< 8.9	-	-	-	-	-	-	-
J1841.9+3220.RXJ1841.7+3218_src2	-	-	20.4 ± 0.7	-	1.04 ± 0.13	0.965 ± 0.095	0.931 ± 0.073	0.688 ± 0.060	0.611 ± 0.067	0.588 ± 0.042
J1841.9+3220_src1	-	-	< 7.7	-	0.503 ± 0.127	< 0.252	0.422 ± 0.062	0.351 ± 0.051	0.457 ± 0.061	0.430 ± 0.037
J1842.3-5845_src1	-	< 10.1	-	-	-	-	-	-	2.38 ± 0.10	2.32 ± 0.09
J1858.1-2218	-	-	< 10.7	-	-	-	-	-	-	-
J1902.0-5110	-	-	-	-	-	-	-	-	-	-
J1916.9-3028	-	-	< 2.8	-	-	-	-	-	-	-
J1926.8+6153.1RXSJ192649.5+615445	-	-	< 2.5	-	-	-	3.43 ± 0.11	5.73 ± 0.17	-	-
J1956.2-0238_src1	-	-	< 10.1	-	-	-	-	-	-	0.37458
J1959.7-4730.SUMSSJ195945-472519	-	23.8 ± 1.1	-	-	3.82 ± 0.32	4.44 ± 0.23	4.55 ± 0.21	4.28 ± 0.20	4.40 ± 0.22	4.02 ± 0.10
J2004.8+7004	-	-	< 11.6	-	-	-	1.37 ± 0.13	-	-	< 1.33
J2014.4+0647_NVSSJ201431+064849	-	-	15.0 ± 0.9	-	2.01 ± 0.11	1.87 ± 0.09	-	2.40 ± 0.29	-	-
J2034.6-4202	-	10.2 ± 1.6	-	-	-	-	-	2.59 ± 0.08	2.61 ± 0.11	2.96 ± 0.08
J2039.4-5621	-	< 5	-	-	-	-	-	-	-	-
J2043.2+1709	-	-	-	-	-	-	-	-	-	-
J2112.5-3044	-	-	< 2.5	-	-	-	-	-	-	-
J2129.8-0427.PSRJ2129-04_src1	-	-	< 4.4	-	-	-	0.657 ± 0.027	0.151 ± 0.012	-	-
J2129.8-0427.PSRJ2129-04_src3	< 0.5	-	-	-	-	-	-	0.261 ± 0.010	-	-
J2134.5-2130_src1	-	-	< 30	-	-	-	-	-	0.153 ± 0.045	0.152 ± 0.022
J2223.3+0103_NVSSJ222329+010226	-	-	6.1 ± 0.5	-	-	-	1.73 ± 0.04	-	-	1.14 ± 0.07
J2228.5-1633_UL	-	-	< 22	-	-	-	-	-	-	-
J2243.4+4104.TXS2241+406	-	-	226.2 ± 6.8	-	3.10 ± 0.42	2.27 ± 0.28	2.37 ± 0.23	1.65 ± 0.20	1.34 ± 0.19	1.08 ± 0.10
J2251.2-4928_src1	-	33.3 ± 1.4	-	-	-	-	0.582 ± 0.020	0.403 ± 0.032	-	-
J2251.2-4928_src2	-	< 34.7	-	-	-	-	0.150 ± 0.012	0.211 ± 0.026	-	-
J2256.9-1024	-	-	-	-	0.284 ± 0.064	0.351 ± 0.043	0.359 ± 0.027	-	-	-
J2257.9-3643_src1	-	-	10.6 ± 0.6	-	-	-	1.26 ± 0.04	-	1.26 ± 0.05	-
J2257.9-3643_src2	-	-	< 11.2	-	-	-	1.30 ± 0.04	-	1.37 ± 0.05	-
J2259.9-8255	-	-	-	-	-	-	-	-	-	-
J2310.0-3627.1RXSJ230940.6-363241	-	-	89.8 ± 3.1	-	-	-	-	3.14 ± 0.07	3.41 ± 0.09	-
J2310.0-3627_src2	-	-	< 92.9	-	-	-	-	1.15 ± 0.03	1.29 ± 0.05	-
J2323.0-4919.1RXSJ232256.7-491658	-	28.3 ± 1.3	-	-	1.79 ± 0.21	1.97 ± 0.14	1.81 ± 0.12	1.87 ± 0.11	2.18 ± 0.14	2.17 ± 0.09
J2330.3-4745.PKS2326-477	-	2820 ± 1	-	-	-	-	-	-	-	-
J2330.3-4745_src1	-	< 15.1	-	-	3.13 ± 0.14	3.53 ± 0.11	4.17 ± 0.12	-	-	1.52 ± 0.04
J2339.7-0531_src2	-	-	< 11.6	-	0.73 ± 0.07	0.52 ± 0.05	0.23 ± 0.02	-	-	-
J2347.3+0710_UL	-	-	< 41.6	-	-	-	-	-	-	-
J2350.1-3005	-	-	< 9.3	-	-	-	-	-	-	-
J2352.1+1752.87GB234934.7+173227	-	-	44.2 ± 1.4	-	0.779 ± 0.234	0.801 ± 0.152	0.631 ± 0.101	0.581 ± 0.083	0.416 ± 0.080	0.469 ± 0.055

Table 6: *Swift*/XRT X-ray fluxes and 2FGL Gamma-ray fluxes plotted in SEDs(Figure 12) are shown here. $U.L._{0.5-8keV}$ shows the upper-limit of X-ray fluxes. Note that all X-ray fluxes are in [E-14 erg/cm²/s], while Gamma-ray fluxes in [E-12 erg/cm²/s].

Name	X-ray (Swift/XRT) [E-14 erg/cm ² /s]						Gamma-ray (2FGL Catalog) [E-12 erg/cm ² /s]				
	$F_{0.32-64keV}$	$F_{0.64-1.28keV}$	$F_{1.28-2.56keV}$	$F_{2.56-5.12keV}$	$F_{5.12-10.24keV}$	$U.L._{0.5-8keV}$	$F_{100-300MeV}$	$F_{0.3-1GeV}$	F_{1-3GeV}	$F_{3-10GeV}$	$F_{10-100GeV}$
J0001.9-4158_src1	104 ± 11	86.2 ± 7.3	57.5 ± 6.4	39.2 ± 8.13	20.2 ± 12.9	-	< 3.47	< 1.63	< 1.21	1.09 ± 0.39	< 1.42
J0001.9-4158_src2	-	2.29 ± 1.29	2.96 ± 1.58	-	-	-	< 3.47	< 1.63	< 1.21	1.09 ± 0.39	< 1.42
J0009.1+5031	18.3 ± 8.45	17.0 ± 4.3	15.1 ± 3.9	6.62 ± 3.86	-	-	< 2.29	2.85 ± 0.53	3.70 ± 0.55	4.10 ± 0.73	3.53 ± 1.04
J0022.2-1850	38.2 ± 17.4	37.2 ± 12.5	40.7 ± 14.5	-	-	-	< 1.27	< 1.34	1.27 ± 0.35	1.80 ± 0.52	3.61 ± 1.16
J0023.5+0930_PSRJ0023+48_src2	-	5.49 ± 2.27	6.68 ± 2.77	9.78 ± 5.08	24.1 ± 18.5	-	< 2.70	2.64 ± 0.53	2.08 ± 0.44	< 1.67	< 1.27
J0023.5+0930_PSRJ0023+48_src3	9.82 ± 4.45	24.1 ± 5.2	2.06 ± 1.52	-	-	-	< 2.70	2.64 ± 0.53	2.08 ± 0.44	< 1.67	< 1.27
J0030.7+0724_src2	3.42 ± 1.91	0.745 ± 0.606	2.27 ± 1.11	1.96 ± 1.57	-	-	3.41 ± 1.13	< 1.20	< 1.38	< 0.609	1.28 ± 0.64
J0030.7+0724_src6	12.3 ± 5.0	19.2 ± 4.1	15.4 ± 3.9	-	-	-	3.41 ± 1.13	< 1.20	< 1.38	< 0.609	1.28 ± 0.64
J0032.7-5519	-	-	-	-	-	< 18.7	3.58 ± 0.91	3.94 ± 0.46	2.92 ± 0.44	1.54 ± 0.45	< 2.46
J0038.0+1236	33.4 ± 8.7	20.5 ± 4.4	16.0 ± 4.0	11.2 ± 5.14	-	-	3.42 ± 1.24	2.51 ± 0.52	1.84 ± 0.42	1.28 ± 0.46	1.38 ± 0.62
J0039.2+4331	31.3 ± 9.9	4.74 ± 2.30	5.38 ± 2.47	6.98 ± 4.23	-	-	< 1.64	< 0.776	< 1.36	0.709 ± 0.334	< 2.28
J0051.4-6242	481 ± 32	255 ± 13	127 ± 9	65.6 ± 10.2	57.9 ± 20.0	-	< 2.38	1.17 ± 0.39	1.82 ± 0.38	3.79 ± 0.68	3.43 ± 1.05
J0054.9-2455	254 ± 41	136 ± 21	41.7 ± 12.6	52.9 ± 21.9	70.7 ± 53.1	-	< 1.31	< 0.701	0.790 ± 0.299	1.51 ± 0.50	< 1.54
J0101.0-6423_PSRJ0101-6422	-	-	-	-	-	< 39.1	< 2.23	2.15 ± 0.36	4.28 ± 0.51	2.30 ± 0.55	< 0.925
J0102.3+0942	-	5.62 ± 2.36	1.93 ± 1.59	4.58 ± 3.60	-	-	< 4.30	< 1.94	< 1.31	1.21 ± 0.46	< 2.08
J0103.1+4840	-	-	-	-	-	< 26.1	< 3.44	2.21 ± 0.63	4.82 ± 0.67	3.00 ± 0.65	< 1.01
J0106.7+4853	-	-	-	-	-	-	< 5.47	5.03 ± 0.77	5.11 ± 0.69	5.60 ± 0.84	< 1.05
J0115.7+0357	30.7 ± 15.4	19.3 ± 8.6	32.0 ± 12.3	-	-	-	< 4.80	2.98 ± 0.50	2.54 ± 0.45	2.69 ± 0.62	1.73 ± 0.76
J0124.6-0616_PMNJ0124-0624	-	-	-	-	-	< 22.9	< 1.73	2.12 ± 0.46	0.943 ± 0.353	0.786 ± 0.377	< 1.06
J0143.9-5845	780 ± 37	650 ± 22	533 ± 22	441 ± 30	311 ± 56	-	< 2.38	1.36 ± 0.37	1.86 ± 0.37	1.62 ± 0.46	4.25 ± 1.15
J0157.0-5259	500 ± 40	607 ± 32	737 ± 39	825 ± 63	579 ± 118	-	< 3.26	< 1.01	< 1.02	1.98 ± 0.52	< 1.46
J0217.9-6630_RBS0300_src1	101 ± 11	86.8 ± 7.5	45.7 ± 5.8	28.0 ± 7.0	-	-	< 2.60	1.52 ± 0.40	< 1.23	1.67 ± 0.48	< 2.05
J0217.9-6630_src2	9.70 ± 3.65	6.58 ± 2.12	4.20 ± 1.88	9.79 ± 4.28	-	-	< 2.60	1.52 ± 0.40	< 1.23	1.67 ± 0.48	< 2.05
J0217.9-6630_src3	4.72 ± 2.68	6.83 ± 2.20	9.13 ± 2.76	4.72 ± 3.13	14.2 ± 12.1	-	< 2.60	1.52 ± 0.40	< 1.23	1.67 ± 0.48	< 2.05
J0223.0-1118_IRXSJ022314.6-111741	78.6 ± 11.9	57.6 ± 7.5	47.5 ± 7.4	17.4 ± 7.0	18.0 ± 16.6	-	< 1.02	< 0.873	< 1.08	< 1.40	< 3.01
J0226.3+0937	-	-	-	-	-	< 93.9	< 3.92	< 2.35	< 1.66	1.50 ± 0.48	< 1.32
J0239.5+1324	-	-	-	-	-	< 9.42	< 5.46	< 2.35	1.20 ± 0.40	1.06 ± 0.47	< 2.35
J0305.2-1601	51.3 ± 11.2	72.4 ± 9.0	77.3 ± 10.2	50.4 ± 12.3	81.7 ± 34.7	-	< 1.45	< 0.765	< 0.838	0.808 ± 0.395	1.78 ± 0.81
J0308.6+7442	-	-	-	-	-	< 4.86	< 1.31	1.84 ± 0.40	6.19 ± 0.65	1.87 ± 0.50	< 0.876
J0316.3-6438	206 ± 20	138 ± 11	120 ± 11	61.3 ± 12.4	-	-	< 3.88	< 1.69	0.813 ± 0.315	1.96 ± 0.52	< 2.92
J0335.5-4501_src1	4.94 ± 3.10	1.57 ± 1.38	5.84 ± 2.69	-	-	-	< 1.31	1.33 ± 0.37	0.930 ± 0.302	0.953 ± 0.378	1.83 ± 0.79
J0335.5-4501_src3	29.4 ± 7.7	15.4 ± 4.1	15.5 ± 4.4	4.98 ± 3.99	-	-	< 1.31	1.33 ± 0.37	0.930 ± 0.302	0.953 ± 0.378	1.83 ± 0.79
J0340.4+4130_PSRJ0340+4130	-	-	-	-	-	< 11.6	< 2.89	2.81 ± 0.57	7.74 ± 0.75	5.13 ± 0.83	< 2.07
J0345.2-2355	6.12 ± 3.20	3.97 ± 1.96	6.25 ± 2.65	6.94 ± 4.30	-	-	4.44 ± 1.53	2.96 ± 0.52	1.49 ± 0.36	0.768 ± 0.337	< 0.886
J0409.9-0357	7.04 ± 4.08	9.58 ± 2.86	9.78 ± 3.07	7.97 ± 4.13	16.7 ± 13.8	-	< 4.47	1.58 ± 0.51	1.34 ± 0.40	1.08 ± 0.43	< 2.53
J0439.8-1857	14.9 ± 5.8	4.22 ± 2.17	5.06 ± 2.61	-	-	-	< 4.02	< 1.07	0.879 ± 0.306	1.58 ± 0.50	< 2.93
J0505.9+6121_NVSSJ050558+611336	755 ± 386	295 ± 34	103 ± 10	41.7 ± 8.6	9.56 ± 9.14	-	< 1.41	< 1.89	< 1.90	1.27 ± 0.49	< 2.60
J0506.9-5435_IES0505-546	539 ± 78	290 ± 36	172 ± 28	138 ± 38	181 ± 94	-	< 1.41	< 1.12	< 1.16	1.51 ± 0.48	1.49 ± 0.71
J0515.9+1528_GB6J0515+1527	-	12.1 ± 6.2	4.81 ± 3.45	9.15 ± 6.97	-	-	< 5.51	< 2.68	2.74 ± 0.61	1.86 ± 0.58	2.58 ± 0.89
J0521.6+0103_src1	11.0 ± 7.0	6.87 ± 2.93	4.30 ± 2.39	-	-	-	< 2.58	< 0.754	< 1.28	1.07 ± 0.44	< 3.49
J0523.5-2529	2.52 ± 2.05	-	2.64 ± 1.66	10.4 ± 4.9	-	-	4.03 ± 0.93	3.18 ± 0.49	4.14 ± 0.53	3.49 ± 0.69	< 1.29

Name	X-ray (Swift/XRT) [E-14 erg/cm ² /s]						Gamma-ray (2FGL Catalog) [E-12 erg/cm ² /s]				
	$F_{0.32-0.64\text{keV}}$	$F_{0.64-1.28\text{keV}}$	$F_{1.28-2.56\text{keV}}$	$F_{2.56-5.12\text{keV}}$	$F_{5.12-10.24\text{keV}}$	$U.L.-0.5-8\text{keV}$	$F_{100-300\text{MeV}}$	$F_{0.3-1\text{GeV}}$	$F_{1-3\text{GeV}}$	$F_{3-10\text{GeV}}$	$F_{10-100\text{GeV}}$
J0533.9+6758_src1	12.3 ± 5.3	19.6 ± 4.6	2.36 ± 1.66	-	-	-	< 1.44	1.38 ± 0.38	2.81 ± 0.46	2.51 ± 0.56	< 1.09
J0533.9+6758_src2	9.35 ± 4.97	3.48 ± 1.83	5.41 ± 2.43	-	-	-	< 1.44	1.38 ± 0.38	2.81 ± 0.46	2.51 ± 0.56	< 1.09
J0537.7-5717_src2	58.3 ± 16.5	49.4 ± 9.6	27.0 ± 7.3	12.9 ± 7.7	-	-	< 4.00	< 0.931	< 1.36	0.888 ± 0.403	< 2.46
J0537.7-5717_SUMSSJ053748-571828	10.5 ± 6.5	40.4 ± 9.2	8.53 ± 4.36	-	-	-	< 4.00	< 0.931	< 1.36	0.888 ± 0.403	< 2.46
J0538.4-3910_1RXSJ053810.0-390839	344 ± 39	261 ± 17	216 ± 15	183 ± 20	102 ± 34	-	< 3.18	1.90 ± 0.51	0.901 ± 0.348	< 1.37	< 2.11
J0600.5-2006	-	-	-	-	-	< 321	< 4.67	2.07 ± 0.52	1.06 ± 0.39	< 1.33	< 0.718
J0603.0-4012	-	-	-	-	-	< 79.4	< 3.02	2.12 ± 0.52	1.76 ± 0.46	2.46 ± 0.61	< 2.53
J0604.2-4817_1ES0602-482	384 ± 26	263 ± 14	208 ± 13	170 ± 17	107 ± 31	-	< 1.57	1.32 ± 0.45	1.24 ± 0.37	< 1.44	1.80 ± 0.79
J0605.1+0005_GB6J0604+0000	-	-	-	-	-	< 203	< 1.99	< 2.35	1.48 ± 0.53	< 1.37	1.53 ± 0.76
J0609.3-0244_NVSSJ060915-024754	98.0 ± 60.0	35.8 ± 14.9	38.9 ± 14.0	19.0 ± 14.2	-	-	5.58 ± 1.89	< 2.62	1.47 ± 0.49	1.93 ± 0.61	2.48 ± 0.97
J0622.2+3751_LATPSR_PSRJ0622+3749	-	-	-	-	-	< 27.1	< 2.25	6.09 ± 0.64	3.95 ± 0.60	< 1.32	< 0.712
J0648.6-6052_PMNJ0647-6058	4.80 ± 2.59	3.64 ± 1.36	6.32 ± 1.92	11.6 ± 3.8	15.5 ± 10.7	-	< 4.13	2.05 ± 0.52	< 1.78	1.07 ± 0.43	< 2.26
J0648.6-6052_src4	-	4.45 ± 1.63	1.52 ± 1.06	0.663 ± 1.343	-	-	< 4.13	2.05 ± 0.52	< 1.78	1.07 ± 0.43	< 2.26
J0707.3+7742_NVSSJ070651+774137	17.2 ± 6.2	5.65 ± 2.39	9.89 ± 3.39	-	-	-	< 2.05	1.57 ± 0.38	2.30 ± 0.38	1.85 ± 0.45	< 1.67
J0718.8-4958_src1	1.22 ± 3.78	7.76 ± 2.80	-	-	-	-	< 4.64	1.73 ± 0.57	< 2.04	1.26 ± 0.47	< 0.902
J0803.1-0339_src1	45.7 ± 10.3	33.1 ± 5.9	27.8 ± 5.8	15.5 ± 6.6	-	-	< 4.67	1.58 ± 0.48	1.89 ± 0.42	2.25 ± 0.58	1.68 ± 0.78
J0814.5-1011_NVSSJ081411-101208	292 ± 206	496 ± 157	261 ± 117	349 ± 201	-	-	< 7.85	2.24 ± 0.67	2.33 ± 0.53	1.36 ± 0.52	< 2.75
J0843.4+6718	-	-	-	-	-	< 24.7	< 2.55	< 1.64	1.06 ± 0.30	1.78 ± 0.45	< 0.623
J0848.6+0504_TXSO846+051	-	-	-	-	-	< 123	< 1.86	< 1.69	< 0.986	1.64 ± 0.52	< 3.69
J0902.4+2050_NVSSJ090226+205045	18.7 ± 6.0	10.9 ± 3.1	3.19 ± 1.85	7.81 ± 4.27	-	-	< 3.11	< 2.05	1.92 ± 0.41	1.63 ± 0.49	< 2.39 ^l
J0906.4-0903_PMNJ0906-0905	19.6 ± 13.9	13.4 ± 7.8	15.3 ± 9.1	22.4 ± 16.8	-	-	< 3.58	< 1.82	1.28 ± 0.38	1.62 ± 0.51	< 2.44 ^l
J0908.7-2119_NVSSJ090858-211854	-	2.67 ± 1.97	-	11.9 ± 6.2	-	-	< 4.65	2.25 ± 0.68	< 1.87	< 1.01	< 1.92 ^l
J0922.0+2337_NVSSJ092145+233548	14.4 ± 6.0	8.10 ± 3.18	3.96 ± 2.48	5.81 ± 4.57	-	-	< 2.27	< 1.10	< 1.33	1.26 ± 0.45	< 2.38
J0922.0+2337_src2	-	2.19 ± 1.75	6.97 ± 3.31	12.9 ± 6.7	-	-	< 2.27	< 1.10	< 1.33	1.26 ± 0.45	< 2.38
J0922.0+2337_src3	5.18 ± 4.14	6.82 ± 3.18	13.1 ± 4.8	7.04 ± 5.45	-	-	< 2.27	< 1.10	< 1.33	1.26 ± 0.45	< 2.38
J0940.2-7605_UL	-	-	-	-	-	< 480	< 5.45	2.53 ± 0.69	1.84 ± 0.50	< 0.841	< 0.805
J0953.6-1505	-	-	-	-	-	< 66.8	< 1.73	1.57 ± 0.48	2.08 ± 0.44	1.38 ± 0.51	< 1.21
J0955.2-3949_src1	-	3.85 ± 2.36	9.25 ± 3.56	13.7 ± 6.5	-	-	4.28 ± 1.33	4.14 ± 0.67	3.20 ± 0.58	1.56 ± 0.52	< 1.14
J1040.5+0616_src1	4.51 ± 2.46	1.71 ± 1.07	4.23 ± 1.83	4.39 ± 2.95	-	-	7.67 ± 1.05	3.10 ± 0.51	1.95 ± 0.40	1.75 ± 0.49	< 0.912
J1040.5+0616_src2	6.64 ± 2.91	4.64 ± 1.69	6.13 ± 2.15	6.07 ± 3.26	12.3 ± 10.9	-	7.67 ± 1.05	3.10 ± 0.51	1.95 ± 0.40	1.75 ± 0.49	< 0.912
J1040.5+0616_src3	4.00 ± 2.28	2.74 ± 1.28	3.22 ± 1.55	5.94 ± 3.16	-	-	7.67 ± 1.05	3.10 ± 0.51	1.95 ± 0.40	1.75 ± 0.49	< 0.912
J1048.7+2335	-	-	-	-	-	< 73.7	< 2.73	1.41 ± 0.47	1.25 ± 0.35	< 1.20	< 1.10
J1119.9-2205_src1	3.52 ± 1.84	4.80 ± 1.39	1.14 ± 0.79	3.78 ± 2.05	-	-	3.90 ± 0.74	4.88 ± 0.53	5.55 ± 0.61	2.06 ± 0.55	< 0.828
J1119.9-2205_src2	2.59 ± 1.58	1.70 ± 0.83	2.81 ± 1.15	-	-	-	3.90 ± 0.74	4.88 ± 0.53	5.55 ± 0.61	2.06 ± 0.55	< 0.828
J1124.4-3654_PSRJ1124-36	3.45 ± 2.50	1.43 ± 0.93	2.17 ± 1.17	3.48 ± 2.25	-	-	< 5.27	3.24 ± 0.68	3.53 ± 0.57	3.08 ± 0.70	< 1.63
J1129.3+3757_src1	3.93 ± 2.59	2.18 ± 1.38	3.65 ± 1.95	3.69 ± 3.16	-	-	3.45 ± 1.14	2.26 ± 0.45	1.83 ± 0.37	1.69 ± 0.50	< 1.21
J1129.3+3757_src2	-	1.35 ± 1.12	4.54 ± 2.17	1.51 ± 2.22	-	-	3.45 ± 1.14	2.26 ± 0.45	1.83 ± 0.37	1.69 ± 0.50	< 1.21
J1141.8-1403_1RXSJ114142.2-140757	128 ± 14	91.5 ± 8.4	84.5 ± 8.7	53.6 ± 10.4	52.1 ± 22.4	-	< 1.42	< 1.60	1.09 ± 0.38	1.18 ± 0.45	< 1.91
J1159.8+0200_GB6J1200+0202	-	-	-	-	-	< 73.8	< 3.99	1.39 ± 0.44	< 1.33	1.41 ± 0.47	< 1.26
J1218.4-0128_PKS1216-010	-	-	21.6 ± 8.8	-	77.0 ± 55.3	-	< 5.70	2.79 ± 0.54	3.47 ± 0.54	2.09 ± 0.56	1.46 ± 0.70
J1221.4-0635_src1	11.6 ± 4.2	8.17 ± 2.46	7.29 ± 2.57	11.2 ± 4.8	14.8 ± 13.1	-	4.21 ± 1.15	2.14 ± 0.51	1.43 ± 0.39	1.25 ± 0.46	< 1.08
J1221.4-0635_src3	-	-	4.24 ± 2.13	7.99 ± 4.32	-	-	4.21 ± 1.15	2.14 ± 0.51	1.43 ± 0.39	1.25 ± 0.46	< 1.07
J1226.0+2954_UL	-	-	-	-	-	< 28.4	< 2.0738	1.98 ± 0.44	2.38 ± 0.46	3.02 ± 0.63	< 1.13
J1232.2-5118_src1	-	3.68 ± 2.33	8.05 ± 3.37	8.72 ± 5.18	37.4 ± 24.4	-	3.19 ± 1.20	5.11 ± 0.72	2.45 ± 0.56	< 0.868	< 0.68
J1249.3-2812	81.2 ± 14.6	67.0 ± 8.3	56.4 ± 7.9	21.5 ± 7.4	41.5 ± 22.0	-	< 2.01	< 1.99	< 1.57	< 1.60	< 2.86
J1251.3+1044_1RXSJ125117.4+103914	77.2 ± 15.1	70.6 ± 10.4	63.2 ± 10.7	29.0 ± 11.0	37.0 ± 27.0	-	< 2.08	< 1.37	< 1.45	< 1.43	< 2.43

Name	X-ray (Swift/XRT) [E-14 erg/cm ² /s]						Gamma-ray (2FGL Catalog) [E-12 erg/cm ² /s]				
	$F_{0.32-0.64\text{keV}}$	$F_{0.64-1.28\text{keV}}$	$F_{1.28-2.56\text{keV}}$	$F_{2.56-5.12\text{keV}}$	$F_{5.12-10.24\text{keV}}$	$U.L_{0.5-8\text{keV}}$	$F_{100-300\text{MeV}}$	$F_{0.3-1\text{GeV}}$	$F_{1-3\text{GeV}}$	$F_{3-10\text{GeV}}$	$F_{10-100\text{GeV}}$
J1254.4+2209_src2	40.3 ± 13.7	18.4 ± 6.6	14.0 ± 6.4	25.2 ± 13.0	-	-	< 3.74	1.15 ± 0.40	1.15 ± 0.35	1.52 ± 0.49	< 1.80
J1254.4+2209_TXS1252+224	23.1 ± 12.9	114 ± 18	22.0 ± 9.2	-	-	-	< 3.74	1.15 ± 0.40	1.15 ± 0.35	1.52 ± 0.49	< 1.80
J1256.9+3650_1RXSJ125716.0+364713	-	-	-	-	-	< 62.4	< 1.44	1.40 ± 0.39	1.65 ± 0.35	0.967 ± 0.437	< 2.41
J1301.8+0837_PSRJ1301+08	-	1.65 ± 1.41	5.69 ± 2.74	8.09 ± 4.86	-	< 41.7	< 1.31	1.62 ± 0.45	1.52 ± 0.39	1.33 ± 0.44	< 0.89
J1301.8+0837_src1	2.91 ± 1.93	1.40 ± 0.83	-	2.89 ± 1.83	-	< 41.7	< 1.31	1.62 ± 0.45	1.52 ± 0.39	1.33 ± 0.44	< 0.89
J1302.3-3255_PSRJ1302-32	2.91 ± 1.93	1.40 ± 0.83	-	2.89 ± 1.83	-	< 9.42	3.48 ± 0.98	4.04 ± 0.60	4.45 ± 0.62	3.06 ± 0.69	< 1.73
J1302.3-3255_src1	473 ± 64	262 ± 28	134 ± 20	118 ± 28	-	< 9.42	3.48 ± 0.98	4.04 ± 0.60	4.45 ± 0.62	3.06 ± 0.69	< 1.73
J1304.3-4352_1RXSJ130421.2-435308	473 ± 64	262 ± 28	134 ± 20	118 ± 28	-	-	< 7.81	4.80 ± 0.73	6.54 ± 0.71	7.55 ± 1.03	5.02 ± 1.26
J1307.0-4030_ESO323-77	0.756 ± 0.267	6.65 ± 1.64	69.1 ± 7.9	653 ± 35	1510 ± 134	-	< 2.88	< 3.06	1.81 ± 0.47	< 1.61	< 0.722
J1307.0-4030_src2	146 ± 16	206 ± 13	274 ± 17	281 ± 25	435 ± 73	-	< 2.878	< 3.06	1.81 ± 0.47	< 1.61	< 0.722
J1307.0-4030_src3	7.21 ± 5.82	3.26 ± 2.33	5.75 ± 3.14	12.5 ± 6.7	-	-	< 2.878	< 3.06	1.81 ± 0.47	< 1.61	< 0.722
J1307.6-4259_1RXSJ130737.8-425940	952 ± 99	872 ± 58	628 ± 51	624 ± 76	-	-	< 6.61	< 3.01	2.95 ± 0.57	4.32 ± 0.82	4.54 ± 1.23
J1311.7-3429	-	-	-	-	-	-	12.8 ± 1.6	15.9 ± 0.9	15.2 ± 1.0	8.75 ± 1.05	< 1.63
J1312.6+0048	-	-	-	-	-	-	< 2.94	2.53 ± 0.61	4.79 ± 0.65	2.69 ± 0.62	< 1.92
J1315.6-0729_src1	138 ± 13	110 ± 8	72.4 ± 7.4	37.4 ± 8.1	33.1 ± 17.2	-	< 3.62	< 1.18	1.53 ± 0.41	0.908 ± 0.417	< 2.63
J1328.2-4729_src1	24.3 ± 9.3	5.60 ± 2.56	13.0 ± 3.9	5.16 ± 3.67	-	-	< 2.13	< 2.21	2.32 ± 0.73	2.01 ± 0.68	4.27 ± 1.25
J1340.5-0413_src1	54.0 ± 8.2	36.0 ± 4.8	24.2 ± 4.2	12.3 ± 4.6	11.7 ± 10.2	-	< 1.72	< 1.59	0.965 ± 0.365	< 1.10	< 2.67
J1340.5-0413_src2	3.82 ± 2.27	2.05 ± 1.19	4.04 ± 1.78	4.57 ± 2.86	-	-	< 1.72	< 1.59	0.965 ± 0.365	< 1.10	< 2.67
J1340.5-0413_src3	8.36 ± 3.26	3.98 ± 1.71	9.35 ± 2.76	13.6 ± 5.1	-	-	< 1.72	< 1.59	0.965 ± 0.365	< 1.10	< 2.67
J1340.5-0413_src4	42.5 ± 19.7	41.4 ± 12.6	16.7 ± 8.7	-	-	-	< 1.72	< 1.59	0.965 ± 0.365	< 1.10	< 2.67
J1406.2-2510_NVSSJ140609-250808	42.5 ± 19.7	41.4 ± 12.6	16.7 ± 8.7	-	-	-	< 2.72	< 1.38	< 1.40	1.76 ± 0.54	2.02 ± 0.83
J1419.7+7731_1RXSJ141901.8+773229	145 ± 16	99.6 ± 9.7	70.3 ± 8.7	55.2 ± 11.9	-	-	< 2.98	< 0.975	< 0.994	< 1.26	< 1.78
J1511.8-0513_src1	753 ± 43.6	649 ± 25	559 ± 24	401 ± 30	289 ± 56	-	< 13.0	< 4.42	2.14 ± 0.62	1.63 ± 0.57	< 2.61
J1511.8-0513_src2	8.83 ± 4.89	10.7 ± 3.3	7.89 ± 3.00	13.0 ± 5.8	30.9 ± 19.3	-	< 13.0	< 4.42	2.14 ± 0.62	1.63 ± 0.57	< 2.61
J1521.0-0350_NVSSJ152048-034850	33.8 ± 7.2	33.1 ± 4.2	18.5 ± 3.2	14.4 ± 4.3	-	-	< 2.89	< 2.28	1.67 ± 0.50	2.68 ± 0.67	1.67 ± 0.80
J1539.0-3328_UL	-	-	-	-	-	< 11.0	< 0.967	< 1.46	3.75 ± 0.67	4.87 ± 0.92	< 1.48
J1544.5-1127_src1	101 ± 24	114 ± 11	143 ± 11	171 ± 17	199 ± 44	-	< 2.86	3.08 ± 0.69	1.89 ± 0.51	< 1.61	< 1.03
J1549.7-0659_PSRJ1549-06	-	-	-	-	-	< 436	< 3.52	< 2.34	1.75 ± 0.50	1.31 ± 0.52	< 1.81
J1549.7-0659_src1	199 ± 26	179 ± 14	152 ± 13	112 ± 16	102 ± 35	< 436	< 3.52	< 2.34	1.75 ± 0.50	1.31 ± 0.52	< 1.81
J1625.3-0019_UL	-	-	-	-	-	< 7.17	< 1.99	1.57 ± 0.39	8.95 ± 0.79	3.40 ± 0.71	< 0.970
J1627.6+3218_src1	7.47 ± 4.03	18.4 ± 4.5	7.91 ± 3.29	5.63 ± 4.36	-	-	< 1.68	< 1.88	1.42 ± 0.34	1.47 ± 0.48	< 1.83
J1627.6+3218_src2	5.86 ± 3.71	4.26 ± 2.32	6.85 ± 3.20	25.9 ± 9.3	-	-	< 1.68	< 1.88	1.42 ± 0.34	1.47 ± 0.48	< 1.83
J1630.5+3735_UL	-	-	-	-	-	< 13.9	< 2.80	< 1.54	1.81 ± 0.41	2.05 ± 0.50	< 0.657
J1653.6-0158_src1	-	3.06 ± 1.84	4.70 ± 2.19	-	-	-	6.16 ± 1.54	9.96 ± 0.88	7.79 ± 0.79	4.99 ± 0.89	< 1.37
J1721.1+0713_UL	-	-	-	-	-	< 225	< 4.79	2.72 ± 0.70	2.57 ± 0.56	< 1.72	< 1.60
J1739.4+8717	-	-	-	-	-	-	< 2.85	2.57 ± 0.47	2.32 ± 0.41	1.88 ± 0.45	1.26 ± 0.60
J1743.8-7620	-	-	-	-	-	-	< 3.38	3.85 ± 0.55	7.63 ± 0.75	4.40 ± 0.79	< 0.862
J1745.5+1018_PSRJ1745+10	-	-	-	-	-	< 30.1	< 6.32	3.49 ± 0.76	2.32 ± 0.54	1.84 ± 0.56	< 0.749
J1754.0-5002_PMNJ1753-5015	-	-	-	-	-	< 235	6.69 ± 1.43	5.57 ± 0.78	3.42 ± 0.62	< 2.21	< 0.890
J1754.0-5002_src1	-	10.6 ± 4.2	4.82 ± 2.72	10.9 ± 5.8	36.2 ± 23.4	-	6.69 ± 1.43	5.57 ± 0.78	3.42 ± 0.62	< 2.21	< 0.890
J1754.0-5002_src2	-	9.44 ± 4.00	6.47 ± 3.11	8.15 ± 5.10	23.2 ± 19.6	-	6.69 ± 1.43	5.57 ± 0.78	3.42 ± 0.62	< 2.21	< 0.890
J1806.2+0609_UL	-	-	-	-	-	< 15.7	< 4.69	2.36 ± 0.74	2.85 ± 0.60	2.21 ± 0.66	< 1.33
J1810.3+1741_LATPSR_PSRJ1810+17	-	4.48 ± 2.42	2.15 ± 1.78	-	35.4 ± 22.4	-	7.55 ± 1.43	6.97 ± 0.73	5.00 ± 0.65	1.63 ± 0.52	< 0.675
J1816.7+4509	-	-	-	-	-	< 19.3	< 3.48	2.28 ± 0.46	3.14 ± 0.48	1.66 ± 0.52	< 2.29
J1824.6+1013	-	-	-	-	-	< 9.31	< 6.78	< 3.36	< 2.24	1.97 ± 0.60	< 1.56
J1841.9+3220_RXJ1841.7+3218_src2	2.85 ± 2.73	3.37 ± 1.64	6.11 ± 2.27	5.04 ± 3.09	-	-	< 7.68	2.92 ± 0.67	1.76 ± 0.48	1.90 ± 0.56	2.60 ± 0.89

Name	X-ray (Swift/XRT) [E-14 erg/cm ² /s]						Gamma-ray (2FGL Catalog) [E-12 erg/cm ² /s]				
	$F_{0.32-0.64\text{keV}}$	$F_{0.64-1.28\text{keV}}$	$F_{1.28-2.56\text{keV}}$	$F_{2.56-5.12\text{keV}}$	$F_{5.12-10.24\text{keV}}$	$U.L_{0.5-8\text{keV}}$	$F_{100-300\text{MeV}}$	$F_{0.3-1\text{GeV}}$	$F_{1-3\text{GeV}}$	$F_{3-10\text{GeV}}$	$F_{10-100\text{GeV}}$
J1841.9+3220_src1	113 ± 15	98.2 ± 8.7	76.1 ± 7.8	36.9 ± 8.2	35.1 ± 17.9	-	< 7.68	2.92 ± 0.67	1.76 ± 0.48	1.90 ± 0.56	2.60 ± 0.89
J1842.3-5845_src1	887 ± 75	701 ± 35	548 ± 30	459 ± 40	303 ± 71	-	< 3.35	< 1.34	< 1.53	1.61 ± 0.51	< 3.02
J1858.1-2218	-	-	-	-	-	< 26.1	< 4.08	< 1.81	3.61 ± 0.66	< 2.29	< 1.58
J1902.0-5110	-	-	-	-	-	-	4.25 ± 0.98	5.74 ± 0.62	5.93 ± 0.67	2.95 ± 0.64	< 1.43
J1916.9-3028	-	-	-	-	-	< 45.4	< 3.86	< 2.66	1.54 ± 0.52	1.83 ± 0.58	< 2.18
J1926.8+6153_1RXSJ192649.5+615445	278 ± 55	206 ± 30	130 ± 24	53.3 ± 23.8	-	-	< 2.58	2.70 ± 0.66	3.41 ± 0.50	3.32 ± 0.62	5.20 ± 1.16
J1956.2-0238_src1	401 ± 78	255 ± 21	208 ± 15	140 ± 17	104 ± 32	< 9.56	< 6.80	4.38 ± 0.79	< 1.52	< 1.64	< 1.35
J1959.7-4730_SUMSSJ195945-472519	128 ± 18	77.9 ± 9.6	47.3 ± 7.8	36.4 ± 10.4	-	-	< 1.47	< 1.66	2.68 ± 0.49	3.21 ± 0.68	2.34 ± 1.04
J2004.8+7004	401 ± 78	255 ± 21	208 ± 15	140 ± 17	104 ± 32	-	< 9.48	< 3.26	1.90 ± 0.51	1.74 ± 0.50	2.30 ± 0.77
J2014.4+0647_NVSSJ201431+064849	1151 ± 182	434 ± 36	143 ± 16	52.1 ± 13.7	65.9 ± 31.3	-	< 2.87	< 2.76	< 1.70	1.19 ± 0.53	< 3.14
J2034.6-4202	111 ± 14	54.7 ± 7.0	36.4 ± 6.0	15.4 ± 5.9	26.1 ± 16.7	-	< 3.29	< 2.06	< 0.885	0.890 ± 0.397	< 2.01
J2039.4-5621	-	-	-	-	-	< 15.6	4.86 ± 1.02	4.83 ± 0.58	4.68 ± 0.59	2.79 ± 0.64	< 1.09
J2043.2+1709	-	-	-	-	-	-	4.14 ± 0.99	5.52 ± 0.62	9.14 ± 0.76	5.70 ± 0.87	< 2.49
J2112.5-3044	-	-	-	-	-	< 12.1	< 1.95	2.72 ± 0.49	6.36 ± 0.69	5.21 ± 0.86	< 1.27
J2129.8-0427_PSRJ2129-04_src1	2.78 ± 1.62	2.06 ± 0.94	6.56 ± 1.76	4.68 ± 2.30	-	-	< 3.25	2.01 ± 0.49	1.85 ± 0.42	1.10 ± 0.42	< 1.63
J2129.8-0427_PSRJ2129-04_src3	17.7 ± 4.46	12.0 ± 2.5	11.8 ± 2.7	16.0 ± 4.8	16.3 ± 11.4	-	< 3.25	2.01 ± 0.49	1.85 ± 0.42	1.10 ± 0.42	< 1.63
J2134.5-2130_src1	6.47 ± 3.21	3.25 ± 1.55	1.44 ± 1.17	5.18 ± 3.25	-	-	< 1.70	2.07 ± 0.49	1.15 ± 0.36	< 1.26	2.23 ± 0.87
J2223.3+0103_NVSSJ222329+010226	11.6 ± 5.3	5.73 ± 2.34	-	-	-	-	< 1.20	< 1.20	< 1.18	1.21 ± 0.44	1.49 ± 0.73
J2228.5-1633_UL	-	-	-	-	-	< 64.3	< 3.82	< 1.90	1.05 ± 0.33	< 1.55	< 2.07
J2243.4+4104_TXS2241+406	15.3 ± 7.9	17.8 ± 4.4	21.3 ± 4.8	31.2 ± 8.5	42.4 ± 22.3	-	5.79 ± 1.52	7.51 ± 0.72	4.70 ± 0.60	3.14 ± 0.66	< 1.94
J2251.2-4928_src1	7.56 ± 3.61	2.40 ± 1.59	-	-	-	-	< 0.894	< 1.52	1.15 ± 0.35	1.41 ± 0.48	< 1.80
J2251.2-4928_src2	6.02 ± 3.29	6.42 ± 2.47	2.08 ± 1.66	-	-	-	< 0.894	< 1.52	1.15 ± 0.35	1.41 ± 0.48	< 1.80
J2256.9-1024	6.39 ± 3.80	4.01 ± 2.11	-	-	-	-	< 2.42	1.84 ± 0.46	2.61 ± 0.44	< 1.03	< 1.36
J2257.9-3643_src1	12.0 ± 4.6	4.81 ± 2.22	3.38 ± 2.16	5.23 ± 4.05	-	-	< 2.09	< 0.914	1.21 ± 0.34	< 0.56	1.43 ± 0.70
J2257.9-3643_src2	3.50 ± 2.75	3.27 ± 1.90	2.52 ± 1.95	12.2 ± 6.3	-	-	< 2.09	< 0.914	1.21 ± 0.34	< 0.56	1.43 ± 0.70
J2259.9-8255	-	-	-	-	-	< 70.8	< 4.89	< 2.58	< 2.18	1.46 ± 0.51	< 0.725
J2310.0-3627_1RXSJ230940.6-363241	118 ± 11	93.3 ± 7.7	55.2 ± 6.4	28.4 ± 7.0	-	-	< 2.34	< 1.50	< 1.11	1.44 ± 0.50	< 3.46
J2310.0-3627_src2	7.39 ± 2.95	3.40 ± 1.52	7.46 ± 2.45	-	-	-	< 2.34	< 1.50	< 1.11	1.44 ± 0.50	< 3.46
J2323.0-4919_1RXSJ232256.7-491658	109 ± 24	43.3 ± 11.3	29.1 ± 9.8	15.4 ± 10.9	-	-	< 3.35	< 1.26	< 0.979	1.08 ± 0.43	< 1.35
J2330.3-4745_PKS2326-477	1.16 ± 1.11	1.04 ± 0.74	1.90 ± 1.06	3.17 ± 2.10	-	-	< 4.58	< 2.28	1.17 ± 0.35	< 0.910	< 0.87
J2330.3-4745_src1	30.0 ± 5.90	35.3 ± 4.7	35.8 ± 5.3	41.9 ± 8.9	40.1 ± 20.4	-	< 4.58	< 2.28	1.17 ± 0.35	< 0.910	< 0.87
J2339.7-0531_src2	5.22 ± 2.27	3.92 ± 1.38	4.18 ± 1.55	6.96 ± 3.05	30.6 ± 14.4	-	3.42 ± 0.69	4.21 ± 0.48	10.3 ± 0.8	6.02 ± 0.89	1.63 ± 0.73
J2347.3+0710_UL	-	-	-	-	-	< 11.2	< 1.58	1.87 ± 0.53	< 1.25	1.37 ± 0.47	1.38 ± 0.67
J2350.1-3005	147 ± 33	78.9 ± 18.0	55.0 ± 16.1	41.4 ± 21.5	-	-	< 6.67	< 1.98	1.06 ± 0.34	< 1.29	< 2.27
J2352.1+1752_87GB234934.7+173227	-	-	-	-	-	< 16.8	< 3.19	< 1.64	1.52 ± 0.36	0.830 ± 0.363	< 3.06